CONDITION MONITORING OF PEM FUEL CELLS

Andrej Debenjak

Doctoral Dissertation
Jožef Stefan International Postgraduate School
Ljubljana, Slovenia

Supervisor: Dr. Janko Petrovčič, Jožef Stefan Institute, Ljubljana, Slovenia
Co-Supervisor: Prof. Dr. Đani Juričić, Jožef Stefan Institute, Ljubljana, Slovenia

Evaluation Board:
Prof. Dr. Stanislav Strmčnik, Chair, Jožef Stefan Institute, Ljubljana, Slovenia
Prof. Dr. Miran Gaberšček, Member, National Institute of Chemistry, Ljubljana, Slovenia, and Faculty of Chemistry and Chemical Technology, University of Ljubljana, Ljubljana, Slovenia
Prof. Dr. Juš Kocijan, Member, Jožef Stefan Institute, Ljubljana, Slovenia, and University of Nova Gorica, Nova Gorica, Slovenia

MEDNARODNA PODIPLOMSKA ŠOLA JOŽEFA STEFANA
JOŽEF STEFAN INTERNATIONAL POSTGRADUATE SCHOOL



Andrej Debenjak

CONDITION MONITORING OF PEM FUEL CELLS

Doctoral Dissertation

SPREMLJANJE STANJA GORIVNIH CELIC PEM

Doktorska disertacija

Supervisor: Dr. Janko Petrovčič

Co-Supervisor: Prof. Dr. Đani Juričić

Ljubljana, Slovenia, May 2015

To Ema, Žiga and Katja.
And in memory of Blaž.

Acknowledgments

First and foremost, I would like to extend my most sincere appreciation to my supervisor Dr. Janko Petrovčič. I am deeply grateful for his selfless sharing of his passion for engineering, knowledge, and commitment to perfection.

I also owe a debt of gratitude to my co-supervisor Prof. Dr. Đani Juričić for sharing his devotion to excellent science and mathematical clarity that enabled me to achieve beyond state-of-the-art results.

I would like to further thank Dr. Pavle Boškoski without whom my research work would not be as fruitful as it is.

My sincere thanks and gratitude to everyone else who has helped or inspired me at any point over the years, notably: Dr. Vladimir Jovan, Dr. Bojan Musizza, Dr. Matej Gašperin, Dr. Boštjan Pregelj, Dr. Biljana Mileva Boshkoska, and Stanislav Černe.

I would like to acknowledge the financial support of the Slovenian Research Agency through the Young Researchers Programme.

I thank my daughter Ema and my son Žiga for simply being there for me. And most importantly, I thank my wife Katja. I am eternally grateful to you for your continued love and support in all phases of our journey. Thank you for everything.

Abstract

The proton exchange membrane (PEM) fuel cells are close to be competitive with the conventional energy converting devices. However, the durability and reliability of PEM fuel cell systems have to be increased in order to meet end-user's expectations. The condition monitoring (CM) of PEM fuel cells is considered as one of the required tools to enhance the operation performance of the PEM fuel cell power systems.

This dissertation addresses the problem of reliable CM of PEM fuel cells. It provides a novel CM methodology, which manages each step of the CM, from the initial data acquisition to the final output in the form of a unit-free condition indicator (CI). The methodology is based on the well adopted electrochemical impedance spectroscopy (EIS) diagnostic method.

The conventional EIS method relies on the consecutive probing of the fuel cell with a set of single-sine signals of particular frequencies and computation of the corresponding points in the impedance curve. The approach proposed in this dissertation differs from the conventional one in (i) the use of frequency-rich excitation signal and (ii) handling impedance as a complex random variable. The excitation signal is the pseudorandom binary sequence (PRBS) waveform. Use of such an excitation signal results in a substantial reduction in the time required for conducting the impedance estimation. The short probing time is especially convenient for the CM systems. Moreover, in order to achieve high time-frequency resolution of the impedance estimates, the continuous wavelet transform (CWT) with the Morlet mother wavelet is used as the focal signal processing tool. The statistical properties of the employed PRBS signal, together with the CWT, enables the impedance at individual frequency to be treated as a complex random variable. This allows for rigorous selection of the initial CM alarm thresholds as well as for the information aggregation into a single CI. The strength of such an approach arises from two important engineering aspects. First, at commissioning or after a maintenance action, the tuning of the CM system requires only the data from normal (i.e., fault-free) operation of the PEM fuel cell system and the tolerated probability of false alarm (PFA). Second, the ultimate output of the CM system is a unit-free CI that describes the current condition of a PEM fuel cell.

The dissertation also presents the designed 90-channel fuel cell voltage monitor (FCVM) and modular direct-current-to-direct-current (DC-DC) converter. The interconnected FCVM and DC-DC converter, together with the CM algorithm, form an embedded CM system for PEM fuel cells. The interconnection enables the injection of the excitation signals and the acquisition of measurements that are required for fast online estimation of the impedance of PEM fuel cells. The system is both commercially viable and accurate enough to perform the measurements required for the CM purposes.

The complete CM setup was tested on a commercially available PEM fuel cell power system. For the validation of the CM methodology, the PEM fuel cells were subjected to water management faults, which were successfully detected and evaluated by the CI.

Povzetek

Gorivne celice s protonsko prevodno membrano (PEM, ang. proton exchange membrane) postajajo vse konkurenčnejše konvencionalnim pretvornikom energije. Da bi zadovoljile pričakovanja končnih uporabnikov in postale tržno zanimive, je potrebno izboljšati vzdržljivost in zanesljivost njihovega delovanja. Spremljanje stanja (CM, ang. condition monitoring) gorivnih celic PEM je prepoznano kot eno izmed orodij, ki so potrebna za izboljšanje zmogljivosti in učinkovitosti delovanja sistemov z gorivnimi celicami PEM.

Ta disertacija obravnava problem zanesljivega spremljanja stanja gorivnih celic PEM. V ta namen je predstavljena nova metodologija, ki opredeljuje vsak korak spremljanja stanja od začetnega zajema signalov do končnega izhoda v obliki brez-enotskega kazalnika stanja (CI, ang. condition indicator). Razvita metodologija temelji na metodi elektrokemijske impedančne spektroskopije (EIS, ang. electrochemical impedance spectroscopy).

Konvencionalna metoda EIS temelji na vzbujanju gorivne celice z nizom sinusnih signalov različnih frekvenc in izračunu pripadajočih točk impedančne krivulje. V disertaciji predstavljeni postopek se od konvencionalnega razlikuje v uporabi frekvenčno bogatega vzbujalnega signala in obravnavanju impedance kot kompleksne naključne spremenljivke. Vzbujalni signal ima obliko psevdonaključnega binarnega zaporedja (PRBS, ang. pseudo-random binary sequence). Uporaba signala PRBS pripomore k znatnemu skrajšanju časa, potrebnega za izvedbo postopka ocene impedance, ki je še posebej pomemben v sistemih za sprotni nadzor stanja. Z namenom doseganja visoke frekvenčno-časovne ločljivosti impedančne ocene je za obdelavo signalov uporabljena zvezna valčna transformacija (CWT, ang. continuous wavelet transform) z Morletovim valčkom. Statistične lastnosti signal PRBS in lastnosti CWT omogočajo obravnavo impedance pri določeni frekvenci kot kompleksne naključne spremenljivke. To pa omogoča natančno določanje odločitvenih meja sistema za spremljanje stanja kot tudi združevanje informacije v končni CI. Dva pomembna inženirska vidika utemeljujeta prednost takšnega pristopa. Prvič, pri prvem zagonu sistema ali po vzdrževalnem posegu zahteva nastavljanje izhodiščnih odločitvenih meja sistema za spremljanje stanja le podatke, pridobljene ob normalnem delovanju celic, in vrednost še sprejemljive verjetnosti lažnega alarma. In drugič, izhod sistema za spremljanje stanja je brez-enotski CI, ki na preprost način popisuje trenutno stanje gorivnih celic PEM.

Predstavljena sta tudi zasnovana 90 kanalni merilnik napetosti za gorivne celice (FCVM, ang. fuel cell voltage monitor) in enosmerni v enosmerni (DC-DC, ang. direct-current-to-direct-current) pretvornik. Medsebojno povezana FCVM in DC-DC pretvornik ter algoritem za spremljanje stanja tvorijo vgrajeni sistem za spremljanje stanja gorivnih celic PEM. Sistem omogoča hkratno vzbujanje sistema z gorivnimi celicami in zajem meritev, potrebnih za hitro oceno impedance. Sistem je cenovno primeren za komercialno uporabo in hkrati dovolj natančen za opravljanje zahtevanih meritev za namen spremljanja stanja.

Celotna predlagana rešitev za spremljanje stanja je bila testirana na komercialnem sistemu z gorivnimi celicami PEM. Za validacijo metodologije so bile v sistemu izzvane napake v obliki poplavljanja gorivnih celic in izsuševanja membran PEM, ki so bile z vrednostjo kazalnika CI uspešno zaznane.

Contents

List of Figures **xv**

List of Tables **xvii**

List of Listings **xix**

Abbreviations **xxi**

1 Introduction **1**
1.1 Brief Background of Condition Monitoring 3
1.2 Aim and Goals 4
1.3 Hypotheses 4
1.4 Scientific Contributions 5
1.5 Structure of the Dissertation 6

2 Fast Impedance Estimation **9**

3 Optimal Selection of Condition Monitoring Thresholds **19**

4 PEM Fuel Cell Condition Indicator **29**

5 Embedded Condition Monitoring System **39**

6 Conclusions **53**

Appendix A Matlab Code for Fast Impedance Estimation **57**

References **63**

Bibliography **73**

Biography **77**

List of Figures

Figure 1.1: A mind map of the connection among the scientific contributions and the underlying concepts. 7

Figure 2.1: Power speallows anctrum of the PRBS signal. 13
Figure 2.2: Cone of influence for the Morlet wavelet with edge e. 14
Figure 2.3: Block diagram of the experimental setup. 14
Figure 2.4: Top and side view of the FCVM connected to the fuel cell stack consisted of 80 PEM fuel cells. 14
Figure 2.5: Sampling frequency f_s of applied PRBS signals and utilized central frequencies ω_0 of complex Morlet wavelet in relation to frequency scale $f = [0.1\ \ 500]$ Hz. 15
Figure 2.6: Measured current and voltage signals during the experiment. 15
Figure 2.7: Bode plot of the measured PEM fuel cell impedance. 16
Figure 2.8: Nyquist plot of the measured PEM fuel cell impedance. 16

Figure 3.1: Graphical presentation of the complex Gaussian circularity of PRBS's frequency components. 20
Figure 3.2: Representation of fuel cell system excited by current and affected by disturbances. 22
Figure 3.3: Contour plot of the probability density function (3.8) for $\rho = 1/2 + j1/4$. 23
Figure 3.4: Probability distribution functions of particular impedance components. 23
Figure 3.5: Block diagram of the experimental setup. 25
Figure 3.6: Top and side view of the FCVM connected to an 8.5 kW PEM fuel cell system. 25
Figure 3.7: Measured current and voltage signals during the experiment. 25
Figure 3.8: Trend of impedance components throughout the experiment. 26
Figure 3.9: Trend of CI of $|Z|$ throughout the experiment. 26

Figure 4.1: Schematic representation of the complete condition monitoring process. 33
Figure 4.2: Regions of best performance for different Archimedean copulas. 35
Figure 4.3: Fully nested Archimedean copula. 35
Figure 4.4: Nyquist plot of the PEM fuel cell impedance. 35
Figure 4.5: Measurement sequences in time. 36
Figure 4.6: Description of the regions for high and low copula outputs. 36
Figure 4.7: Example of current and voltage signals during the experiment. 36
Figure 4.8: Evolution of the health index (copula output). 37

Figure 5.1: Block diagram of a PEM fuel cell power system. 41
Figure 5.2: Assembly of three DC-DC converter modules paralleled together providing 5 kW of power conversion capability. 43
Figure 5.3: Block diagram of the DC-DC module. 43
Figure 5.4: Power output stage of the current-mode DC-DC converter. 43

Figure 5.5: Key waveforms of the DC-DC converter operating at two different input voltages U_{in} and the same output current I_{out}. 44
Figure 5.6: FCVM connected to an 8.5 kW PEM fuel cell system Hydrogenics HyPM-HD 8-200. 45
Figure 5.7: Floating power supply scheme, which allows an industry-standard multiplexer to operate in floating mode. 45
Figure 5.8: Connection of two industry-standard multiplexers to measure up to 30 fuel cell leads in order to reduce componentcount. 45
Figure 5.9: Block diagram of the FCVM. 46
Figure 5.10: Connection scheme between the FCVM and the DC-DC converter for online CM. 46
Figure 5.11: Probability distribution function of $|Z|$ at 157 Hz. 47
Figure 5.12: Example of acquired current and voltage signals. 49
Figure 5.13: Trend of $|Z|$ at 157 Hz throughout the experiment. 49
Figure 5.14: Trend of the CI throughout the experiment. 50

Figure A.1: An impedance characteristic from 50 mHz to 20 kHz – the output of the publicly available package. 62

List of Tables

Table 4.1: Archimedean copulas. 34

List of Listings

Listing A.1: `compute_impedance.m` Matlab script. 57
Listing A.2: `fc_impedance_cwtft.m` Matlab script. 60

Abbreviations

CDF	...	cumulative distribution function
CI	...	condition indicator
CM	...	condition monitoring
CWT	...	continuous wavelet transform
DC-DC	...	direct-current-to-direct-current
EIS	...	electrochemical impedance spectroscopy
FCVM	...	fuel cell voltage monitor
FFT	...	fast Fourier transform
FNAC	...	fully nested Archimedean copula
HI	...	health indicator
NFRA	...	non-linear frequency response analysis
PDF	...	probability density function
PEM	...	proton exchange membrane
PFA	...	probability of false alarm
PRBS	...	pseudorandom binary sequence

Chapter 1

Introduction

The increasing energy demand, together with the ecological concerns related to the conventional electric energy production, is pushing science to search for alternatives. A hydrogen fuel cell with the proton exchange membrane (PEM) (Barbir, 2005; Sadiq Al-Baghdadi, 2013) presents a potential alternative to the existing energy conversion devices (i.e., internal combustion engine, thermal power station, etc.). A PEM fuel cell is an electrochemical device that converts the chemical energy of hydrogen directly into electrical energy. In the commercially available PEM fuel cell-based power systems, the net efficiency of the chemical-to-electrical energy conversion at nominal output power varies between 45 to 60%, which is substantially higher compared to the conventional energy converting devices. In addition to the high conversion efficiency, a PEM fuel cell-based power system generates no greenhouse gases and emits only low level noise. The PEM fuel cells are considered as the most appropriate for utilisation in the transportation and stationary applications of up to 100 kW of power. Features that make PEM fuel cells usable in such a wide range of applications are low temperature of operation, the ability to use oxygen from the air, short start-up and shut-down time, and high power density (Barbir, 2005).

The success of the large-scale market penetration of PEM fuel cell technology depends on the durability and reliability of the technology on the one hand, and on the reduction in costs of production, operation, and maintenance on the other hand (de Bruijn, Dam, & Janssen, 2008; Schmittinger & Vahidi, 2008; J. Wu, Yuan, Martin, et al., 2008). For instance, the US Department of Energy has put a set of requirements according to which the fuel cells for automotive applications will need to have a durability of 5,000 hours at a cost of €25/kW, and stationary fuel cell systems will require about 60,000 to 80,000-hour durability at a cost of about €800/kW to €1,200/kW ("The Department of Energy Hydrogen and Fuel Cells Program Plan," 2011). At the time being, the PEM fuel cell technology is close to being competitive. However, a major hurdle to reach a high commercialisation level of PEM fuel cell power system remains their relatively low reliability of operation and insufficient lifetime outside the laboratory environment.

There are several phenomena that affect PEM fuel cell condition (Wilkinson & St-Pierre, 2010) of which most notable are as follows:

- Corrosion of the electrodes and the degradation of the catalyst and membranes (Ciureanu, 2004; R. L. Borup, Davey, Garzon, Wood, & Inbody, 2006; Lee et al., 2006; B. Wu et al., 2014).
- The carbon monoxide poisoning of the catalyst and the contamination of the PEMs with sulphur, which are irreversible processes (Le Canut, Abouatallah, & Harrington, 2006; Farrell, Gardner, & Ternan, 2007; W.-M. Yan et al., 2009; Sethuraman & Weidner, 2010).

- High temperatures induce membrane drying, which result in decreased conducting characteristics of the membranes. On the other side, the PEM fuel cells are sensitive to the sub-zero temperatures, which lead to freezing and destruction of the membranes (Schmittinger & Vahidi, 2008; Q. Yan, Toghiani, Lee, Liang, & Causey, 2006).

Studies have also shown that the durability and reliability of a PEM fuel cell is also vitally affected by water management faults (Ciureanu, 2004; Yi, Yang, & King, 2004; Mulyazmi, Daud, Majlan, & Rosli, 2013). A precise balance of liquid water and water vapour inside a fuel cell needs to be maintained to ensure the optimal performance. Inadequate water balance directly affects the cell's performance:

- Insufficient removal of produced water at the cathode side of a PEM fuel cell leads to flooding of the gas-diffusion layer and gas channels. In normal operation, the most of the produced water is evaporated and carried away by oxidant stream, and the rest is consumed for humidification of a PEM. If the water removal is not sufficient, water starts to condense in the pores of the gas diffusion layer and in the gas channels, where the water droplets prevent the diffusion of oxygen to the reaction site. The result of fuel cell flooding is loss of voltage potential due to shortage of the reactant gases.

- An excessive water removal or too dry inlet gases cause membrane drying. Typically, the PEM membranes are made of perfluorocarbon-sulphonic acid ionomer. The SO_3^- group in the side chain of the ionomer is an SO_3^- ion with an H^+ ion. The SO_3^- group is extremely hydrophilic and when the membrane is properly hydrated, the hydrated regions around the SO_3^- groups conduct protons H^+. If the inlet gas streams are too dry, or if the operating temperature of a fuel cell is too high, water evaporates from the PEM, and is removed from the fuel cell by the gas stream. In this case drying of the membrane occurs, which decreases proton conductivity of the membrane and cell voltage potential.

An effectual handling of the water management faults and the contamination processes is an important underlying research problem to be solved in order to promote more intensive deployment of the PEM fuel cell technology to the market. A way to reduce the impact of these faults on the durability and reliability of PEM fuel cells is through the employment of advanced diagnostic approaches. In a broader sense, this dissertation addresses the condition monitoring (CM) for PEM fuel cells, where the focal point of the research are the water management faults.

Generally, the aforelisted faults, which occur in PEM fuel cells, cannot be detected and evaluated by direct measurements. Therefore, advanced diagnostic methods have to be applied for this task, allowing detection of faults in the incipient stage. This will enable the (supervisory) control system to react in a way to recover the fuel cell system from faulty operation, thus avoiding any irreversible damage or to prepare an appropriate maintenance procedure. Moreover, an upgrade of diagnostics with the prognostics information can be exploited for the appropriate maintenance planning. Consequently, a higher reliability of operation, increased durability and life time of the overall system, and better maintenance planning should be achieved.

1.1 Brief Background of Condition Monitoring

According to Isermann and Ballé (1997), the CM is defined as follows:

> *"A continuous real-time task of determining the conditions of a physical system, by recording information, recognising and indicating anomalies in the behaviour".*

The condition of a PEM fuel can be determined through various diagnosis approaches. In general, these approaches can be applied before or after assembly of a fuel cell, or can be performed online (during the operation of a fuel cell). Only a subset of basic diagnostic approaches have the potential of being successfully adjusted and applied outside the laboratory environment on the industry-grade PEM fuel cell systems. These approaches include:

- polarisation curve,
- current interrupt, and
- electrochemical impedance spectroscopy (EIS).

To obtain a polarisation curve of a fuel cell, its load current is gradually increased from open circuit to short circuit current (or decreased in the opposite direction). Meanwhile, the load current and the corresponding voltage response of the fuel cell are measured. The polarisation curve-based diagnostics is done by fitting the measured voltage and current data to the equations describing the polarisation curve. The complexity and effectiveness of the method are directly linked to the complexity of the presumed equations of the curve. Simple equations go along with simpler fitting methods that produce little, but robust information. On the other hand, complex equations request powerful fitting methods, which in turn result in more information on the account of higher uncertainty of the estimated parameter values. The final result of the diagnostic method gives insight into the parameters of the fuel cell under test (i.e., reversible cell potential, cell resistance, etc.). A change in value of a particular parameter can be interpreted as an indication of the presence of a fault. However, the impact on the polarisation curve is similar regardless of the type of fault. Therefore, the method can only detect the presence of faults, but fails to distinguish among them. Moreover, the method is very intrusive because it requires time-consuming measurement at currents of entire operation region. This makes the method unsuitable for many of out-of-laboratory fuel cell applications, where changing the load current of a fuel cell during operation is not desirable, or it is even impossible.

In terms of invasivity and ability to distinguish among different kinds of faults, the current interrupt method performs better compared to the one based on the polarisation curve (Büchi, Marek, & Scherer, 1995; Rubio, Urquia, & Dormido, 2010). The acquisition of the required measurements takes place in a short time window, when the load current of the fuel cell is interrupted for a few milliseconds. The measured data is fitted to the presumed equivalent circuit model in order to obtain values of the circuit parameters, which are differently affected by different kind of faults. The current interrupt method is proved to be a powerful diagnostic tool that provides insight into the fuel cell parameters. As such, it can diagnose different faulty conditions. Its main limitations include the need for extremely precise measurement of the current and voltage following the interruption, which implies sophisticated and costly measurement equipment.

The EIS is a diagnostic method used in various fields of electrochemistry (Yuan, Sons, Wang, & Zhang, 2010). An electrochemical device involves many electrochemical, transportation, thermodynamic and electric processes and physical parameters. In most cases,

the contributions of these factors overlap and consequently make analysis nearly impossible. However, the power of the EIS involves the capability to recognise and to analyse all the involved processes. The EIS method has already been applied to PEM fuel cells as a diagnostic tool and has been proven as effective (Yuan, Wang, Sun, & Zhang, 2007). In comparison to other diagnostic methods, the EIS is less invasive, is able to distinguish among fuel cell flooding, membrane drying, poisoning of the catalyst, sulphur contamination, and enables monitoring of the fuel cell ageing. Moreover, it can be performed during operation of the fuel cell with acceptable amount of perturbation. It is a so-called *active* diagnostic approach which relies on using probing signals.

Although the EIS-based diagnostic concept for PEM fuel cells is known and thoroughly researched, it is not yet at a point of maturity to be fully introduced into industrial-grade applications. Research is mainly concentrated on the development of model-based diagnosis methodologies, whereas the acquisition and processing of the signals is getting only negligible attention since researchers are using dedicated data acquisition laboratory equipment. The equipment utilises basic measurement principles, resulting in precise yet unacceptable long and over-intrusive measurements. Furthermore, at this stage the measurement equipment is bulky and prohibitively costly for the industrial applications. Also, an improvement in the segment of data acquisition should pave the way for the diffusion of the EIS-based diagnostics into the PEM fuel cell systems outside the laboratory environment.

1.2 Aim and Goals

The aim of this dissertation is to provide new concepts and methodologies in order to raise reliability of operation and longevity of PEM fuel cell systems by relying on EIS-oriented CM. In line with the aim, the dissertation is foreseen to meet the following goals:

- to derive an approach for time efficient estimation of the impedance characteristic of PEM fuel cells with possibly no interruptions of the regular operation,
- to develop algorithms for EIS-based fault detection of water management faults in PEM fuel cells,
- to propose an overall condition indicator (CI) for PEM fuel cells that reflects the condition of the cells,
- to design an embedded low-cost CM system for PEM fuel cell power systems,
- to evaluate the designed CM system and the proposed methodology on laboratory test runs.

1.3 Hypotheses

The hypotheses of this dissertation are as follows.

Hypothesis 1. Compared to the conventional approaches, a more time-efficient estimation of a PEM fuel cell impedance characteristic is achievable by utilising frequency-rich excitation signal and advanced signal processing tools.

Hypothesis 2. The decision thresholds of a CM algorithm are attainable based solely on the data collected from the fuel cell under normal (i.e., fault-free) operation.

Hypothesis 3. Since the information about the fuel cell condition is incorporated in its impedance characteristic, a unit-free CI should be constructed from that impedance information.

1.4 Scientific Contributions

The research work and findings presented within this dissertation mainly contribute to the field of CM of PEM fuel cells. Partly, the work also adds to the field of electrochemical energy systems in general. The original scientific contributions are as follows.

An approach for fast impedance estimation

Published in: Debenjak, A., Boškoski, P., Musizza, B., Petrovčič, J., & Juričić, Đ. (2014). Fast measurement of proton exchange membrane fuel cell impedance based on pseudo-random binary sequence perturbation signals and continuous wavelet transform. *Journal of Power Sources*, *254*, 112–118. doi:10.1016/j.jpowsour.2013.12.094

The approach enables a fast estimation of the impedance characteristic of a PEM fuel cell, where the impedance estimates exhibit a high time-frequency resolution. It covers all the required elements from the experiment design phase to the final estimate of the impedance. It proposes an unconventional waveform for the perturbation signal and advanced tools for the signal processing. To estimate the impedance characteristic of a PEM fuel cell, a small amplitude signal of the pseudorandom binary sequence (PRBS) waveform is superimposed to the load current of the cell. This current perturbation signal excites the fuel cell over wide frequency band, thus enabling shorter data acquisition time. During the perturbation, the current (i.e., perturbation) and voltage (i.e., response) signals are acquired and further processed. Finally, the impedance estimate is obtained by applying the continuous wavelet transform (CWT) with the Morlet mother wavelet. Although the approach has been designed for the impedance estimation of PEM fuel cells, it has been proven to be applicable to any type of electrochemical cell.

A method for optimal selection of condition monitoring thresholds

Published in: Boškoski, P. & Debenjak, A. (2014). Optimal selection of proton exchange membrane fuel cell condition monitoring thresholds. *Journal of Power Sources*, *268*, 692–699. doi:10.1016/j.jpowsour.2014.06.110

The method offers an analytic solution to the problem of tuning the threshold values of an EIS-based diagnostic system for the PEM fuel cells. It builds on the proposed concept, according to which the impedance at individual frequency is regarded as a complex random variable. The complex probability density functions (PDFs) of the cell impedance is the ratio distribution of the CWT coefficients of the voltage response and current excitation signals. The decision thresholds are determined based on the cumulative distribution function (CDF) of the impedance amplitude and the value of the predetermined probability of false alarm (PFA). To determine the initial optimal threshold values, the method requires solely the operational data on the PEM fuel cell in the nominal state of operation (i.e., no characteristic data about the operation under faulty conditions) and the level of PFA.

A unit-free condition indicator

Published in: Mileva Boshkoska, B., Boškoski, P., Debenjak, A., & Juričić, Đ. (2015). Dependence among complex random variables as a fuel cell condition indicator. *Journal of Power Sources*, *284*, 566–573. doi:10.1016/j.jpowsour.2015.03.044

The CI for fault detection in PEM fuel cells is constructed from a set of fuel cell impedance values at a number of frequencies. Since the fuel cell condition (i.e., faults) affects the impedance over a broad frequency range, the complex impedance values at individual frequencies are treated as dependent complex random variables. The information about PEM fuel cell condition is incorporated into the dependence

structure of these variables and is described through the corresponding joint CDF by employing copula functions. As the copula function, constructed in such a way, itself is a CDF, its output is a probability of observing a particular fuel cell impedance characteristic. Therefore, the copula output is regarded as an overall unit-free CI describing the overall PEM fuel cell condition.

A condition monitoring system for PEM fuel cells

Published in: Debenjak, A., Petrovčič, J., Boškoski, P., Musizza, B., & Juričić, Đ. (2015). Fuel cell condition monitoring system based on interconnected DC-DC converter and voltage monitor. *IEEE Transactions on Industrial Electronics*, *62*(8), 1–13. doi:10.1109/TIE.2015.2434792

The system is an embedded solution for the CM of PEM fuel cell power systems. It consists of a modular direct-current-to-direct-current (DC-DC) converter and a 90-channel fuel cell voltage monitor (FCVM). The DC-DC converter, interconnected with the FCVM, forms a self-sufficient diagnostic system capable of performing various diagnostic tasks. In addition to its basic functionality (i.e., power conditioning), the DC-DC also performs diagnostic probing of fuel cells by injecting current excitation signals. On the other side, the FCVM acquires precise measurement of the current and voltage signals of all individual cells in the fuel cell stack. The embedded diagnostic algorithms, which are executed on the FCVM, process the acquired signals and provide online CM information. Besides its present functionality, the system hardware represents a solid base for further diagnostic algorithm development and evaluation.

1.5 Structure of the Dissertation

The structure of the dissertation goes in line with the listed scientific contributions. Accordingly, Chapters 2 through 5 include published journal articles, each covering the individual contribution. Figure 1.1 shows the connections among all the scientific contributions and the conceived underlying concepts in the form of a mind map.

Chapter 2 covers the approach for fast impedance estimation of a PEM fuel cell (Debenjak et al., 2014). Chapter 3 introduces the concept of treating the impedance at individual frequency as a complex random variable. Furthermore, the method for optimal selection of condition monitoring thresholds is laid out, which builds on the complex random variable concept (Boškoski & Debenjak, 2014). Chapter 4 deals with the construction and evaluation of the unit-free CI for PEM fuel cells (Mileva Boshkoska et al., 2015). Chapter 5 presents the designed embedded CM system for PEM fuel cell power systems (Debenjak et al., 2015). Finally, Chapter 6 summarises the research findings, provides some suggestions for the further work, and concludes the dissertation.

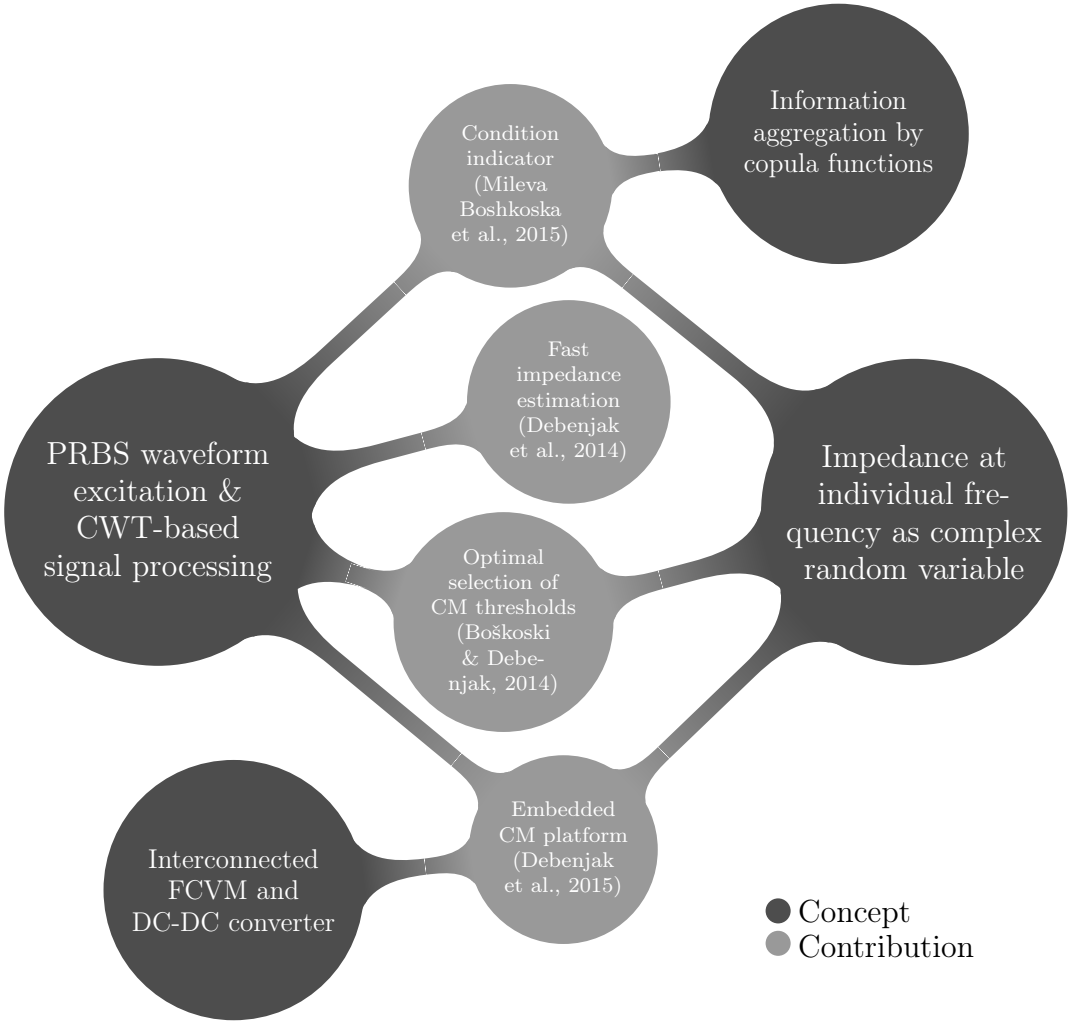


Figure 1.1: A mind map of the connection among the scientific contributions and the underlying concepts.

Chapter 2

Fast Impedance Estimation

The conventional EIS approach utilises the sine waveform as a perturbation signal (i.e., single-sine approach) (Yuan et al., 2010). In order to measure the impedance in a frequency range of interest Ω, the procedure of applying the sine perturbation at a frequency ω_i ($\omega_i \in \Omega$) has to be repeated multiple times. On the one hand, the single-sine approach exhibits high accuracy, since at each particular measurement i, all the energy of the perturbation signal is condensed at the frequency ω_i. But on the other hand, measurements required by the approach are inherently time-consuming.

To compute the impedance of a fuel cell from the voltage and current signals, the signals have to be transformed into the frequency domain. Commonly, the transformation is performed by the fast Fourier transform (FFT) that implies inflexible time-frequency resolution, which is especially unsuitable at low frequencies.

Such an approach is time-consuming and in some cases even inappropriate for online CM of industrial PEM fuel cell power systems. To speed up the required probing time and to minimise the intrusion into the operation of a system, a time efficient approach for estimation of the fuel cell impedance was conceived. The proposed approach employs the PRBS waveform as a perturbation signal and the impedance is estimated by utilising the CWT with the Morlet mother wavelet.

The main advantage of the PRBS approach, compared to the conventional one, is a shorter probing time. To estimate the frequency characteristic of a fuel cell in a frequency band from 0.1 Hz to 500 Hz, the required probing time is 60 s. For comparison, Fouquet, Doulet, Nouillant, Dauphin-Tanguy, and Ould-Bouamama (2006) who used conventional single-sine approach, reported approximately 5 min long measurements required to estimate the impedance characteristic in a comparable frequency band.

The length of the probing time is tightly linked to the lower frequency limit of the frequency band. Only a slightly higher limit significantly shortens the required probing time. Additionally, as the PEM fuel cell is perturbed by a broadband PRBS signal and the CWT is utilised for the signal processing, the value of the impedance can be computed at any frequency of interest only by an adjustment of the algorithm parameters.

The approach also addresses the selection of parameter values of the PRBS signal (i.e., order n, sampling period Δt, and amplitude a) and of the CWT with the Morlet mother wavelet (i.e., length of the signals, central frequency ω_0, cone of influence e[1]) that have a significant influence on the effectiveness and accuracy of the proposed approach. With

[1]The cone of influence is rather a consequence than a direct parameter of the CWT. However, it is addressed because if not handled carefully, it has a significantly negative effect on the quality of the final results. The cone of influence for the Morlet mother wavelet is presented in Figure 2.2. Note that the naming *cone* refers to the shape of influenced area's edge in case of logarithmic y-axis. Since the y-axis in Figure 2.2 is linear, the shape of cone is somehow deformed.

properly tuned parameters, the approach provides fast and reliable impedance estimates along the entire frequency band. Additionally, it yields the statistical information about the confidence interval of the impedance estimates.

An attention is also given to the computationally efficient implementation of the CWT algorithms. Since the frequency-domain representation of the Morlet wavelet exists in a closed form, the required time-domain convolution can be efficiently conducted in the frequency-domain as a multiplication. This implies significant practical advantage for the implementation of online EIS-based fault detection and diagnostics, where the computation resources are limited.

Although the approach has been designed for the impedance estimation of PEM fuel cells, it is applicable to any type of electrochemical cell. For instance, Figure A.1 shows the impedance characteristic of a lithium-sulphur battery. The measurements required to estimate the impedance from the Figure A.1 were conducted on a laboratory-grade lithium-sulphur battery and processed according to the fast impedance estimation approach. The figure is the output of the publicly available package that includes the Matlab code for the fast impedance estimation and the sample dataset. The Matlab code is listed in the Appendix A.

This chapter includes the following publication:
Debenjak, A., Boškoski, P., Musizza, B., Petrovčič, J., & Juričić, Đ. (2014). Fast measurement of proton exchange membrane fuel cell impedance based on pseudo-random binary sequence perturbation signals and continuous wavelet transform. *Journal of Power Sources*, *254*, 112–118. doi:10.1016/j.jpowsour.2013.12.094

Journal of Power Sources 254 (2014) 112–118

Contents lists available at ScienceDirect

Journal of Power Sources

journal homepage: www.elsevier.com/locate/jpowsour

Fast measurement of proton exchange membrane fuel cell impedance based on pseudo-random binary sequence perturbation signals and continuous wavelet transform

Andrej Debenjak [a,*], Pavle Boškoski [a], Bojan Musizza [a], Janko Petrovčič [a,b], Đani Juričić [a]

[a] Jožef Stefan Institute, Department of Systems and Control, Jamova cesta 39, 1000 Ljubljana, Slovenia
[b] Centre of Excellence for Low-carbon Technologies – CO NOT, Hajdrihova 19, 1000 Ljubljana, Slovenia

HIGHLIGHTS

- A new approach to the estimation of PEM fuel cell impedance is proposed.
- The approach employees PRBS waveform as perturbation signals.
- The impedance characteristic is computed based on continuous wavelet transform.
- Guidance for optimal parameter selection is presented.
- The impedance characteristic of a PEM fuel cell is obtained in 60 seconds.

ARTICLE INFO

Article history:
Received 29 August 2013
Received in revised form
9 December 2013
Accepted 17 December 2013
Available online 30 December 2013

Keywords:
PEM fuel cell
Impedance characteristic
Electrochemical impedance spectroscopy
Pseudo-random binary sequence
Continuous wavelet transform
Morlet wavelet

ABSTRACT

This paper proposes an approach to the estimation of PEM fuel cell impedance by utilizing pseudo-random binary sequence as a perturbation signal and continuous wavelet transform with Morlet mother wavelet. With the approach, the impedance characteristic in the frequency band from 0.1 Hz to 500 Hz is identified in 60 seconds, approximately five times faster compared to the conventional single-sine approach. The proposed approach was experimentally evaluated on a single PEM fuel cell of a larger fuel cell stack. The quality of the results remains at the same level compared to the single-sine approach.
© 2013 Elsevier B.V. All rights reserved.

1. Introduction

Electrochemical Impedance Spectroscopy (EIS) is a widely adopted method for the characterization and diagnostics of Proton Exchange Membrane (PEM) fuel cells. Its use is comprehensively covered in reviews [1–4]. Nowadays, for the purpose of the EIS, the impedance characteristic is measured at a fixed operating point defined by current I_{DC}. To perturb the cells, small-amplitude sinusoidal perturbations with frequencies $\omega \in \Omega$ are applied [5]. Assuming linearity of the fuel cell dynamics around the operating point I_{DC}, the fuel cell responds with sinusoid voltage change with the same frequency ω and particular amplitude and phase. From these signals one can compute the fuel cell impedance at the frequency ω. In order to cover the whole desired frequency range Ω one has to repeat the same procedure multiple of times. Such an approach can be time consuming and in some cases even inappropriate for on-line monitoring of operational fuel cell system. Therefore, to speed up the experiment with minimal intrusion into system's operation, a new time efficient approach for measurement of impedance characteristic is proposed in this paper. The method uses Pseudo-Random Binary Sequence (PRBS) as perturbation signal and the impedance is estimated using continuous wavelet transform (CWT) with Morlet mother wavelet.

With currently adopted single-sine perturbation approach, the impedance plot of a fuel cell is constructed at discrete frequencies. The approach provides precise impedance estimates because all the

* Corresponding author.
E-mail address: andrej.debenjak@ijs.si (A. Debenjak).

0378-7753/$ – see front matter © 2013 Elsevier B.V. All rights reserved.
http://dx.doi.org/10.1016/j.jpowsour.2013.12.094

energy of the perturbation signal is condensed at one frequency only, as such enabling maximal perturbation at this frequency at the expense of long execution time period of the measurements. Despite the obvious deficiencies, the approach has been employed by the majority of authors. For instance Fouquet et al. [6] used the EIS based methodology to monitor the state-of-health of a PEM fuel cell, estimating the impedance at frequencies ranging from 0.1 Hz to 1 kHz with 10 frequency points per decade. Reportedly, one frequency sweep took approximately 5 minutes to complete. Similarly, Le Canut et al. [7] successfully detected water management faults and catalyst poisoning occurrence by examining the impedance in a higher frequency band from 1 Hz to 10 kHz, where one full measurement sweep took approximately 3 minutes. Long measurement times lead to the problems associated with low-frequency stability and non-linearity of a fuel cell. Additionally, from a practical point of view, such time consuming measurements make this approach inadequate for on-line industrial applications.

Some attempts to reduce the required time of impedance measurement have already been made. Brunetto et al. [8] proposed a multi-sine approach, where the fuel cell under test is perturbed with a signal composed of multiple sinusoids, hence economizing the required measurement time. In the work of Wasterlain et al. [9], the authors clearly exposed the idea of employing multi-sine signals in their further work, even though the single-sine approach was used in the work. In spite of the fact that the multi-sine approach shortens the required time period for the EIS measurements, the approach is not widely adopted. One possible reason might be that time reduction is not significant enough to justify additional complexity of measurement equipment and computation.

Addressing the issues of time consuming measurements and complexity of measurement equipment, this paper presents a novel approach for fast measurement of the PEM fuel cell impedance for the EIS purposes. The proposed approach utilizes PRBS as a perturbation signal. The PRBS is well-established perturbation signal in the field of system identification since it has suitable white-noise-like spectral properties in a predefined frequency band [10]. However, to the best of the authors knowledge PRBS has been neglected for EIS impedance measurements in the context of fuel cell diagnostics. Recently published study by Boghani et al. [11] is the nearest available study to the field of "conventional" fuel cells that uses the PRBS system identification concept. In their study, the PRBS was utilized together with step waveform to analyse performance of a microbial fuel cell by measuring the time constant and steady-state gain of a predefined first order model over the operation range of a cell. In the same manner, Fairweather et al. [12] employed a very low frequency PRBS in order to estimate model parameters of a valve-regulated lead-acid batteries affected by operational temperature. Unlike these studies, the novel approach presented in this paper deals with measuring the impedance characteristic in a frequency band from 0.1 Hz to 500 Hz and it is not limited or predefined by any linear or non-linear model.

The main advantage of the proposed PRBS approach compared to the single-sine and multi-sine ones is a shorter time period required for the measurements. In the case of 0.1 Hz–500 Hz frequency band, the measurements take 60 seconds to complete. The length of measurement time is tightly linked to the lower frequency limit of the frequency band, therefore only slightly higher limit (e.g. 0.5 Hz instead of 0.1 Hz) significantly shortens the required measurement time period. Additionally, as the cell is perturbed by the broadband signal, the value of impedance can be computed at any frequency of interest just with properly adjusted parameters of the computational algorithm.

In the case of sinusoid waveform signals, the Fourier transform is applied to transform the signals into frequency domain [8,13]. However, when using broad-band random signals such as PRBS, it is preferred to perform time-frequency analysis for the impedance computation. One approach is the application of Short-time Fourier transform or wavelet transform. The former one suffers from fixed time-frequency resolution, whereas the latter one allows flexibility in the time–frequency resolution by achieving good time resolution for high-frequency events, and good frequency resolution for low-frequency event. Therefore, in this study CWT approach based on the Morlet mother wavelet was employed for impedance computation. With properly tuned CWT parameters, this approach provides reliable impedance results along the entire frequency band. Additionally, it yields statistical information about confidence interval of the impedance measurement.

The wavelet transform is widely used tool in a variety of scientific fields ranging from diagnostics of human cardiovascular systems [14] and analysis of life signals in mammals [15] to fault detection in mechanical drives [16]. In the field of PEM fuel cell diagnostics, Steiner et al. [17] used discrete wavelet transform to diagnose PEM fuel cell flooding directly from the voltage signals. The flooding was diagnosed based on the pattern of the wavelet packet coefficients derived with the wavelet packet transform.

The paper also addresses the problem of proper parameter selection of both PRBS and CWT with the Morlet wavelet, which has significant influence on the effectiveness of the proposed approach. Special attention is given to the computationally efficient implementation of the algorithms which brings significant practical advantages in implementation of on-line EIS based diagnostic systems. Finally, the paper presents experimental results, where the PRBS approach was applied to a commercial PEM fuel cell system. The PEM fuel cell impedance results acquired using the PRBS approach are thoroughly discussed. The impedance characteristic measured with use of PRBS perturbation signal is compared to the reference impedance characteristic obtained by standard single-sine approach.

2. Pseudo-Random Binary Sequence

According to Ljung [10], PRBS is a periodic and deterministic signal with white-noise-like properties. As such, it is highly appropriate as an input test signal for system identification purposes. The maximum length PRBS can be generated by employing feedback shift registers [18,19]. The maximum length PRBS is characterized by its order n, the maximum length period N, amplitude a and its sampling period Δt. The order n determines the maximum length period N (number of discrete points in time, when the PRBS signal can change its value):

$$N = 2^n - 1 \tag{1}$$

The discrete power spectrum density Φ of maximum length PRBS signal with amplitude a and length N is [19]:

$$\Phi^{\mathrm{d}}(m) = \begin{cases} \frac{a^2}{N} & m = 0 \\ \frac{a^2(N+1)}{N} & 0 < m < N \end{cases} \tag{2}$$

Therefore, the power spectrum of periodical PRBS with period N and sampling period Δt is:

$$\Phi^{\mathrm{p}}\left(m\frac{2\pi}{N\Delta t}\right) = \frac{1}{N}\Phi^{\mathrm{d}}(m)\left|\frac{\sin\frac{m\pi}{N}}{\frac{m\pi}{N}}\right|^2 \tag{3}$$

Fig. 1 resembles the power spectrum of the PRBS signal given by the Equation (3). It can be seen, that the value of the power spectrum hits zero exactly at integer multiples of sampling frequency f_s, which is related to the sampling period Δt as follows:

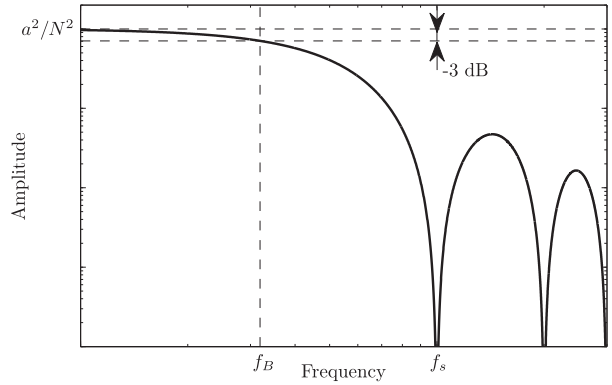


Fig. 1. Power spectrum of the PRBS signal.

$$f_s = \frac{1}{\Delta t} \tag{4}$$

However, the system under test has to be sufficiently perturbed, therefore the useful frequency band is determined by −3 dB frequency limit. In this way, the useful frequency band f_B is approximately determined as:

$$f_B = \frac{1}{3} f_s \tag{5}$$

3. Continuous wavelet transform

The application of Fourier transform is suitable for roughly stated smooth periodic signals. However for signals describing transient phenomena, located in a narrow time interval, the application of Fourier transform turns to be inadequate. Moreover, the Fourier transform performs poorly at lower frequencies.

Wavelet transform is based on a set of specifically designed functions called wavelets. The continuous wavelet transform (CWT) of a square integrable function $f(t) \in \mathbf{L}^2(\mathbb{R})$ is defined as [20]:

$$Wf(s,u) = \langle f(t), \psi_{u,s}(t) \rangle = \int_{-\infty}^{\infty} f(t) \psi_{u,s}^*(t) dt, \tag{6}$$

where $\psi_{u,s}(t)$ is a scaled and translated version of the mother wavelet $\psi(t)$:

$$\psi_{u,s}(t) = \frac{1}{\sqrt{s}} \psi\left(\frac{t-u}{s}\right). \tag{7}$$

The CWT transform (6) describes the analysed signal $f(t)$ on the time-scale plane. The conversion between scale s and actual frequency f is straightforward and depends on the selection of the mother wavelet (7).

Each scaling s alters the time-frequency resolution of the mother wavelet. As a result, CWT offers adaptive time-frequency resolution. High frequency resolution is preserved for lower frequencies, whereas high time resolution is preserved for higher frequencies.

3.1. The Morlet wavelet

For the impedance estimation, one needs information about the instantaneous amplitude and phase of the electrical current $i(t)$ and voltage $u(t)$. Therefore, a logical choice for mother wavelet (7) is the Morlet wavelet defined as [21]:

$$\psi(t) = \pi^{-1/4} \left(e^{j\omega_0 t} - e^{-\omega_0^2/2} \right) e^{-t^2/2}, \tag{8}$$

where ω_0 stands for the ratio between the highest and the second most highest peak and is usually set to $\omega_0 = 5$. For such $\omega_0 > 5$ the second term in (8) can be neglected.

The Morlet wavelet (8) is an analytical function i.e. it has only positive frequencies. Consequently, the wavelet coefficients $Wf(s,u)$ in (6) are complex values. Therefore, the CWT is plotted in modulus-phase form i.e. one plot for $|\langle f,\psi_{u,s}\rangle|$ and another plot for $\arg(\langle f,\psi_{u,s}\rangle)$, both on time-frequency plane. As a result, at each time translation u and scale s the CWT with Morlet wavelet gives the instantaneous amplitude and phase.

3.2. Scale to frequency transform for Morlet wavelet

The frequencies in CWT (6) are represented by scale s, which corresponds to a particular dilatation of the mother wavelet $\psi(x)$. Transforming scale to frequency for the Morlet wavelet is defined as [22]:

$$\frac{1}{f} = \frac{4\pi s}{\omega_0 + \sqrt{2 + \omega_0^2}}, \tag{9}$$

where s is the scale of CWT and ω_0 is the parameter of the Morlet wavelet governing the peak ratios.

3.3. Cone of influence

Due to the finite length of the measured signals, the wavelet coefficients (6) will be influenced by the discontinuities at the beginning and the end of the signal. These discontinuities introduce false broad frequency components. The presence of these effects is different over different wavelet scales, defining the so-called cone of influence. It is defined as the e-folding time for the autocorrelation of wavelet power at each scale [22], which for the Morlet wavelet reads:

$$e = s\sqrt{2}. \tag{10}$$

The cone of influence for the Morlet wavelet is shown as hatched region in Fig. 2. The hatched regions show the wavelet coefficients whose values are influenced by the edge effects. These coefficients should be omitted from further analysis. In Fig. 2, it can be noticed that all of the low frequency wavelet coefficients are influenced by the discontinuities occurring on both edges. One can overcome this limitation by either using longer signal or by oversampling the existing one.

3.4. Influence of the Morlet wavelet central frequency

The definition of Morlet wavelet (8) states that the wavelet is dependent upon parameter ω_0. The choice of this parameter is a compromise between localization in time and frequency [14,15]. For smaller ω_0, the shape of the wavelet favours localization of singular time events, whilst for larger ω_0 more periods of the sine-carrier in the Gaussian window (envelope) make the frequency localization better.

The broad frequency band and relatively short duration of measured signals (in case of lower frequencies) raise a problem in relation to variance of the calculated impedance. In order to minimize the variance the frequency resolution is increased by increasing the central frequency of the wavelet ω_0.

While this minimizes the variance for high frequencies it simultaneously raises the variance for lower frequencies. This is

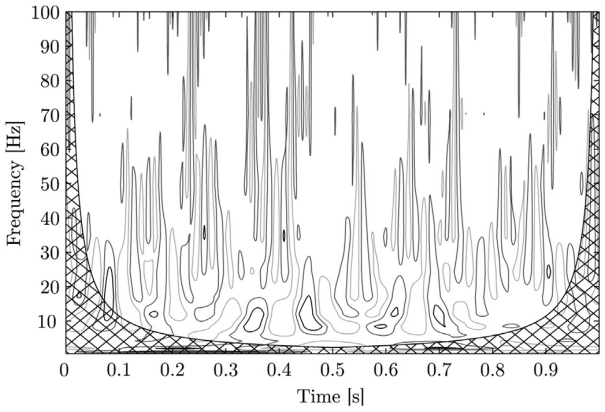


Fig. 2. Cone of influence for the Morlet wavelet with edge e defined by Equation (10).

due to the fact that at lower frequencies the whole signal contains less periods than the wavelet itself, which increases the variance. To remedy this situation the parameter ω_0 is lowered to decrease the number of periods in the wavelet. While this trade-off lowers frequency resolution it improves the reliability of the calculated impedance.

4. Experimental

4.1. Experimental setup

The experimental setup consisted of a PEM fuel cell power unit, electronic load, arbitrary function generator, voltage and current measurement equipment, and desktop computer. The measurements were performed on PEM fuel cells of a commercial 8.5 kW fuel cell system HyPM HD8-200, produced by Hydrogenics Inc. The stack of the system consists of 80 PEM fuel cells with surface area of 200 cm^2 each.

The electronic load was connected to the fuel cell system and it was used to perturb the system with PRBS perturbation signal in galvanostatic mode. The waveform of the load current was controlled by an arbitrary function generator. The generator was generating the PRBS reference signal, which was feed to the electronic load as a reference signal for the load current. Block diagram in Fig. 3 presents the experimental setup. Here, all the signal flows can be distinctly observed.

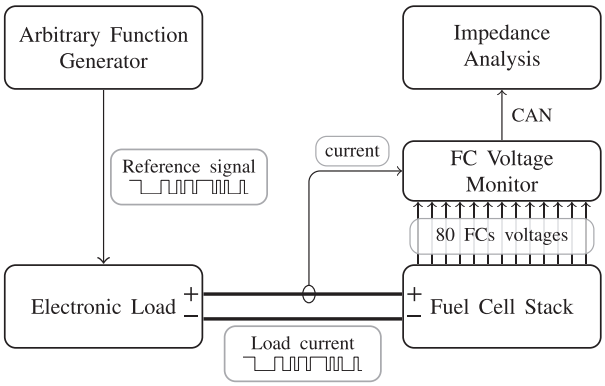


Fig. 3. Block diagram of the experimental setup.

Voltage and current signals were measured with an in-house developed fuel cell voltage monitor (FCVM) described in Ref. [23] and presented in Fig. 4. The top view of the figure shows the printed circuit board of the FCVM. The board is mounted directly on top of the stack and the galvanic contacts to all the fuel cells are implemented by spring contact probes, which are visible in the side view of Fig. 4. The FCVM provides means for fast and accurate measurements of voltage and current signals of any individual fuel cell inside the stack (the contacts to all fuel cells of the stack are clearly seen at the bottom edge of Fig. 4). The FCVM utilizes a Hall-effect current sensor to measure current, and an analogue circuitry to precisely measure changes in voltage of any individual fuel cell inside the stack. Any cell of the stack can be selected to be measured, however only three of them can be measured simultaneous at the same time.

With the FCVM, voltage and current signals are measured with the resolution of 80 μV and 10 mA, respectively, at sampling frequency of 5 kHz. The FCVM has the frequency range up to 660 Hz. The acquired measurements are transferred to a PC via CAN bus interface. The signal processing and impedance computational algorithms are performed on the PC.

4.2. Selection of the PRBS bandwidth and Morlet wavelet central frequency values

Due to the limitations set by the FCVM (i.e. frequency range of 660 Hz), the impedance characteristic was measured in the frequency band from 0.1 Hz to 500 Hz. Since such a frequency band spans over more than three frequency decades, two PRBS waveforms with different sampling frequency f_s were employed as perturbation signals. First one with $f_s = 500$ Hz covered the frequencies from 0.1 Hz to 10 Hz, whereas the other with $f_s = 2$ kHz

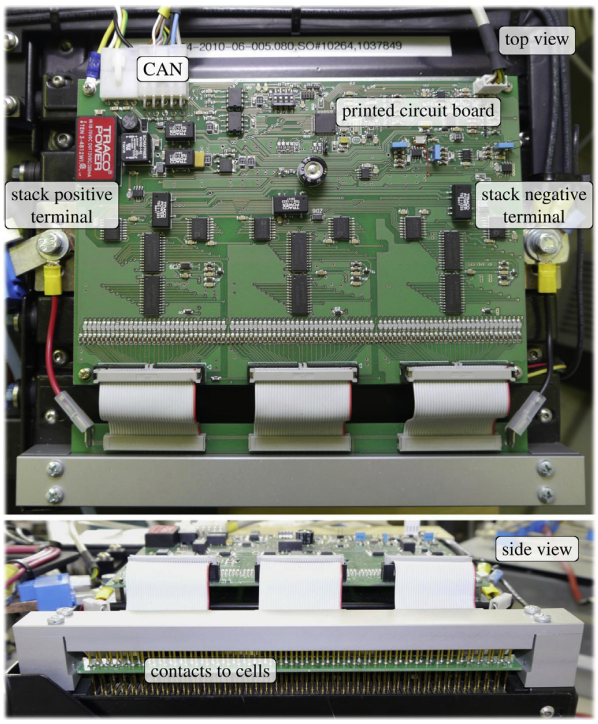


Fig. 4. Top and side view of the FCVM connected to the fuel cell stack consisted of 80 PEM fuel cells.

covered the frequencies from 10 Hz to 500 Hz. According to (5), the useful bandwidths f_B of the two signals are approximately 166 Hz and 660 Hz, respectively.

Accordingly to the analysis given in Section 3.4, for proper estimation of impedance at various frequencies, the central frequency ω_0 of the used Morlet wavelet was accordingly adjusted along the frequency axis. Three values of the central frequency ω_0 were selected, each covering separate frequency band.

Fig. 5 graphically depicts the selected bandwidth f_B of the PRBS signal and the corresponding central frequency ω_0 of the Morlet wavelet for different frequency ranges. The selection of the PRBS bandwidth was done accordingly to the analysis given in Section 2. The wavelet central frequency ω_0 was chosen in line with the analysis given in Section 3.4.

4.3. Experimental procedure

During the experiments, the fuel cell system was operating at constant operating and environmental conditions. The DC current operating point I_{DC} was set to 50 A, whereas the amplitude of the superposed PRBS waveform was set to 2 A. As such, the peak-to-peak amplitude was 4 A and therefore small enough not to cause difficulties due to non-linearity of the PEM fuel cells.

The order n of the PRBS was selected to be $n = 16$. Therefore, according to (1) the length of PRBS sequence is 65535 samples. The two PRBS signals were applied to the fuel cell system in consecutive manner one after another. The first PRBS signal ($f_B = 166$ Hz) was applied for 45 s and the second ($f_B = 660$ Hz) for 15 s, therefore one individual measurement of impedance characteristic took 60 s in total to complete. The first PRBS signal was applied for longer time period since it excites lower frequencies. Fig. 6 shows time plots of current and voltage signals of a PEM fuel cell during measurements. Current was measured as an absolute value, whereas the fuel cell voltage was measured as differential value.

5. Results and discussion

Utilizing the PRBS perturbation signals and CWT computational algorithm, the obtained impedance characteristic of a PEM fuel cell is presented in Fig. 7 in the form of Bode plot. The impedance characteristic was computed at 450 different frequency points. However, since the measured current and voltage signals comprise all frequency components in the frequency band, the algorithm allows to arbitrary choose frequencies and the number of frequency points at which the impedance is to be computed. In every such a configuration set of frequency points, the input signals for the algorithm are the same, the only thing is the computation time (i.e. more frequency points lead to longer computation time, and vice versa).

The plotted impedance characteristic in Fig. 7 is the median value of the impedance through measurement time period. Alongside the median impedance value, the 10th and 90th percentiles are provided in order to show the reliability of the impedance estimation. As such, the two percentiles account for 80%

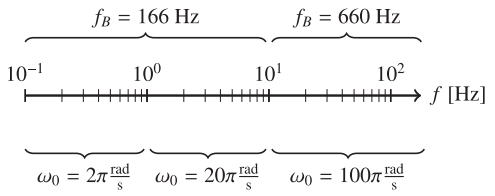


Fig. 5. Sampling frequency f_s of applied PRBS signals and utilized central frequencies ω_0 of complex Morlet wavelet in relation to frequency scale $f = [0.1, 500]$ Hz.

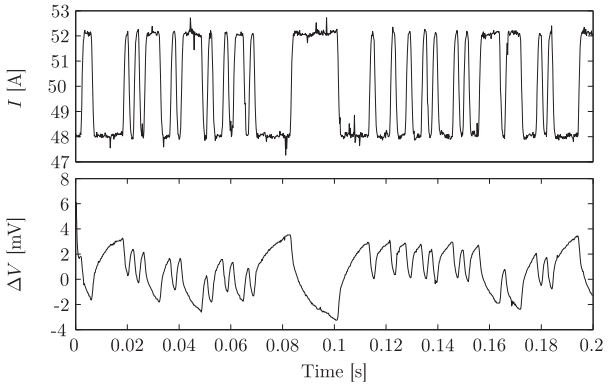


Fig. 6. Measured current and voltage signals during the experiment.

of the population. Additionally, the figure also provides the reference values of the impedance, which are presented with dots. The reference values were measured with single-sine technique at 4 points per decade.

Fig. 7a shows the Bode amplitude plot of the measured PEM fuel cell impedance. In the frequency band from 1 Hz to 500 Hz, the results exhibit high alignment with the reference impedance values. Moreover, the span between 10th and 90th percentile is quite narrow, meaning that the impedance results exhibit high confidence in this frequency band. At slightly lower frequencies in the frequency band between 0.5 and 1 Hz, the median amplitude value of the impedance still exhibit steady behaviour, but the 80% confidence interval is noticeable extended. In the lowest frequency band from 0.1 to 0.5 Hz, the 80% confidence interval is wide, therefore the results in this frequency band has always to be interpreted together with the confidence interval. However, the median value is informative, but it should not be declared as the exact value of the impedance amplitude without considering the confidence interval. The reasons for the occurrence of result with such relatively high uncertainty can be found in at least two causes. Firstly, impedance estimation at low frequencies requires sufficiently long signals in order to obtain more reliable results. Secondly, the aforementioned cone of influence of the Morlet wavelet decreases the number of eligible samples for calculating the impedance statistics at very low frequencies.

The Bode phase plot of the measured PEM fuel cell impedance is presented in Fig. 7b. The previous discussion about amplitude results applies equally to the phase results. As can be seen in Fig. 7b, the results indicate that the measured PEM fuel cell exhibits inductive behaviour at low frequencies. According to Roy and Orazem [24], the low-frequency inductive behaviour can be attributed to PEM fuel cell characteristic itself and not solely to non-stationary artefacts. Roy et al. [25] suggested the reactions of hydrogen peroxide intermediate formation and PtO formation as possible causes of the low-frequency inductive behaviour. Since the inductive behaviour was observed with the PRBS approach as well as with the single-sine one, most probably, the inductive behaviour was not introduced by the PRBS or CWT methodology.

Fig. 8 summarizes the impedance result in the form of Nyquist plot. The plot presents only the median value of the impedance without 80% confidence interval since there is no straightforward manner of presenting the confidence interval of the impedance characteristic in the Nyquist plot.

The Nyquist plot in Fig. 8 clearly expresses two semicircle arcs in the PEM fuel cell impedance characteristic. The high-frequency arc ranges from approximately 5 Hz up to high frequencies. The low-

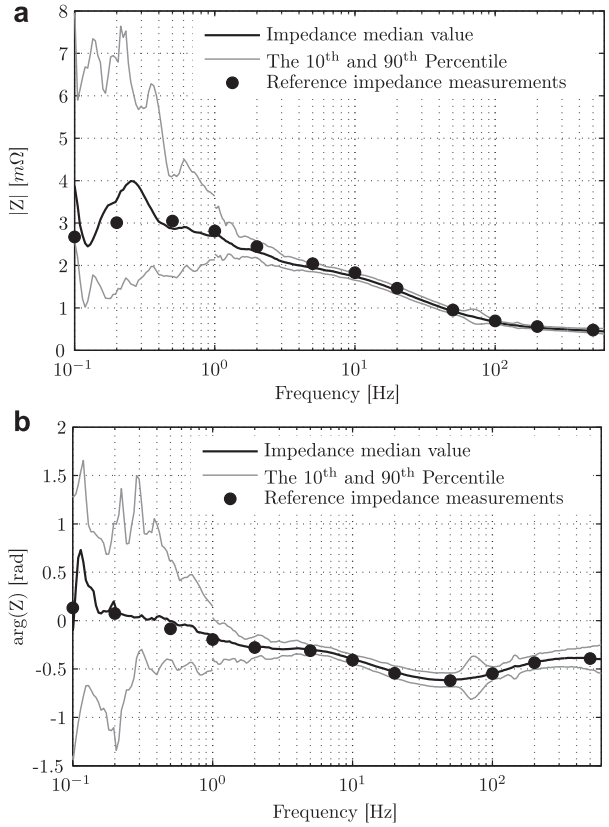


Fig. 7. Bode plot of the measured PEM fuel cell impedance. (a) Bode amplitude plot (b) Bode phase plot.

frequency one starts at approximately 0.5 Hz and extends up to 5 Hz, where the high-frequency arc starts. The Nyquist plot also clearly shows the already discussed inductive behaviour at lowest frequencies.

The study has confirmed the hypothesis that the measurements of the PEM fuel cell impedance utilizing the PRBS perturbation signal can be performed in a substantially shorter time period than with accepted single-sine approach. In the case of the proposed PRBS approach, the required time period for the measurements is approximately five times shorter compared to the single-sine technique. With such a reduction of time required for the measurements, the feasibility and acceptability of the EIS based diagnostics in industrial applications is significantly enhanced. Moreover, unlike the single-sine approach, where the impedance can be obtained only at frequencies that have been perturbed, in the case of the proposed PRBS approach, the impedance can be computed at any frequency of interest by simple adjustment of the computational algorithm.

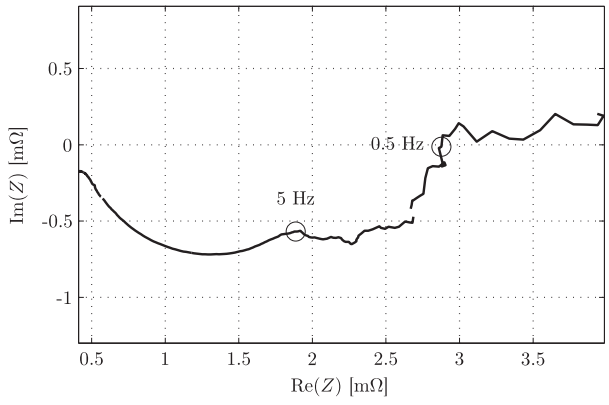


Fig. 8. Nyquist plot of the measured PEM fuel cell impedance.

6. Conclusion

The PEM fuel cell impedance characteristic obtained by employing PRBS perturbation signals and CWT computation algorithm shows high similarity to the impedance characteristics obtained by the single-sine approach. The similarity between the two characteristics confirm the suitability of the proposed PRBS perturbation and CWT computational approach. Regardless of the fact, that the present study has been performed on a PEM fuel cell, the proposed approach for impedance measurement can be easily applied to other types of electrochemical cells as well.

In this study impedance characteristic in the frequency band from 0.1 Hz to 500 Hz was measured. For such a measurement, the PRBS approach takes 60 s to complete. However, if the impedance only at frequencies above 1 Hz is to be measured, the required time for the measurements is further reduced. Additionally, the upper bandwidth frequency can be freely selected even at higher frequencies.

The computational algorithm besides the median value of the population provides also the confidence interval of the results. The information about the confidence interval is very beneficial, since it expresses how far the results can be trusted. In this manner, the study revealed that the impedance results below 0.5 Hz expresses wide confidence interval, therefore they have to be interpreted with great care if used for the EIS based diagnostics or are employed for any other purposes.

The presented approach of measuring PEM fuel cell impedance clearly provides the impedance characteristic. However, the approach still uses some kind of perturbation signal. Therefore, the possibility of using no external perturbation signal at all should be investigated in the future work. This way, solely the readily available signals (i.e. the operation signal of the fuel cell system) should be employed for impedance characteristic identification. Such obtained data could be further used for improving the operation of in-the-field fuel cell power units [26].

In this study, the approach was applied to estimate the impedance of a PEM fuel cell. However, the employed hardware and proposed approach are broadly applicable in the field of electrochemical impedance spectroscopy. With minor modifications the approach may be applied to any other type of electrochemical cells, for instance lithium ion cells.

Acknowledgements

The research leading to these results has received funding from the European Union's Seventh Framework Programme (FP7/2007-2013) for the Fuel Cells and Hydrogen Joint Technology Initiative under grant agreement №301782. The authors also thank the Centre of Excellence for Low-carbon Technologies – CO NOT, financed by the Slovenian Ministry of Higher Education, Science and Technology and co-financed by the European Regional Development Fund, and the Slovenian Research Agency (P2-0001) for the financial support.

References

[1] X.-Z. Yuan, H. Wang, J.C. Sun, J. Zhang, Int. J. Hydrogen Energy 32 (2007) 4365–4380.
[2] J. Wu, X.Z. Yuan, H. Wang, M. Blanco, J.J. Martin, J. Zhang, Int. J. Hydrogen Energy 33 (6) (2008) 1735–1746.
[3] R. Petrone, Z. Zheng, D. Hissel, M. Péra, C. Pianese, M. Sorrentino, M. Becherif, N. Yousfi-Steiner, Int. J. Hydrogen Energy 38 (17) (2013) 7077–7091.
[4] S.M. Rezaei Niya, M. Hoorfar, J. Power Sources 240 (0) (2013) 281–293.
[5] X.-Z. Yuan, C. Sons, H. Wang, J. Zhang, Electrochemical Impedance Spectroscopy in PEM Fuel Cells, Fundamentals and Applications, Springer, London, 2010.
[6] N. Fouquet, C. Doulet, C. Nouillant, G. Dauphin-Tanguy, B. Ould-Bouamama, J. Power Sources 159 (2005) 905–913.
[7] J.-M. Le Canut, R.M. Abouatallah, D.A. Harrington, J. Electrochem. Soc. 153 (2006) A857–A864.
[8] C. Brunetto, A. Moschetto, G. Tina, Electr. Power Syst. Res. 79 (2008) 17–26.
[9] S. Wasterlain, D. Candusso, F. Harel, D. Hissel, X. François, J. Power Sources 196 (12) (2011) 5325–5333.
[10] L. Ljung, System Identification: Theory for the User, in: Prentice-Hall Information and System Sciences Series, Prentice-Hall, 1999.
[11] H.C. Boghani, J.R. Kim, R.M. Dinsdale, A.J. Guwy, G.C. Premier, J. Power Sources 238 (0) (2013) 218–226.
[12] A. Fairweather, M. Foster, D. Stone, J. Power Sources 207 (2012) 56–59.
[13] A. Debenjak, M. Gašperin, B. Pregelj, M. Atanasijević-Kunc, J. Petrovčič, V. Jovan, J. Mech. Eng. 59 (1) (2013) 56–64.
[14] A. Stefanovska, M. Bračič, Contemp. Phys. 40 (1) (1999) 31–55.
[15] B. Musizza, A. Stefanovska, P.V. McClintock, M. Paluš, J. Petrovčič, S. Ribarič, F.F. Bajrović, J. Physiol. 580 (1) (2007) 315–326.
[16] P. Boškoski, Đ. Juričić, Mech. Syst. Signal Process. 31 (0) (2012) 369–381.
[17] N.Y. Steiner, D. Hissel, P. Moçotéguy, D. Candusso, Int. J. Hydrogen Energy 6 (1) (2011) 740–746.
[18] W. Davies, System Identification for Self-adaptive Control, John Wiley & Sons, New York, 1970.
[19] R. Isermann, M. Münchhof, Identification of Dynamic Systems: an Introduction with Applications, Advanced Textbooks in Control and Signal Processing, Springer-Verlag, Berlin Heidelberg, 2011.
[20] S. Mallat, A Wavelet Tour of Signal Processing: the Sparse Way, third ed., Elsevier Academic Press, Burlington, MA, 2008.
[21] I. Daubechies, Ten Lectures on Wavelets, CBMS-NSF Regional Conference Series in Applied Mathematics, Society for Industrial and Applied Mathematics, 1992.
[22] C. Torrence, G.P. Compo, Bull. Am. Meteorol. Soc. 79 (1998) 61–78.
[23] A. Debenjak, M. Gašperin, J. Petrovčič, Chem. Eng. Trans. 33 (2013) 1003–1008.
[24] S.K. Roy, M.E. Orazem, J. Electrochem. Soc. 154 (8) (2007) B883–B891.
[25] S.K. Roy, M.E. Orazem, B. Tribollet, J. Electrochem. Soc. 154 (12) (2007) B1378–B1388.
[26] Boštjan Pregelj, Darko Vrečko, Vladimir Jovan, J. Power Sources 196 (22) (15 November 2011) 9419–9428, http://dx.doi.org/10.1016/j.jpowsour.2011.06.077, ISSN 0378-7753.

Chapter 3

Optimal Selection of Condition Monitoring Thresholds

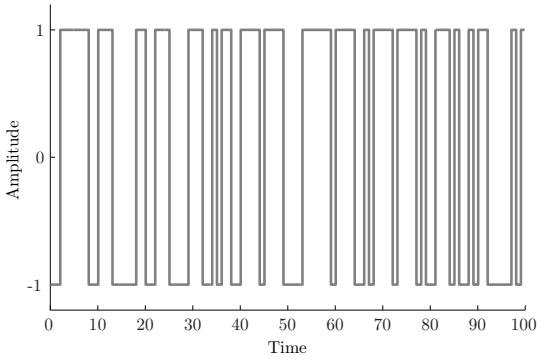
Crucial parameters of any CM system are threshold values that define when a specific alarm is to be raised. These threshold values have to be set during commissioning of a new PEM fuel cell power system or tuned after a maintenance activity. Improperly tuned threshold values may result either in a too high number of false alarms, or in a reduced sensitivity of the CM system to deviant conditions (i.e., faults). From the user (or control system) point of view, either a too high alarm rate or missed alarms reduce the reliability of the CM system. Therefore, a method for tuning the CM system's threshold values is of a great practical merit.

The proposed method for optimal selection of CM thresholds extends the fast impedance estimation approach (Debenjak et al., 2014) to the field of CM. It builds on the fact that the excitation signal, which is used for the impedance estimation, is of the PRBS waveform. The novelty of the method is the concept of treating the impedance at individual frequency as a complex random variable.

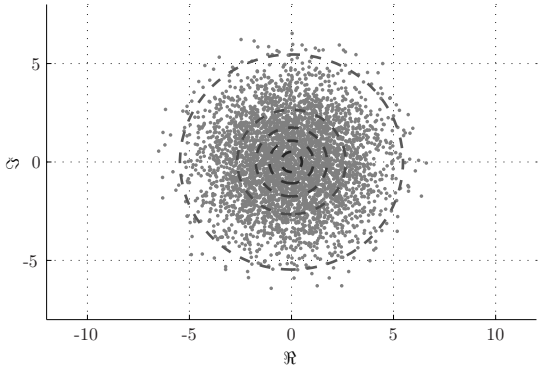
The analysis for the thresholds selection exploits the statistical properties of the PRBS signal. The essential property is the complex Gaussian circularity of the PRBS's frequency components (Priestley, 1981). This property implies that in the frequency domain, the real and imaginary parts of an individual frequency component, which can be written as $z = x + jy$, have zero-mean Gaussian distribution (i.e., $x \sim \mathcal{N}\left(0, \sigma^2\right)$ and $y \sim \mathcal{N}\left(0, \sigma^2\right)$).

The complex Gaussian circularity of the PRBS's frequency components is graphically presented in Figure 3.1 on the following page. Figure 3.1a shows the PRBS signal in the time domain with arbitrary units. Figure 3.1b shows the CWT coefficients of the PRBS signal at a certain frequency in the complex plane. From Figure 3.1b it can be observed that the CWT coefficients exhibit complex Gaussian circularity. This is further supported by Figure 3.1c and 3.1d. These two figures separately present the real and imaginary parts of the CWT coefficients from Figure 3.1b. The values are plotted as histograms and the maximum likelihood estimates for the Gaussian distribution are given.

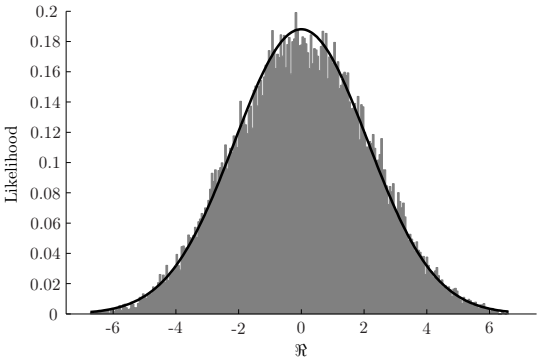
The design of the complete method for optimal CM thresholds selection also includes the analytical derivation of various PDFs. These PDFs are essential for the proposed methodology and they include: (i) the PDF of the complex impedance at individual frequency, which is a ratio distribution of two dependent random variables, that are derived from voltage and current signals, (ii) the PDF of the real and imaginary parts of the complex impedance, and (iii) the PDF of the module (i.e., amplitude) of the complex impedance. These PDFs are employed for the optimal CM threshold selection, where the proposed methodology provides the guidelines how the PDFs' parameters that are required for the CM thresholds selection should be estimated.



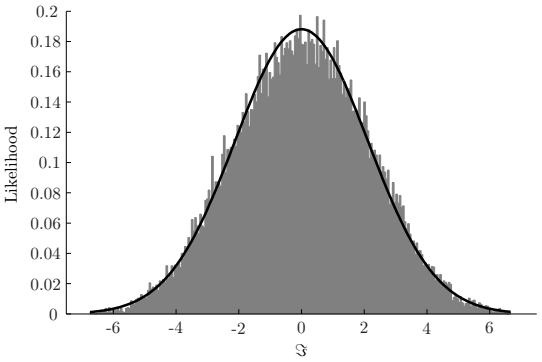
(a) The representation of the PRBS signal in the time domain.



(b) The CWT coefficients at a certain frequency in the complex plane.



(c) Histogram of the CWT coefficients' real part values and the maximum likelihood estimate of the distribution.



(d) Histogram of the CWT coefficients' imaginary values and the maximum likelihood estimate of the distribution.

Figure 3.1: Graphical presentation of the complex Gaussian circularity of PRBS's frequency components.

The main strengths of the method are as follows:

- The initial CM thresholds are determined based on data acquired from the PEM fuel cell power system solely under fault-free condition.
- The only design parameter is the tolerated PFA.

This chapter includes the following publication:
Boškoski, P. & Debenjak, A. (2014). Optimal selection of proton exchange membrane fuel cell condition monitoring thresholds. *Journal of Power Sources*, *268*, 692–699. doi:10.1016/j.jpowsour.2014.06.110

Journal of Power Sources 268 (2014) 692–699

Contents lists available at ScienceDirect

Journal of Power Sources

journal homepage: www.elsevier.com/locate/jpowsour

Optimal selection of proton exchange membrane fuel cell condition monitoring thresholds

Pavle Boškoski [a, *], Andrej Debenjak [a, b]

[a] Jožef Stefan Institute, Department of Systems and Control, Jamova cesta 39, SI-1000 Ljubljana, Slovenia
[b] Jožef Stefan International Postgraduate School, Jamova cesta 39, SI-1000 Ljubljana, Slovenia

HIGHLIGHTS

- An analytical method for optimal condition monitoring thresholds is proposed.
- The approach regards the electrical impedance as complex random variable.
- Impedance statistical properties are calculated via Morlet wavelet coefficients.
- Thresholds are determined based on the probability of false alarm.
- Unified and scale-free condition indicator for PEM fuel cells is proposed.

ARTICLE INFO

Article history:
Received 24 February 2014
Received in revised form
9 May 2014
Accepted 19 June 2014
Available online 7 July 2014

Keywords:
PEM fuel cell system
Fault detection
Complex random variable
Probability of false alarm

ABSTRACT

When commissioning or restarting a system after a maintenance action there is a need to properly tune the decision thresholds of the diagnostic system. Too low or too high thresholds may implicate either missed alarms or false alarm rates. This paper suggests an efficient data-driven approach to optimal setting of decision thresholds for a PEM fuel cell system based solely on data acquired from the system in reference state of health (i.e. under fault free operation). The only design parameter is the desired false alarm rate. Technically, the problem reduces to analytically determining the probability distribution of the fuel cell's complex impedance and its particular components. Employing pseudo-random binary sequence perturbation signals, the distribution of the impedance is estimated through the complex wavelet coefficients of the fuel cell voltage and current. The approach is validated on a PEM fuel cell system subjected to various faults.

© 2014 Elsevier B.V. All rights reserved.

1. Introduction

Like any other item of equipment the reliability and durability of proton exchange membrane (PEM) fuel cells is affected by faults on various components [1,2]. These faults include corrosion of the electrodes and degradation of membranes [3–6], catalyst and membrane poisoning [7–10], and water management faults (i.e. flooding of gas channels and membrane drying) [11–13]. Timely detection and diagnosis of these faults is of great importance for future employment of PEM fuel cell technology on larger scale [14,15].

Majority of faults that may occur on PEM fuel cells can be detected with multitude of approaches based on electrochemical impedance spectroscopy (EIS) [16–21]. EIS characterization of fuel cell flooding and membrane drying was reported by plethora of authors [22–28]. Portion of these authors used EIS measurement data to directly detect faults [26–28], meanwhile others proposed model based approaches [22–25]. Employing somehow more advanced approach, Kadyk et al. [29,30] proposed a non-linear extension of the EIS diagnostic approach with non-linear frequency response analysis (NFRA) to diagnose fuel cell flooding and membrane dehydration. In addition to the detection of water management faults, Le Canut et al. [27] and Kadyk et al. [31] also tackled detection of anode catalyst poisoning with CO by employing more complex NFRA. All these numerous studies confirm that various PEM fuel cell faults can be observed through EIS impedance measurements. Therefore, an autonomous and effectual condition monitoring system for fuel cells can be implemented by using EIS features.

To the best of the authors' knowledge, at this stage of PEM fuel cell diagnostic's development, using EIS features for condition monitoring requires beforehand EIS characterisation of fuel cell

* Corresponding author.
E-mail address: pavle.boskoski@ijs.si (P. Boškoski).

http://dx.doi.org/10.1016/j.jpowsour.2014.06.110
0378-7753/© 2014 Elsevier B.V. All rights reserved.

behaviour under normal and faulty operation. Having such data, one can set up threshold values that mark the border between fault free and faulty regions.

However, performing such characterisation procedures may be infeasible in many practical situations, since they may lead to irreversible damage of the fuel cell system (e.g. extensive drying and CO poisoning [1,2]). Moreover, due to variation in parameters from one fuel cell to another, once the EIS data is obtained for one particular fuel cell, there is no straightforward way to transfer this particular knowledge to another cell without conducting new complete set of characterisation procedure. Therefore a vital question arises how to design a condition monitoring system employing measurements conducted solely under fault free (normal) operation of a fuel cell.

Implementing an effective condition monitoring system can significantly improve the operation of in-the-field fuel cell power units [32]. Many of the problems for designing an effective condition monitoring system have been addressed in the context of mechanical systems [33,34]. The main difficulty is to determine the statistical properties of the selected features and model their behaviour under faulty conditions [35,36]. Achieving this goal has significant practical importance for any system integrator.

Addressing the issue of beforehand characterisation, this paper proposes a systematic approach for determining the bounds of the fault free region of operation without inducing any faults. In the proposed approach the fuel cell impedance is considered as a complex random variable. The corresponding probability distribution functions are derived, allowing complete statistical characterisation of the behaviour of the complex impedance. As a result, the only design parameter is the desired false alarm rate, which is intuitive and very well understood even by non-specialists in the area of condition monitoring. The effectiveness of the proposed approach was evaluated on a 8.5 kW PEM fuel cell subjected to various water management faults.

The first step towards specifying the fault free region is the analysis of the statistical properties of the feature set as described in Section 2. Using these statistical properties the method for calculating the bounds of the fault free region as well as the overall condition indicator are presented in Section 3. Experimental evaluation of the proposed condition indicator is presented in Section 4.

2. Statistical properties of the fuel cell impedance

Fuel cell electrical impedance is a complex variable that is defined as a frequency domain ratio of the voltage to the current. Regarding the fuel cell system as linear and time invariant one, the electrical impedance can be referred as its transfer function which has a deterministic nature for each frequency. However, when dealing with real world scenarios the observed fuel cell system is influenced by external disturbances, which are generally modelled as stochastic signals [37], as shown in Fig. 1. Since these disturbances are in many cases unmeasurable, their influence is incorporated into the model thus making the mapping between the current and voltage a stochastic one. Therefore, the observed electrical impedance should be treated as a complex random variable.

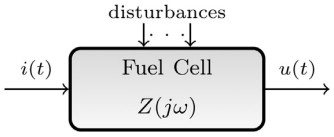


Fig. 1. Representation of fuel cell system excited by current and affected by disturbances.

In order to properly describe the electrical impedance as a complex random variable, the first step is determining its probability distribution function. For that purpose the fuel cell system can be excited using (PRBS) signal [38]. Following the procedure described by Debenjak et al. [38], the impedance characteristic can be efficiently estimated by using the complex wavelet coefficients of the continuous wavelet transform of the fuel cell's current $i(t)$ and voltage $u(t)$ using the Morlet mother wavelet, which is used in a variety of fields [38–41].

2.1. Continuous wavelet transform using the Morlet wavelet

The continuous wavelet transform (CWT) of a square integrable function $f(t) \in \mathbf{L}^2(\mathbb{R})$ is defined as [42]:

$$Wf(s,u) = \langle f(t), \psi_{u,s}(t) \rangle = \int_{-\infty}^{\infty} f(t)\psi^*_{u,s}(t)dt, \tag{1}$$

where $\psi_{u,s}(t)$ is a scaled and translated version of the mother wavelet $\psi(t)$:

$$\psi_{u,s}(t) = \frac{1}{\sqrt{s}}\psi\left(\frac{t-u}{s}\right). \tag{2}$$

The wavelet coefficients (1) describe the analysed signal $f(t)$ on the time-scale plane. The conversion between scale s and frequency f is straightforward and depends on the selection of the mother wavelet (2). Therefore, in the remaining of the paper instead of scale s all subsequent relations will rely on actual frequency f.

For the impedance estimation, one needs information about the instantaneous amplitude and phase of the electrical current $i(t)$ and voltage $u(t)$. Therefore, the Morlet wavelet was chosen as a mother wavelet (2), which reads [43]:

$$\psi(t) = \pi^{-1/4}\left(e^{j\omega_0 t} - e^{-\omega_0^2/2}\right)e^{-t^2/2}, \tag{3}$$

where ω_0 is the ratio between the highest and the second most highest peak and is usually set to $\omega_0 = 5$.

The Morlet wavelet (3) is an analytical function i.e. it has only positive frequencies. As a result, the wavelet coefficients $Wf(t,f)$ in (1) are complex values and at each time translation t and frequency f the wavelet coefficients give the instantaneous amplitude and phase.

2.2. PRBS as excitation signal

PRBS can be regarded as sufficiently close to stationary random noise whose amplitude probability distribution is Gaussian [44]. Analysing such a signal with continuous wavelet transform preserves its statistical properties with in the wavelet coefficients. As a result the complex wavelet coefficients of the measured current $i(t)$ and voltage $u(t)$ for a particular frequency can be regarded as zero-mean Gaussian circular complex random variables:

$$\begin{aligned} Wi(t,f) &= \Re\{Wi(t,f)\} + j\Im\{Wi(t,f)\} \\ Wu(t,f) &= \Re\{Wu(t,f)\} + j\Im\{Wu(t,f)\}, \end{aligned} \tag{4}$$

where $Wi(t,f)$ and $Wu(t,f)$ are the complex wavelet coefficients of the current $i(t)$ and voltage $u(t)$ respectively. Basic definitions about complex circular random variables are given in the Appendix B.

Due to the circularity of the complex random variables as well as the statistical properties of the prbs signal, the complex wavelet coefficients have the following properties:

$$\begin{aligned} \Re\{Wi(t,f)\}, \Im\{Wi(t,f)\} &\sim \mathcal{N}(0,\sigma_i^2) \\ \Re\{Wu(t,f)\}, \Im\{Wu(t,f)\} &\sim \mathcal{N}(0,\sigma_u^2). \end{aligned} \tag{5}$$

Using the complex wavelet coefficients (5), the impedance at particular frequency $f = f_0$ can be calculated as a ratio of the complex wavelet coefficients as:

$$z(t) = \left.\frac{Wu(t,f)}{Wi(t,f)}\right|_{f=f_0} = z_r + jz_i. \tag{6}$$

2.3. Probability distribution of the complex impedance z(t)

The ratio of two independent circular Gaussian complex random variables is a known result [45]. However, the current $i(t)$ and voltage $u(t)$ are correlated. This correlation can be expressed with the covariance matrix

$$\Sigma = \begin{bmatrix} \sigma_u^2 & \rho\sigma_u\sigma_i \\ \rho^*\sigma_u\sigma_i & \sigma_i^2 \end{bmatrix}, \tag{7}$$

where $\rho = \rho_r + j\rho_i$ is complex correlation coefficient, such as $|\rho| \leq 1$. As a result the distribution of the ratio (6) reads [46]:

$$f_z(z) = \frac{1-|\rho|^2}{\pi\sigma_u^2\sigma_i^2}\left(\frac{|z|^2}{\sigma_u^2} + \frac{1}{\sigma_i^2} - 2\frac{\rho_r z_r - \rho_i z_i}{\sigma_u\sigma_i}\right)^{-2}, \tag{8}$$

The location of the mode of $f_z(z)$ depends on the correlation coefficient ρ. For $\rho = 1/2 + j1/4$ the shape of (8) is shown in Fig. 2.

2.4. Probability distribution functions of the real z_r and imaginary z_i impedance components

The distribution of the real z_r and imaginary z_i components of the impedance (6) can be derived from the distribution (8). The probability distribution functions of the imaginary component z_i reads [46]:

$$f_{z_i}(z_i|\rho_r,\rho_i) = \frac{\left(1-|\rho|^2\right)\sigma_x^2\sigma_y}{2\left((1-\rho_r^2)\sigma_x^2 + 2z_i\rho_i\sigma_x\sigma_y + z_i^2\sigma_y^2\right)^{3/2}} \tag{9}$$

For the real component z_r the probability distribution function has the same shape and reads:

$$f_{z_r}(z_r|\rho_r,\rho_i) = f_{z_i}(z_r|-\rho_i,-\rho_r). \tag{10}$$

The shape of the (9) and (10) are shown in Fig. 3(a) and (b).

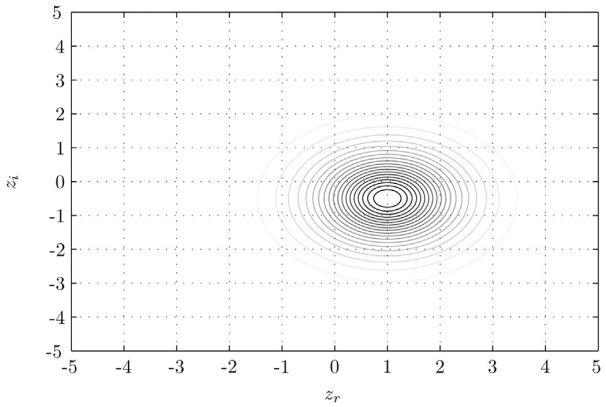
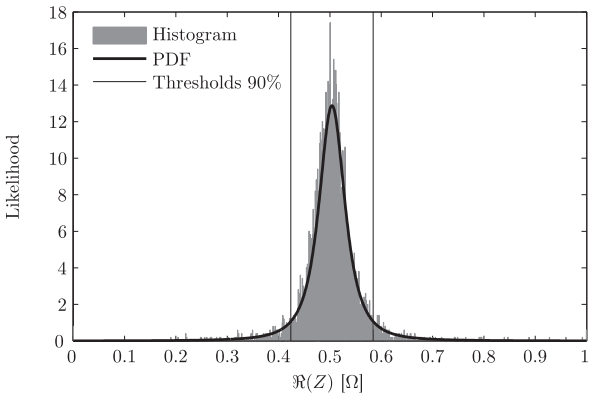


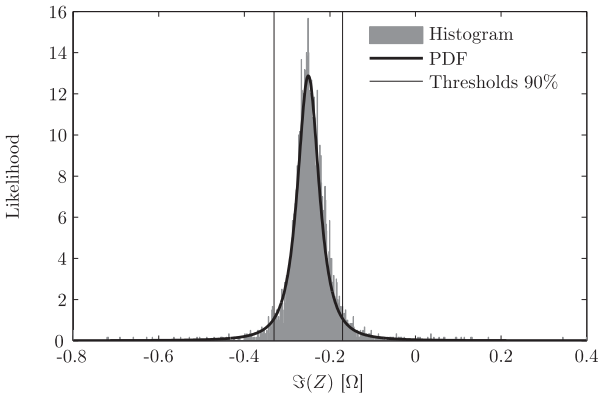
Fig. 2. Contour plot of the probability density function (8) for $\rho = 1/2 + j1/4$

2.5. Probability distribution function of the impedance amplitude |z(t)|

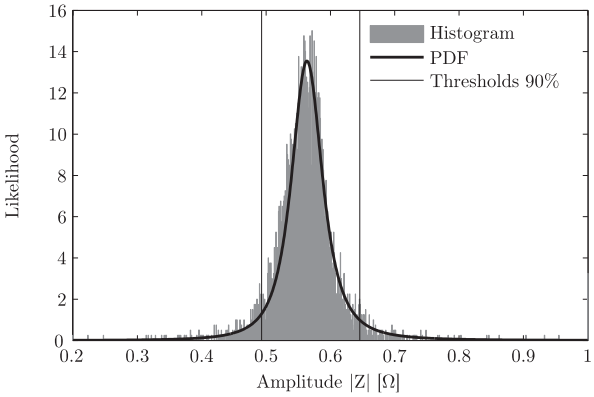
Besides the probability distribution of the real z_r and imaginary z_r components of the impedance in many cases the module of the complex impedance can be used as a feature in the process of condition monitoring. For the circular Gaussian complex random



(a) Distribution of $\Re(Z)$



(b) Distribution of $\Im(Z)$



(c) Distribution function of the module of the impedance (12)

Fig. 3. Probability distribution functions of particular impedance components (a) Distribution of $\Re(Z)$, (b) Distribution of $\Im(Z)$, (c) Distribution function of the module of the impedance (12).

variables (5), their corresponding modules $|Wu(t,f_0)|$ and $|Wi(t,f_0)|$ are distributed with Rayleigh distribution as:

$$\begin{array}{rcl} |Wu(t,f_0)| & \sim & \text{Rayleigh}(\sigma_u) \\ |Wi(t,f_0)| & \sim & \text{Rayleigh}(\sigma_i). \end{array} \tag{11}$$

As the current $i(t)$ and voltage $u(t)$ are correlated, the probability distribution function of the module of the ratio (6) reads [47]:

$$p_{|Z|}(|z|) = \frac{2\sigma_i^2\sigma_u^2(1-\rho^2)|z|(\sigma_i^2|z|+\sigma_u^2)}{\left[\left(\sigma_i^2|z|^2+\sigma_u^2\right)^2 - 4\rho^2\sigma_u^2\sigma_i^2|z|^2\right]^{3/2}}, |z| \geq 0, \tag{12}$$

where $|\rho| \leq 1$ is the correlation coefficient, as defined in (7). The probability distribution function (12) is positively skewed and defined on the non-negative semi axis. A typical realisation of the probability distribution function (12) is shown in Fig. 3(c).

2.6. Parameter estimation

The probability distribution functions (8), (9) and (12) depend on three parameters σ_u, σ_i and the correlation coefficient ρ. These parameters can be easily estimated through the covariance matrix (7) by using the calculated wavelet coefficients as:

$$\begin{aligned} E\{Wu(t,f_0)Wu(t,f_0)^*\} &= \frac{\sigma_u^2}{2} \\ E\{Wi(t,f_0)Wi(t,f_0)^*\} &= \frac{\sigma_i^2}{2} \\ E\{Wi(t,f_0)Wu(t,f_0)^*\} &= \frac{\sigma_u\sigma_i}{2}\rho. \end{aligned} \tag{13}$$

The histogram of the impedance components and its module, using a single realisation of the complex wavelet coefficients (5), are shown in Fig. 3. Using the estimated parameters σ_u, σ_i and ρ, the corresponding probability distribution functions clearly correspond to the empirically estimated histograms.

3. Fuel cell condition indicator based on the probability of false alarm

The statistical properties of the complex impedance are completely determined by estimating the parameters (13) using the data from the fault free operation. Deciding whether the fuel cell's condition deteriorated can be performed by calculating the probability of observing a particular impedance value. Determining the optimal values at which the deterioration can be regarded as significant is of great importance for an autonomous condition monitoring system. The most commonly used criterion for determining these boundary values selection is low (PFA) [35].

Condition monitoring system based on low PFA will raise alarms only when the condition of the fuel cell is suboptimal. Having derived the probability distribution functions (9) and (12), determining optimal boundary values based on low PFA is straight forward and can be defined as:

$$T = 1 - F^{-1}(PFA) = 1 - \inf\{F(z) \geq PFA\}, \tag{14}$$

where $F(z)$ is the cumulative distribution function of either (9) or (12)[1] and z is the corresponding impedance component. This approach was used for calculating the thresholds values in Fig. 3 for $PFA = 10\%$.

[1] Corresponding cumulative distribution functions are derived in the Appendix A.

3.1. Condition indicator

Selected threshold values (14) can be additionally used for mapping the complex impedance values into an so-called condition indicator (CI). It is an abstract feature defined on the interval $[0,\infty)$ that can be directly related to the condition of the system [35]. For a healthy system CI should acquire low values, typically $CI = 0$. As the condition deteriorates, the value of CI should increase in accordance with the severity of the fault(s) present in the system. Using PFA value, the value of CI are typically scaled in such a way that values close to one should indicate imminent failure. Having such a feature value with fixed threshold determining imminent failure has two major advantages:

1. it gives an unified and scale-free view of the overall system condition and
2. its trend can be used for prognostics i.e. estimation of the remaining useful life.

In the context of fuel cells, the presence of fault can either increase or decrease certain impedance components. Therefore, for fault free operation the value of the CI will be in the middle of the region bounded by thresholds at certain PFA, as shown in Fig. 3.

The mapping into the corresponding CI can be easily achieved by using the cumulative distribution functions of either (9) or (12) for the corresponding impedance components. As a result the impedance components of the fault free region will acquire values in the vicinity of 1/2. Setting the maximal value for the CI to be the chosen PFA, the final scaling relation reads:

$$CI = 2 \times (1 - PFA)^{-1}\left|F(z) - \frac{1}{2}\right|, \tag{15}$$

where $F(z)$ is the cumulative distribution function of the corresponding impedance component, as derived in the Appendix A.

4. Experimental evaluation

4.1. Experimental setup

The test bed incorporated a PEM fuel cell power unit, electronic load, arbitrary function generator, voltage and current measurement equipment, and desktop computer. The measurements were performed on a commercially available PEM fuel cell system HyPM HD 8 produced by Hydrogenics Corporation. The stack consists of 80 PEM fuel cells each with surface area of 200 cm^2, providing 8.5 kW of electric power in total. The fuel cell system operates on pure hydrogen and ambient air.

The electronic load was used to simulate real electrical load and to perturb the fuel cell system with PRBS perturbation signal in galvanostatic mode. The e-load's current was controlled by an arbitrary function generator, which was generating the PRBS reference signal. Block diagram of the experimental setup is presented in Fig. 4.

Voltage and current signals were measured with an in-house developed fuel cell voltage monitor (FCVM) presented in Fig. 5 [23]. The top view of the Fig. 5 shows the printed circuit board of the FCVM. The board is mounted directly on top of the stack and the galvanic contacts to all the fuel cells are implemented by spring contact probes, which are visible in the side view of the Fig. 5. The FCVM provides the means for fast and accurate measurements of voltage and current signals of any individual fuel cell inside the stack (the contacts to all fuel cells of the stack are clearly seen at the bottom edge of Fig. 5). The FCVM utilizes a Hall-effect current sensor to measure current, and an analogue circuitry to precisely

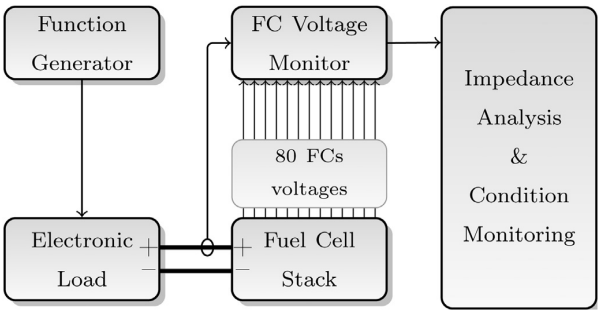


Fig. 4. Block diagram of the experimental setup.

measure changes in voltage of any individual fuel cell inside the stack.

The FCVM enables measurement of voltage and current signals with the resolution of 80 μV and 10 mA, respectively, at sampling frequency of 5 kHz. It has a frequency range of up to 660 Hz. The FCVM contains a CAN bus interface for data transmission to external device (e.g. personal computer). Signal processing and computational algorithms were performed on a PC.

4.2. Experimental procedure

During the experiments, the fuel cell system was kept at constant operating and environmental conditions. The fuel cell stack temperature and the stoichiometry were kept constant by the built-in controller supplied by the fuel cell manufacturer Hydrogenics at 50 °C and 2.5, respectively. At the cathode side, the temperature and relative humidity of the inlet air were measured with Vaisala HMP235A transducer and controlled by external PID

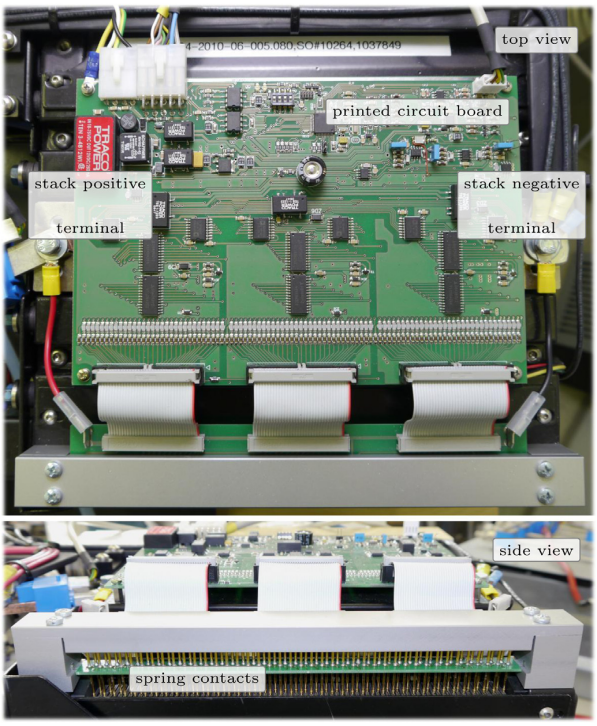


Fig. 5. Top and side view of the FCVM connected to an 8.5 kW PEM fuel cell system.

controllers. The temperature of the air flow was kept constant at 50 °C and the relative humidity changed in order to introduce drying or flooding accordingly. At the anode side, the fuel cell was fed with pure and dry hydrogen at constant temperature of 20 °C. The DC current operating point I_{dc} was set to 70 A resulting in the stack voltage of 55 V, whereas the amplitude of the superposed PRBS waveform was set to 2 A. As such, the peak-to-peak amplitude was 4 A and therefore small enough not to cause difficulties due to non-linearity of the PEM fuel cells. Fig. 6 shows time plots of current and voltage signals of a PEM fuel cell during measurements. Current was measured as an absolute value, whereas the fuel cell voltage was measured as differential value.

During the experiment, an acquisition of measurements occurred every 40 s. The experiment went through five stages. In the first stage of approx. 11 min, 18 measurements were performed in the fault free state at which the relative humidity of the inlet air was kept at 9% (which at 50 °C corresponds to 7.5 g m^{-3} - grams of water per cubic metre of air). Then, air fed to the fuel cell was slightly dried down to relative humidity of 5% (4.1 g m^{-3}) for about 10 min, between the 12 and the 22 min, in order to induce membrane drying, and again humidified to 9%. Afterwards, between the 34 and the 58 min, saturated air with relative humidity of 100% (83 g m^{-3}), was fed into the fuel cell system inducing flooding of fuel cells. Finally, the air humidity was decreased down to the initial 9%. Using such a cycle we were able to determine the response of the cell under different fault scenarios with various fault severity. These stages of the experiment are clearly indicated in Fig. 7.

4.3. Time evolution of particular impedance components

Using the complex wavelet coefficients (4), calculated from the initial fault free operation signals, the parameters of probability distribution functions (8) and (12) were estimated employing (13). With the estimated parameters, the threshold values were calculated for four different $PFA = \{25\%, 20\%, 15\%, 10\%\}$. The resulting thresholds for each impedance component are shown in Fig. 7. The threshold values clearly define the fault free region.

The first departure from the fault free condition was between the 12th and the 22nd minute, when the fuel cell was fed with somewhat drier air (5% relative humidity). In that particular region the real component of the impedance increased and surpasses the threshold of 70%, as shown in Fig. 7(a) and (b). Similar observation can be made also for the module of the impedance, as shown in Fig. 7(c). Despite the minute changes in the relative humidity of the inflow air, there are clear change in the value of the impedance, with 30% probability of false alarm. Without the threshold values such an quantification would have been impossible.

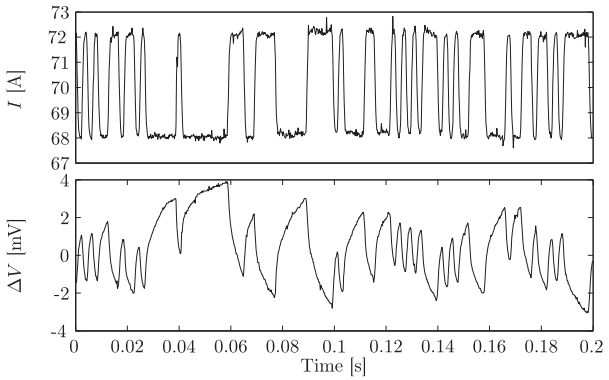


Fig. 6. Measured current and voltage signals during the experiment.

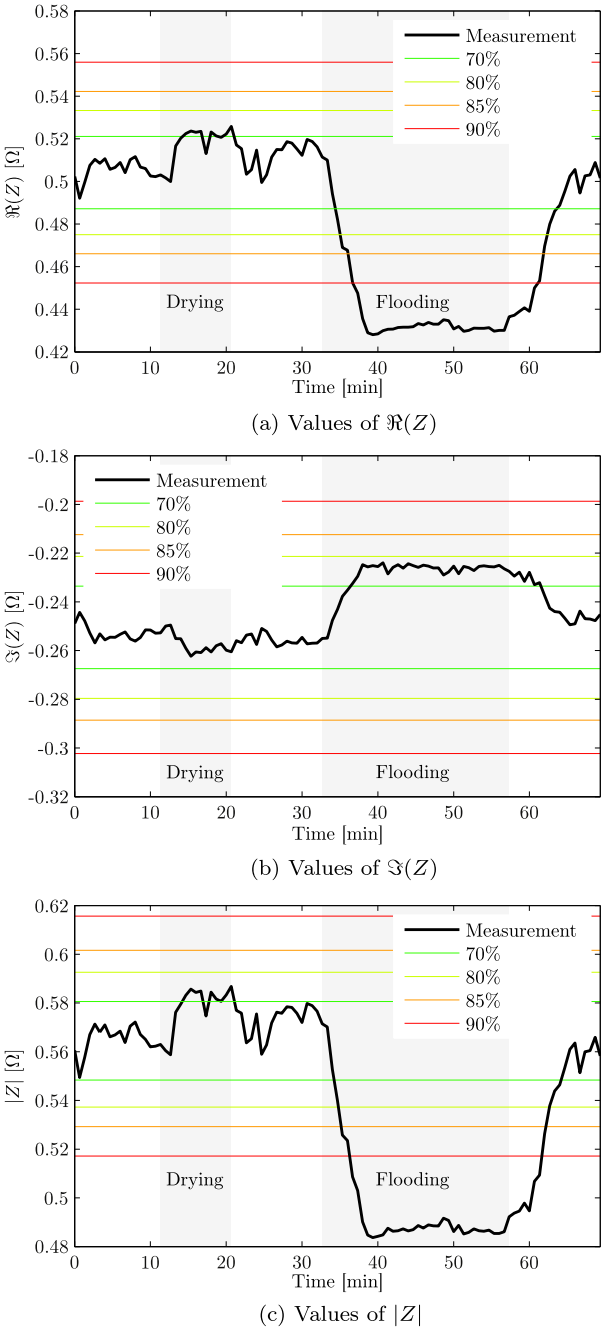


Fig. 7. Trend of impedance components throughout the experiment (a) Values of $\Re(Z)$, (b) Values of $\Im(Z)$, (c) Values of $|Z|$.

Unlike the minor changes caused by the mild decrease in the humidity, the flooding with 100% saturated air inflow shows significant changes in al three impedance components. The values of $\Re(z)$ and $|z|$, between the 34th and the 58th minute, indicate that the condition of the fuel cell departed from the fault free area, with less then 10% probability of false alarm, as shown in Fig. 7(a) and (c). The change in the imaginary component $\Im(z)$ is somewhat smaller, the probability of false alarm is less then 30%.

Finally, when the relative humidity of the air inflow was returned to normal the impedance components returned to the initial values within the fault free region.

4.4. Time evolution of the CI

The time evolution of the CI (15) of the impedance module $|z|$ is shown in Fig. 8. The values of the CI were calculated using the mapping relation (15) with $PFA = 90\%$.

By analysing this time evolution one can notice that during the fault free operation CI acquires low values. As the first fault was induced, the values of CI increased up to 0.5, which indicates that the condition of the fuel cell deteriorated. The acquired value of 0.5 clearly shows departure from fault free operation while in the same time is inline with the low severity of the induced drying, relative humidity change of 8%. Unlike the low severity of the drying fault, during the flooding phase of the experiment, the value of CI surpasses the limit value of 1. The overwhelming flooding of the system is directly reflected in the high value of the CI. Finally, at the end of the experiment, when the air condition was back to nominal, the values of CI decreased indicating almost fault free operation.

The results confirm the behaviour of CI. It is sufficiently sensitive on deviation in the condition of the water management. In the same time its value is directly related to the severity of the deviation with respect to the selected PFA.

5. Conclusion

Observing the impedance of a fuel cell in the context of random variables, this paper specifies probability distribution functions of the real and imaginary components as well as its module. Using the data solely from the fault free operation, one can estimate the free parameters of these distribution functions. As a result, threshold values defining the fault free region can be calculated by specifying a specific probability of false alarm.

Determining the threshold values using the probability of false alarm has significant practical merit. For each of the measured impedance components one can calculate the probability of false alarm and use this value as an indicator of confidence that the current condition of the fuel cell has sufficiently departed from the fault free region. Furthermore, the proposed condition indicator scaled with the chosen PFA is directly related to the fault severity and can be used for both fault detection as well as estimation of the remaining useful life. The evaluation of the proposed method confirms that the calculated condition indicator based on the PFA corresponds to the severity of the induced faults.

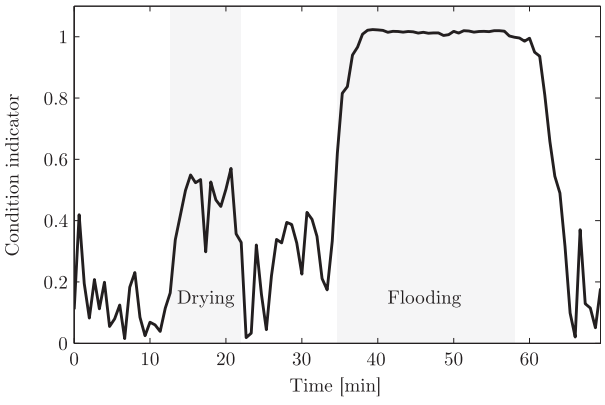


Fig. 8. Trend of CI of $|Z|$ throughout the experiment.

Acknowledgement

The research leading to these results has received funding from the European Union's Seventh Framework Programme (FP7/2007-2013) for the Fuel Cells and Hydrogen Joint Technology Initiative under grant agreement No 301782. The authors also acknowledge the financial support of the Slovenian Research Agency through the Research Programme P2-0001 and the Research Project Z2-5477.

Appendix A. Cumulative distribution functions

Appendix A.1. Cumulative distribution function of z_i

According to [46] integrating out z_r from (8) results into the following cumulative distribution function:

$$F_{z_i}(z_i|\rho_r,\rho_r) = \frac{1}{2} + \frac{\rho_i\sigma_u + z_i\sigma_i}{2\sqrt{(1-\rho_r^2)\sigma_u^2 + 2z_i\rho_i\sigma_u\sigma_i + z_i^2\sigma_i^2}} \tag{A.1}$$

Solution of (A.1) for arbitrary $y = PFA$ reads:

$$z_i = \frac{-2(y-1)y\rho_i\sigma_u\sigma_i}{2(-1+y)y\sigma_i^2} \pm \frac{\sqrt{(1-2y)^2(y-1)y\left(|\rho|^2-1\right)\sigma_u^2\sigma_i^2}}{2(-1+y)y\sigma_i^2} \tag{A.2}$$

Appendix A.2. Cumulative distribution function of $|z|$

The cumulative distribution function that corresponds to (12) reads [47]:

$$F_{|z|}(z) = \frac{1}{2} - \frac{\sigma_u^2 - z^2\sigma_i^2}{2\sqrt{4z^2(1-\rho^2)\sigma_i^2\sigma_u^2 + \left(\sigma_u^2 - z^2\sigma_i^2\right)^2}}, \tag{A.3}$$

where $z \geq 0$. Solution of (A.3) for $y = PFA$ reads:

$$z = \sigma_u\left(\frac{-1+2y-2y^2+(1-2y)^2\rho^2}{2(-1+y)y\sigma_i^2} \pm \frac{(1-2y)\sqrt{-1+\rho^2}\sqrt{(1-2y)^2\rho^2-1}}{2(-1+y)y\sigma_i^2}\right)^{1/2} \tag{A.4}$$

Appendix B. Circular complex random variables

A Gaussian complex random variable can analysed through its real and imaginary components

$$Z = X + jY, \tag{B.1}$$

where both X and Y and real Gaussian random variables. In order for the complex Gaussian random variable Z to be circular the following conditions have to be fulfilled [48]:

$$E\left[Z^2\right] = E\left[X^2\right] - E\left[Y^2\right] + jE[XY] = 0. \tag{B.2}$$

As both X and Y are Gaussian random variables in order for (B.2) to be fulfilled

$$\begin{aligned} E\left[X^2\right] &= E\left[Y^2\right] \\ E[XY] &= 0. \end{aligned} \tag{B.3}$$

Therefore the random variables X and Y are independent with same variance.

Appendix B.1 Circularity of spectral components

A stationary random signal can be represented using Cramer representation [49]:

$$x(t) = \int_{-\infty}^{\infty} e^{j\omega t}dZ(\omega), \tag{B.4}$$

where $dZ(\omega)$ are complex random variables directly related to the signals power spectrum with the following properties:

$$E[dZ(\omega)] = 0, \quad E[dZ(\omega_1)dZ(\omega_2)] = 0, \text{ for } \omega_1 \neq \omega_2. \tag{B.5}$$

Therefore for stationary signals the complex random variables $dZ(\omega)$ are circular [48].

References

[1] F.A. de Bruijn, V.A.T. Dam, G.J.M. Janssen, Fuel Cells 8 (2008) 3–22, http://dx.doi.org/10.1002/fuce.200700053.
[2] W. Schmittinger, A. Vahidi, J. Power Sources 180 (2008) 1–14, http://dx.doi.org/10.1016/j.jpowsour.2008.01.070.
[3] H.R. Colón-Mercado, B.N. Popov, J. Power Sources 155 (2006) 253–263, http://dx.doi.org/10.1016/j.jpowsour.2005.05.011.
[4] R. Borup, J. Meyers, B. Pivovar, Y.S. Kim, R. Mukundan, N. Garland, D. Myers, M. Wilson, F. Garzon, D. Wood, P. Zelenay, K. More, K. Stroh, T. Zawodzinski, J. Boncella, J.E. McGrath, M. Inaba, K. Miyatake, M. Hori, K. Ota, Z. Ogumi, S. Miyata, A. Nishikata, Z. Siroma, Y. Uchimoto, K. Yasuda, K.-i. Kimijima, N. Iwashita, Chem. Rev. 107 (2007) 3904–3951, http://dx.doi.org/10.1021/cr050182l.
[5] P.T. Yu, Z. Liu, R. Makharia, J. Electrochem. Soc. 160 (2013) F645–F650, http://dx.doi.org/10.1149/2.120306jes.
[6] J.D. Fairweather, D. Spernjak, A.Z. Weber, D. Harvey, S. Wessel, D.S. Hussey, D.L. Jacobson, K. Artyushkova, R. Mukundan, R.L. Borup, J. Electrochem. Soc. 160 (2013) F980–F993, http://dx.doi.org/10.1149/2.024309jes.
[7] C. Farrell, C. Gardner, M. Ternan, J. Electrochem. Soc. 171 (2007) 282–293, http://dx.doi.org/10.1016/j.jpowsour.2007.07.006.
[8] X. Cheng, Z. Shi, N. Glass, L. Zhang, J. Zhang, D. Song, Z.-S. Liu, H. Wang, J. Shen, J. Power Sources 165 (2007) 739–756.
[9] W.-M. Yan, H.-S. Chu, M.-X. Lu, F.-B. Weng, G.-B. Jung, C.-Y. Lee, J. Power Sources 188 (2009) 141–147, http://dx.doi.org/10.1016/j.jpowsour.2008.11.107.
[10] G. Postole, A. Auroux, Int. J. Hydrogen Energy 36 (2011) 6817–6825, http://dx.doi.org/10.1016/j.ijhydene.2011.03.018.
[11] H. Li, Y. Tang, Z. Wang, Z. Shi, S. Wu, D. Song, J. Zhang, K. Fatih, J. Zhang, H. Wang, Z. Liu, R. Abouatallah, A. Mazza, J. Electrochem. Soc. 178 (2008) 103–117, http://dx.doi.org/10.1016/j.jpowsour.2007.12.068.
[12] N. Yousfi-Steiner, P. Moçotéguy, D. Candusso, D. Hissel, A. Hernandez, A. Aslanides, J. Power Sources 183 (2008) 260–274, http://dx.doi.org/10.1016/j.jpowsour.2008.04.037.
[13] T. Ous, C. Arcoumanis, J. Power Sources 240 (2013) 558–582, http://dx.doi.org/10.1016/j.jpowsour.2013.04.044.
[14] M. Jouin, R. Gouriveau, D. Hissel, M.-C. Péra, N. Zerhouni, Int. J. Hydrogen Energy 38 (2013) 15307–15317, http://dx.doi.org/10.1016/j.ijhydene.2013.09.051.
[15] M. Jouin, R. Gouriveau, D. Hissel, M.-C. Péra, N. Zerhouni, Int. J. Hydrogen Energy 39 (2014) 481–494, http://dx.doi.org/10.1016/j.ijhydene.2013.10.054.
[16] J. Stumper, M. Löhr, S. Hamada, J. Power Sources 143 (2005) 150–157, http://dx.doi.org/10.1016/j.jpowsour.2004.11.036.

[17] X.-Z. Yuan, H. Wang, J.C. Sun, J. Zhang, Int. J. Hydrogen Energy 32 (2007) 4365–4380.
[18] J. Wu, X.Z. Yuan, H. Wang, M. Blanco, J.J. Martin, J. Zhang, Int. J. Hydrogen Energy 33 (2008) 1735–1746, http://dx.doi.org/10.1016/j.ijhydene.2008.01.013.
[19] R. Petrone, Z. Zheng, D. Hissel, M. Péra, C. Pianese, M. Sorrentino, M. Becherif, N. Yousfi-Steiner, Int. J. Hydrogen Energy 38 (2013) 7077–7091, http://dx.doi.org/10.1016/j.ijhydene.2013.03.106.
[20] Z. Zheng, R. Petrone, M. Péra, D. Hissel, M. Becherif, C. Pianese, N.Y. Steiner, M. Sorrentino, Int. J. Hydrogen Energy 38 (2013) 8914–8926, http://dx.doi.org/10.1016/j.ijhydene.2013.04.007.
[21] S.M. Rezaei Niya, M. Hoorfar, J. Power Sources 240 (2013) 281–293, http://dx.doi.org/10.1016/j.jpowsour.2013.04.011.
[22] N. Fouquet, C. Doulet, C. Nouillant, G. Dauphin-Tanguy, B. Ould-Bouamama, J. Electrochem. Soc. 159 (2005) 905–913.
[23] A. Debenjak, M. Gašperin, J. Petrovčič, Chem. Eng. Trans. 33 (2013) 1003–1008, http://dx.doi.org/10.3303/CET1333168.
[24] S. Cruz-Manzo, R. Chen, J. Electrochem. Soc. 160 (2013) F1109–F1115, http://dx.doi.org/10.1149/2.025310jes.
[25] M. Gašperin, P. Boškoski, A. Debenjak, J. Petrovčič, Fuel Cells 14 (2014) 457–465, http://dx.doi.org/10.1002/fuce.201300217.
[26] W. Merida, D. Harrington, J.L. Canut, G. McLean, J. Power Sources 161 (2006) 264–274, http://dx.doi.org/10.1016/j.jpowsour.2006.03.067.
[27] J.-M. Le Canut, R.M. Abouatallah, D.A. Harrington, J. Electrochem. Soc. 153 (2006) A857–A864.
[28] A. Debenjak, M. Gašperin, B. Pregelj, M. Atanasijević-Kunc, J. Petrovčič, V. Jovan, J. Mech. Eng. 59 (2013) 56–64, http://dx.doi.org/10.5545/sv-jme.2012.640.
[29] T. Kadyk, R. Hanke-Rauschenbach, K. Sundmacher, J. Electroanal. Chem. 630 (2009) 19–27, http://dx.doi.org/10.1016/j.jelechem.2009.02.001.
[30] T. Kadyk, R. Hanke-Rauschenbach, K. Sundmacher, Int. J. Hydrogen Energy 37 (2012) 7689–7701, http://dx.doi.org/10.1016/j.ijhydene.2012.01.148, 7th Petite Workshop on the Defect Chemical Nature of Energy Materials, 14–17 March 2011, Storaas, Kongsberg, Norway.
[31] T. Kadyk, R. Hanke-Rauschenbach, K. Sundmacher, J. Appl. Electrochem 41 (2011) 1021–1032, http://dx.doi.org/10.1007/s10800-011-0298-8.
[32] B. Pregelj, D. Vrečko, V. Jovan, J. Power Sources 196 (2011) 9419–9428, http://dx.doi.org/10.1016/j.jpowsour.2011.06.077.
[33] G. Vachtsevanos, F.L. Lewis, M. Roemer, A. Hess, B. Wu, Intelligent Fault Diagnosis and Prognosis for Engineering Systems, Wiley, 2006.
[34] A. Jardine, D. Lin, D. Banjevi&ccaron, Mech. Syst. Signal Process 20 (2006) 1483–1510.
[35] E. Bechhoefer, A. Bernhard. in: IEEE Aerospace Conference, pp. 1–9.
[36] P. Boškoski, Đ. Juričić, Mech. Syst. Signal Process 31 (2012) 369–381.
[37] R. Isermann, M. Münchhof, Identification of Dynamic Systems: An Introduction with Applications, Advanced textbooks in control and signal processing, Springer-Verlag Berlin Heidelberg, 2011, http://dx.doi.org/10.1007/978-3-540-78879-9.
[38] A. Debenjak, P. Boškoski, B. Musizza, J. Petrovči&ccaron, Đ. Juričić, J. Power Sources 254 (2014) 112–118, http://dx.doi.org/10.1016/j.jpowsour.2013.12.094.
[39] B. Musizza, A. Stefanovska, P.V. McClintock, M. Paluš, J. Petrovčič, S. Ribarič, F.F. Bajrovi&cacute, J. Physiol. 580 (2007) 315–326, http://dx.doi.org/10.1113/jphysiol.2006.126748.
[40] W. Liu, B. Tang, Expert Syst. Appl. 38 (2011) 7575–7581, http://dx.doi.org/10.1016/j.eswa.2010.12.107.
[41] P. Kvandal, L. Sheppard, S.A. Landsverk, A. Stefanovska, K.A. Kirkeboen, J. Clin. Monit. Comput. 27 (2013) 375–383, http://dx.doi.org/10.1007/s10877-013-9484-z.
[42] S. Mallat, A Wavelet Tour of Signal Processing: the Sparse Way, 3rd ed., Elsevier Academic Press, Burlington, MA, 2008.
[43] I. Daubechies, Ten Lectures on Wavelets, CBMS-NSF Regional Conference Series in Applied Mathematics, Society for Industrial and Applied Mathematics, 1992.
[44] E.O. Doebelin, System Modeling and Response, John Wiley & Sons Inc, 1980.
[45] N. Goodman, Ann. Math. Stat. 34 (1963) 152–177.
[46] R.J. Baxley, B.T. Walkenhorst, G. Acosta-Marum, Global Telecommunications Conference (GLOBECOM 2010), IEEE, 2010, pp. 1–5.
[47] M.K. Simon, Probability Distributions Involving Gaussian Random Variables, Springer Science, New York, 2006.
[48] P.O. Amblard, M. Gaeta, J.L. Lacoume, Signal Proc. 53 (1996) 1–13.
[49] M. Priestley, Spectral Analyses and Time Series, Academic Press, London, 1981.

Chapter 4

PEM Fuel Cell Condition Indicator

The final step towards an effectual CM system for PEM fuel cells is a unit-free CI. The proposed PEM fuel cell CI is a continuation (or extension) of the fast impedance estimation approach (Chapter 2) and the statistical analysis of impedance frequency components (Chapter 3). It provides the answer to the question: how can the fast impedance estimation be utilised for online CM of PEM fuel cells?

The construction of the proposed PEM fuel cell CI involves the following four steps (also presented in Figure 4.1 of the journal article in the sequel of this chapter):

- data acquisition,
- signal processing,
- statistical analysis, and
- information aggregation.

The first three steps are covered by Debenjak et al., 2014 (Chapter 2) and Boškoski and Debenjak, 2014 (Chapter 3). The last one – the information aggregation step is the topic of this chapter. In essence, it provides a solution to the problem of aggregating a high cardinality feature set into a single unit-free CI. The feature set comprises a large number of impedance estimates at distinct frequencies over a broad frequency band (i.e., the output of the fast impedance estimation procedure).

As stated in Chapter 3, the impedance estimates at individual frequencies are complex random variables with PDFs of a known shape. Consequently, the set of impedance estimates should be regarded as a set of dependent complex random variables. The dependence originates from the fact that physical system's impedance at a particular frequency cannot be changed without affecting impedance at other frequencies. An appropriate way to aggregate dependent random variables is through construction of their joint CDF. In this manner, the information aggregation of the set of impedance estimates into the CI is performed by utilising the copula functions. These functions offer a solution to the problem of estimating the joint CDF solely by using the marginal distributions.

The PEM fuel cell CI is defined as the output of the constructed copula structure. The copula models the dependence among the random variables (i.e., impedance at individual frequencies) under fault-free operation condition of the PEM fuel cell. By its very nature, its sensitivity to the changes of the underlying marginal distributions (i.e., distributions of the impedance at individual frequencies) enables the detection of the departure from the fault-free condition region described by the original copula structure. Therefore, the proposed CI expresses the probability of observing particular impedance values. Hence, it is directly related to the current condition of a PEM fuel cell, as well as to the severity of the present fault.

The proposed approach exhibits the following advantages:

- The CI can be implemented without any prior characterisation of the PEM fuel cell under various fault conditions. The required copula structure is constructed from data acquired solely from measurements under fault-free operation.
- The estimates of the PDFs' parameters and the transformation of the impedance data into uniform random variables exist in closed form.
- Once the copula structure is constructed, the CM algorithm is computationally efficient.

The validation of the proposed CI was performed on an industrial-grade PEM fuel cell power system. The fuel cells were subjected to water management faults. The validation procedure confirmed that the CI is able to detect presence of faults and that its value is also related to the severity of the faults. However, the applicability of the proposed approach is not limited either to PEM fuel cells or to water management faults. It can be applied in an unmodified form wherever the fast impedance estimation method is applicable.

This chapter includes the following publication:
Mileva Boshkoska, B., Boškoski, P., Debenjak, A., & Juričić, Đ. (2015). Dependence among complex random variables as a fuel cell condition indicator. *Journal of Power Sources*, *284*, 566–573. doi:10.1016/j.jpowsour.2015.03.044

Journal of Power Sources 284 (2015) 566–573

Contents lists available at ScienceDirect

Journal of Power Sources

journal homepage: www.elsevier.com/locate/jpowsour

Dependence among complex random variables as a fuel cell condition indicator

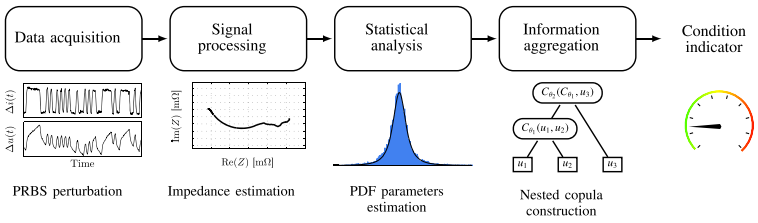
Biljana Mileva Boshkoska [a, b, *], Pavle Boškoski [b], Andrej Debenjak [b, c], Đani Juričić [b]

[a] Faculty of Information Studies, Ulica talcev 3, SI-8000 Novo mesto, Slovenia
[b] Jožef Stefan Institute, Jamova cesta 39, SI-1000 Ljubljana, Slovenia
[c] Jožef Stefan International Postgraduate School, Jamova cesta 39, SI-1000 Ljubljana, Slovenia

HIGHLIGHTS

- A condition indicator for fault detection in PEM fuel cells is proposed.
- The condition indicator is constructed from a set of fuel cell impedance values.
- Individual impedance values are treated as dependent complex random variables.
- Copula functions aggregate the impedance values into the condition indicator.
- Indicator's sensitivity to water management faults is experimentally validated.

GRAPHICAL ABSTRACT



ARTICLE INFO

Article history:
Received 10 July 2014
Received in revised form
4 March 2015
Accepted 6 March 2015
Available online 11 March 2015

Keywords:
PEM fuel cell
Condition monitoring
Flooding
Drying
Dependence structure
Copula functions

ABSTRACT

As various faults alter the PEM fuel cell impedance characteristic over a broad frequency range, the electrochemical impedance spectroscopy is frequently employed for the purpose of condition monitoring. The proposed methodology treats the impedance components among different frequencies as dependent complex random variables. The information about fuel cell condition is incorporated into the dependence structure of these complex random variables. This dependence is described through the corresponding joint cumulative density function by employing copula functions. The benefits of such an approach are threefold: (i) the estimation of the joint cumulative density function requires only several measurements of a fuel cell in a fault-free condition, (ii) the procedure is computationally efficient, and (iii) the output of the copula function is directly used as an overall unit-free condition indicator. The approach was evaluated on a kW-range PEM fuel cell stack subjected to water management faults of various severities. The results show that the ci corresponds with the severity of the induced faults.

© 2015 Elsevier B.V. All rights reserved.

1. Introduction

A proton exchange membrane (PEM) fuel cell is an electrochemical device that converts the chemical energy of hydrogen directly into electrical energy [1]. When both electricity and heat are utilised in a cogeneration system, the overall efficiency of such a system can reach up to 90% [2]. However, the large-scale market

* Corresponding author. Faculty of Information Studies, Ulica talcev 3, SI-8000 Novo mesto, Slovenia.
E-mail address: biljana.mileva@unm.fis.si (B. Mileva Boshkoska).

http://dx.doi.org/10.1016/j.jpowsour.2015.03.044
0378-7753/© 2015 Elsevier B.V. All rights reserved.

penetration of PEM fuel cell technology is still impeded due to the durability and reliability issues of the technology [3–5]. Studies conducted over the last two decades have pointed out several kinds of faults influencing the optimal exploitation of PEM fuel cell systems [6,7]. These faults include corrosion of the electrodes and degradation of membranes [8–11], catalyst and membrane poisoning [12–15], and water management faults (i.e., flooding of gas channels and membrane drying) [16–18]. Detection of these faults can be achieved by employing effectual diagnostics techniques [19,20]. Such effective diagnostic information can be beneficial in various applications [21–23].

The majority of faults occurring in a PEM fuel cell affect its impedance characteristic. Consequently, the faults can be detected with a multitude of approaches based on electrochemical impedance spectroscopy (EIS) [24–28]. EIS is a technique of analysing electrochemical device through measurements of its electrical impedance characteristic. Typically, small-amplitude electrical current perturbation signals in the form of sine waves are applied to the fuel cell. By measuring the voltage response of the fuel cell, the impedance characteristic can be easily estimated [29]. In the field of PEM fuel cells, the EIS technique was already proven to be effective in detecting fuel cell flooding, membrane drying, and anode poisoning [30–35].

Despite the effectiveness of the EIS technique, current implementations have three major drawbacks:

1. The application of sine waves as perturbation signals covering a wide frequency region is time-consuming, hence inappropriate for online condition monitoring (CM).
2. Determining appropriate threshold values requires a priori characterisation of a fuel cell, which in many cases is infeasible.
3. Performing EIS characterisation over a large number of frequencies results in a feature set with large cardinality. Therefore, specifying a single overall value describing the fuel cell condition is of significant practical merit.

The first issue can be resolved by employing a pseudo-random binary sequence (PRBS) perturbation signal and continuous wavelet transform (CWT) [36], which significantly decreases the time for impedance estimation. In an attempt to address the second issue, Boškoski and Debenjak [37] provided a solution in which the individual impedance components are treated as complex random variables. Consequently, the probability density functions (PDFs) of the complex impedance components at a particular frequency exist and were mathematically derived [37]. The corresponding threshold values were determined by specifying the probability of false alarm (PFA). This study deals with the third issue by treating the impedance values at individual frequencies as dependent complex random variables. Using copula functions, their joint cumulative distribution function (CDF) is estimated and used to calculate the fuel cell condition indicator (CI). The complete condition monitoring process, from the data acquisition to the calculation of the CI, is shown in Fig. 1.

Since the fuel cell condition affects the impedance components over a broad frequency range, in the statistical context, this implies that the complex impedance values at various frequencies should be regarded as dependent random variables. An appropriate description of the dependence among random variables is their multidimensional joint CDF. Specifying the joint CDF is a difficult task especially for a large number of dimensions [38], such as the issue at hand. Copula functions offer a solution to this problem by estimating the joint CDF using the marginal distributions. In the context of EIS, the marginal distributions are the CDFs of impedance at specific frequencies of interest. The multivariate joint CDF, specified in such a way, is capable of describing various types of dependences, including nonlinear ones. So far, copulas were successfully applied in the petroleum industry [39], finance [40,41], hydrology [42], biology [43], change detection in images [44], quality control [45], and machine learning [46]. To the authors' knowledge, this is the first application of this concept for condition monitoring of fuel cell systems.

The application of this concept has three practical merits. First, the initial estimation of the fault-free multivariate joint CDF is time efficient since it relies only on several measurements acquired while a fuel cell is in a fault-free condition. Second, the evaluation process is computationally efficient, which makes it suitable for implementation as an online CM system. Finally, as the copula function itself is a CDF, its output is a probability of observing a particular impedance characteristic. Therefore, the output is regarded as a unit-free CI describing the overall fuel cell condition.

The paper is organised as follows: Section 2 presents the way features are generated and discusses the statistical properties of the complex impedance values. The concept of copula functions is presented in Section 3. The complete CI computation process is presented in Section 4. Finally, Section 5 presents the evaluation results of the proposed technique, employed on an 8.5 kW fuel cell stack.

2. Feature set

The straightforward approach for impedance estimation is to excite the fuel cell using sine current excitation signal $i(t)$ with frequency f_0 and to measure the corresponding voltage signal $u(t)$. The impedance $Z(f_0)$ is then calculated as a ratio between the Fourier transform coefficients of the two signals [29]:

$$Z(f_0) = \left.\frac{\mathscr{F}[u(t)]}{\mathscr{F}[i(t)]}\right|_{f_0} \tag{1}$$

In order to cover a broad frequency range, the sine signals have to be separately generated and applied for each frequency of interest, which is time inefficient. An attempt to overcome this issue is by using compound multisine signals [47]. However, even in such a case, the impedance values are calculated only at discrete frequencies that are present in the generated multisine signal.

2.1. Impedance estimation with PRBS and CWT

In order to jointly cover a broad frequency range and perform the required measurements in a reasonably short time period, a broadband excitation is required. In this study, the PRBS signal is used as proposed by Debenjak et al. [36]. The PRBS can be regarded as sufficiently close to stationary random noise, and in a predefined frequency band, it exhibits power spectral density similar to the one of the white noise. Furthermore, the amplitudes of its frequency components have Gaussian distribution [48].

Using such an excitation signal, the Fourier analysis is unable to describe transient phenomena, located in a narrow time interval. Therefore, it is necessary to perform time-frequency analysis for the estimation of the impedance. The possible candidates are the short-time Fourier transform or wavelet transform. The former offers only fixed time-frequency resolution, whereas the latter one allows flexibility in the time-frequency resolution by interchangeably achieving good time resolution for the high-frequency events, and good frequency resolution for the low-frequency events. Therefore, in this study, the CWT approach based on the Morlet mother wavelet was employed for the impedance estimation. With properly tuned CWT parameters, this approach provides reliable impedance results along the entire frequency band. Additionally, it yields statistical information about the confidence interval of the

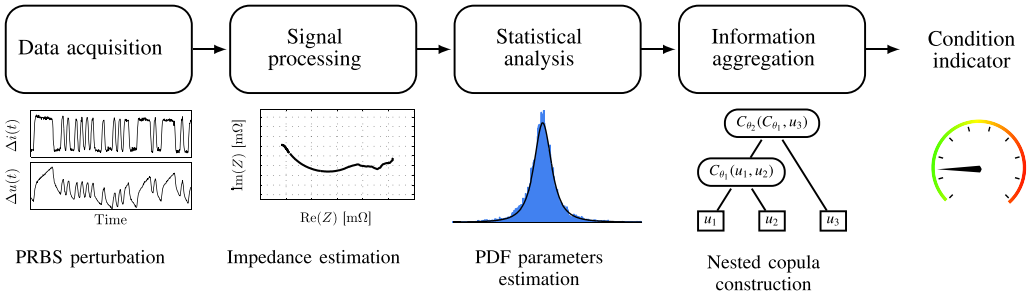


Fig. 1. Schematic representation of the complete condition monitoring process.

impedance measurement.

The process of impedance estimation starts by superimposing the PRBS on the DC current $i_{dc}(t)$ supplied by the fuel cell. As a result, the fuel cell responds with the corresponding voltage $u(t)$ signal, which is directly related to the cell impedance. Performing the CWT with the Morlet mother wavelet on both $i(t)$ and $u(t)$ signals results in two sets of complex wavelet coefficients:

$$\begin{aligned} Wi(\tau,s) &= \langle i(t), \psi_{\tau,s}(t)\rangle = \int_{-\infty}^{\infty} i(t)\psi^*_{\tau,s}(t)\mathrm{d}t, \\ Wu(\tau,s) &= \langle u(t), \psi_{\tau,s}(t)\rangle = \int_{-\infty}^{\infty} u(t)\psi^*_{\tau,s}(t)\mathrm{d}t, \end{aligned} \tag{2}$$

where $\psi_{\tau,s}(t)$ is the translated and scaled version of the Morlet wavelet [49]:

$$\psi_{\tau,s}(t) = \frac{1}{\sqrt{s}}\psi\left(\frac{t-\tau}{s}\right) \tag{3}$$

and

$$\psi(t) = \pi^{-1/4}\left(e^{-j\omega_0 t} - e^{-\omega_0^2/2}\right)e^{-t^2/2}. \tag{4}$$

The relation between scale s and frequency f reads as follows:

$$\frac{1}{f} = \frac{4\pi s}{\omega_0 + \sqrt{2+\omega_0^2}} \tag{5}$$

and, since the translation τ directly corresponds to time t, the impedance $z(t,f)$ is calculated as a ratio of the corresponding complex wavelet coefficients (2) [36]:

$$z(t,f) = \frac{Wu(t,f)}{Wi(t,f)}. \tag{6}$$

This segment of the condition monitoring process is presented by the first two modules in Fig. 1.

2.2. Probability distribution function of impedance at individual frequency

By treating the fuel cell as a piecewise linear system, the response to such an excitation preserves the statistical properties of the PRBS excitation signal. Since the CWT is a linear transformation, the signal's properties are preserved in the calculated wavelet coefficients. Therefore, the wavelet coefficients (2) should be regarded as random variables as well.

In order to perform a statistical analysis of the impedance components, the PDF of the impedance components at a particular frequency $z(t,f)|_{f=f_0}$ has to be determined. This is a two-step process. First, the PDFs of the wavelet coefficients (2) have to be derived. Second, the PDF of their ratio (i.e., $z(t,f)|_{f=f_0}$ has to be derived in a closed form, bearing in mind that wavelet coefficients $Wi(t,f)$ and $Wu(t,f)$ are dependent complex random variables.

The wavelet coefficients $Wi(t,f)$ and $Wu(t,f)$ can be rewritten as

$$\begin{aligned} Wi(t,f) &= \Re\{Wi(t,f)\} + j\Im\{Wi(t,f)\}, \\ Wu(t,f) &= \Re\{Wu(t,f)\} + j\Im\{Wu(t,f)\}. \end{aligned} \tag{7}$$

Since the voltage $u(t)$ is the fuel cell response to the current excitation $i(t)$, and the excitation has the shape of PRBS, these coefficients are dependent zero-mean Gaussian circular complex random variables [37,50]:

$$\begin{aligned} \Re\{Wi(t,f)\}, \Im\{Wi(t,f)\} &\sim \mathcal{N}\left(0, \frac{\sigma_i^2}{2}\right) \\ \Re\{Wu(t,f)\}, \Im\{Wu(t,f)\} &\sim \mathcal{N}\left(0, \frac{\sigma_u^2}{2}\right). \end{aligned} \tag{8}$$

Under these conditions, the PDF of the complex impedance (6) at a particular frequency f_0 reads as follows [37]:

$$p_Z(z) = \frac{1-|\rho|^2}{\pi\sigma_u^2\sigma_i^2}\left(\frac{|z|^2}{\sigma_u^2} + \frac{1}{\sigma_i^2} - 2\frac{\rho_r z_r - \rho_i z_i}{\sigma_u\sigma_i}\right)^{-2}, \tag{9}$$

where z_r and z_i are real and imaginary components and $\rho = \rho_r + j\rho_i$ is a complex correlation coefficient, such that $|\rho| \le 1$. For the purpose of condition monitoring, the module $|z|$ of the complex impedance is of particular interest. Under the same assumption for the stochastic nature of the impedance z, the PDF of its module reads as follows [37]:

$$p_{|Z|}(|z|) = \frac{2\sigma_i^2\sigma_u^2(1-\rho^2)|z|(\sigma_i^2|z| + \sigma_u^2)}{\left[\left(\sigma_i^2|z|^2 + \sigma_u^2\right)^2 - 4\rho^2\sigma_u^2\sigma_i^2|z|^2\right]^{3/2}}, |z| \ge 0, \tag{10}$$

where $|\rho| \le 1$ is the correlation coefficient. The CDF of $|z|$ reads as follows [51]:

$$P_{|Z|}(z) = \frac{1}{2} - \frac{\sigma_u^2 - z^2\sigma_i^2}{2\sqrt{4z^2(1-\rho^2)\sigma_i^2\sigma_u^2 + \left(\sigma_u^2 - z^2\sigma_i^2\right)^2}}, \tag{11}$$

where $z \ge 0$.

The parameters σ_u, σ_i and the correlation coefficient ρ can be estimated through the calculated wavelet coefficients as [52,53]:

$$E\{Wu(t,f_0)Wu(t,f_0)^*\} = \frac{\sigma_u^2}{2}$$
$$E\{Wi(t,f_0)Wi(t,f_0)^*\} = \frac{\sigma_i^2}{2} \quad (12)$$
$$E\{Wi(t,f_0)Wu(t,f_0)^*\} = \frac{\sigma_u\sigma_i}{2}\rho.$$

2.3. Dependence structure among the impedance components

The deterioration of the fuel cell condition alters the impedance characteristic over a wide frequency range. Since the impedance at individual frequency is a random variable, the impedance values should be regarded as dependent random variables. Therefore, in order to properly determine the presence and the root cause of the fault, the overall change in the impedance characteristics has to be characterised. A proper way of describing the joint behaviour of random variables is through the corresponding joint CDF. In this study, the joint CDF is estimated by using copula functions.

3. Basics of copula functions

The joint PDF of two continuous random variables X_1 and X_2 is equal to:

$$p_{X_1,X_2}(x_1,x_2) = p_{X_2|X_1}(x_2|x_1)p_{X_1}(x_1) = p_{X_1|X_2}(x_1|x_2)p_{X_2}(x_2), \quad (13)$$

where $p_{X_1}(x_1)$ and $p_{X_2}(x_2)$ are the marginal PDFs, and $p_{X_1|X_2}(x_1|x_2)$ and $p_{X_2|X_1}(x_2|x_1)$ are the corresponding conditional PDFs. The marginal distributions either are known or can be easily estimated from the available data. On the other hand, when x_1 and x_2 are dependent, the conditional PDFs are generally unknown and are usually difficult to estimate. Consequently, the derivation of the joint PDF is not trivial. An elegant way to connect the marginal PDFs of the random variables with their joint PDF is given through copulas.

3.1. Copula functions

For two random variables X_1 and X_2, which are defined on the same probability space, the joint CDF $P_{X_1,X_2}(x_1,x_2)$ defines the probability of events in terms of the simultaneous occurrences of X_1 and X_2. An explicit estimation of the joint CDF is a difficult task due to possibly complicated forms and the dimensionality issues [38]. Copulas simplify this process by expressing the joint CDF of dependent random variables as a function of their marginal distributions.

A bivariate copula function C:$[0,1]^2 \rightarrow [0,1]$ is an aggregation function that satisfies [54]:

1. $C(x,0) = C(0,x) = 0$ and $C(x,1) = C(1,x) = x$ for all $x \in [0,1]$ (boundary conditions);
2. $C(x_1,y_1) - C(x_1,y_2) - C(x_2,y_1) + C(x_2,y_2) \geq 0$, for all $x_1,y_1,x_2,y_2 \in [0,1]$ such that $x_1 \leq x_2$ and $y_1 \leq y_2$ (2-increasing property).

Let the two random variables X_1 and X_2 have marginal CDFs $P_{X_1}(x_1)$ and $P_{X_2}(x_2)$, respectively, and joint CDF $P_{X_1,X_2}(x_1,x_2)$. According to Sklar's theorem [54,55], there exists a multivariate CDF $C_\theta(u,v)$, where θ is a parameter that has to be estimated, and u and v are uniformly distributed random variables on the unit interval [0,1]. Therefore, the joint CDF $P_{X_1,X_2}(x_1,x_2)$ reads as follows:

$$P_{X_1,X_2}(x_1,x_2) = C_\theta(P_{X_1}(x_1),P_{X_2}(x_2)) = C_\theta(u,v), \quad (14)$$

where u and v are obtained by using the inverse probability integral transform [56]:

$$\begin{aligned} u &= P_{X_1}(x_1), \quad u \sim \mathscr{U}(0,1), \\ v &= P_{X_2}(x_2), \quad v \sim \mathscr{U}(0,1). \end{aligned} \quad (15)$$

From (14), it follows that copula $C_\theta(u,v)$ is a function that couples the marginal CDFs $P_{X_1}(x_1)$ and $P_{X_2}(x_2)$ of the random variable $X = (X_1,X_2)$ with its joint distribution $P_{X_1,X_2}(x_1,x_2)$.

From the large collection of bivariate copulas, the paper addresses the Archimedean family, where copulas are constructed by using the following relation [57]:

$$C_\theta(u,v) = \varphi_\theta^{[-1]}(\varphi_\theta(u) + \varphi_\theta(v)) \quad (16)$$

where $u = P_{X_1}(x_1)$, $v = P_{X_2}(x_2)$, and $\varphi\theta(\cdot)$ is called a generator function and $\varphi_\theta^{[-1]}(\cdot)$ is

$$\varphi_\theta^{[-1]}(t) = \begin{cases} \varphi_\theta^{-1}(t), & \text{if} \quad 0 \leq t \leq \varphi_\theta(0); \\ 0, & \text{if} \quad \varphi_\theta(0) \leq t \leq \infty. \end{cases} \quad (17)$$

The generator function $\varphi_\theta(t)$:$[0,1] \rightarrow [0,\infty]$ must be continuous and strictly decreasing. Table 1 shows different types of Archimedean copulas constructed with the different generators $\varphi_\theta(t)$ [54]. Each of the families in Table 1 describes a different dependence structure. The selection is performed intuitively, as shown in Fig. 2, Clayton and Gumbel copulas exhibit best results in the tails of the distribution, while Frank copula performs best under the bell of the distribution.

3.2. From bivariate to multivariate copulas

The copula, as defined by (14), couples two random variables into their joint CDF, hence the name bi-variate copula. However, majority of problems are multidimensional, and thus, the bivariate copulas should be extended to accommodate multidimensional cases. There are two approaches to extending to higher dimensional copulas [40,58]:

1. The first approach extends the bivariate copula to multivariate copula using only one dependence parameter θ. Such copulas are known as exchangeable Archimedean copulas [59]. The main drawback is that copulas for higher dimensions are tedious to derive [60].
2. The second approach uses bivariate copulas to form a hierarchical structure with at most $n-1$ dependence parameters θ_i for n random variables. This construction of multivariate copulas is called fully nested Archimedean copula (FNAC) [59,61].

As shown in Fig. 3, FNAC is a treelike structure that is obtained using an iterative procedure that starts with coupling two random

Table 1
Archimedean copulas.

	$C_\theta(u,v)$	$\varphi_\theta(t)$	Solve$\left(\frac{\partial C_\theta(u,v)}{\partial u} = q, v\right)$
Clayton	$[\max(u^{-\theta} + v^{-\theta} - 1, 0)]^{-1/\theta}$	$1/\theta(t^{-\theta} - 1)$	$\left(1 - u^{-\theta} + (qu^{1+\theta})^{-\frac{\theta}{1+\theta}}\right)^{-\frac{1}{\theta}}$
Frank	$-\frac{1}{\theta}\ln\left(1 + \frac{(e^{-\theta u}-1)(e^{-\theta v}-1)}{e^{-\theta}-1}\right)$	$-\ln\frac{e^{-\theta t}-1}{e^{-\theta}-1}$	$\frac{1}{\theta}\log\frac{-e^\theta(1-q+qe^{\theta u})}{-e^\theta+qe^\theta-qe^{\theta u}}$
Gumbel-Hougaard	$\exp(-[(\ln u)^\theta + (-\ln v)^\theta]^{1/\theta})$	$\ln\frac{1-\theta(1-t)}{t}$	Only numerical solution

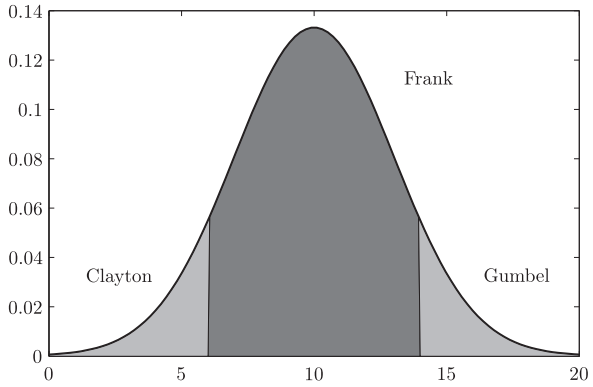


Fig. 2. Regions of best performance for different Archimedean copulas.

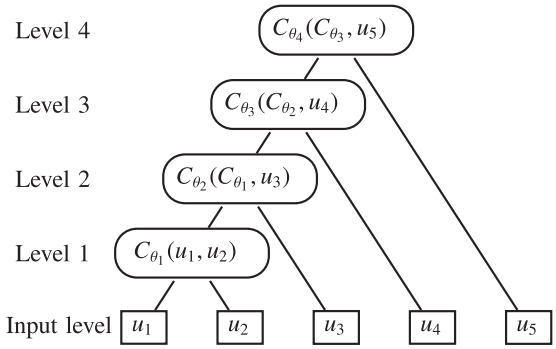


Fig. 3. Fully nested Archimedean copula.

variables. For this particular FNAC structure, u_1 and u_2 are coupled into copula $C_{\theta_1}(u_1, u_2)$ with parameter θ_1. In all subsequent iterations, the obtained copula is coupled with a new random variable; for example, copula C_{θ_1} is coupled with u_3 into $C_{\theta_2}(C_{\theta_1}, u_2)$ with parameter θ_2 and so on. The final output of the topmost copula reads

$$C_{\theta_4}(u_1, u_2, u_3, u_4, u_5) = C_{\theta_4}\left(u_5, C_{\theta_3}\left(u_4, C_{\theta_2}\left(u_3, C_{\theta_1}(u_1, u_2)\right)\right)\right). \tag{18}$$

Generally, an FNAC structure with n input variables has $n-1$ parameters θ_i. The final function (18) represents a valid copula only if the following condition is fulfilled [62]:

$$\theta_1 > \theta_2 > \cdots > \theta_{n-1} \tag{19}$$

where θ_1 is the parameter of the most nested copula, θ_2 is the parameter of the second most nested copula, and so on. The estimations of the values of $\theta_i, i = 1,\ldots,n-1$ are obtained using the maximum likelihood algorithm.

Sometimes, it is not possible to build an FNAC structure that satisfies condition (19) for the desired order of variables in the FNAC. In such a case, a valid FNAC could be found in the set of all FNACs obtained by permuting the order of the variables entering the FNAC [63].

4. Condition indicator formation

The process of computing the CI by using the impedance joint CDF is composed of several steps. First, from the available frequency range, a low cardinality frequency set is selected, in a way that the fuel cell characteristic is preserved. Second, the impedance values (6) are calculated at the selected frequencies by using CWT (2). Afterwards, the parameters of the PDFs (9) and (10) are estimated by employing relation (12). It has to be noted that for each frequency f_i, the PDF of the wavelet coefficients (2) has different parameters. As a result, n different sets of parameters are calculated, one for each frequency f_i. In order to use the copula concept, the selected impedance values are transformed into a uniform random variable by using the CDF (11). Finally, the CI is computed as the output of the estimated multivariate copula.

4.1. Selection of the appropriate frequencies

Impedance values (6) are calculated on a broad frequency range. The results are represented by a Nyquist plot, as shown in Fig. 4. Usually, the number of selected frequencies is quite large, which leads to a high cardinality feature set. The first step is to reduce the number of features while at the same time preserving the necessary diagnostic information.

In the context of PEM fuel cells, the shape of the Nyquist plot suggests that the characteristic is predominantly capacitive, and it embodies two depressed semicircles, as shown in Fig. 4:

- The low-frequency one, $f \leq 5$ Hz, which is attributed to diffusion processes
- The high-frequency semicircle, $f > 5$ Hz, which is attributed to kinetic processes

Therefore, it is reasonable to choose a similar number of impedance values from both frequency regions sampled at logarithmically equal intervals. As a result, the final feature set comprises $N_f = 10$ impedance values that preserve the information about the impedance shape. This feature set with reduced cardinality is subsequently used for the estimation of the fuel cell condition. A possible future improvement of the feature selection process can be achieved by employing, for instance, correlation-based feature selection methods, sequential forward (backward) feature selection, or minimum redundancy maximum relevance feature selection [64,65].

4.2. Estimating the copula parameters

First, the impedance is calculated by using the measured current $i(t)$ and voltage $u(t)$ signals. For each measurement, a complex

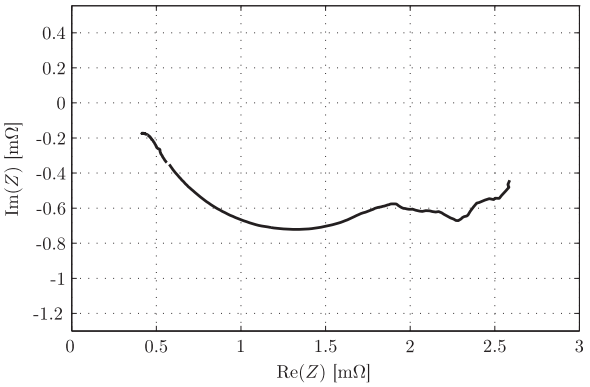


Fig. 4. Nyquist plot of the PEM fuel cell impedance.

matrix $Z(t,f)$ is obtained as a result of the CWT (6), which represents the instantaneous amplitude and phase of the impedance at each time moment over the selected frequency range. The complex matrix $Z(t,f)$ has dimensions $m \times N_f$, where m is the number of time moments at which $u(t)$ and $i(t)$ were measured, in the case at hand, $m = 40{,}000$, $N_f = 10$.

By using the calculated impedance values at each of the selected frequencies f_i, $i = 1,\ldots,N_f$, the corresponding parameters (12) of the CDFs are estimated. Afterwards, using the corresponding CDF, each value of the matrix $Z(t,f)$ is transformed into its uniform feature. As a result, a matrix $\mathbf{U}$ with dimension $m \times N_f$ is obtained. Finally, the copula θ_i parameters (19) are estimated by employing the matrix $\mathbf{U}$.

4.3. Copula output as a fuel cell condition indicator

Since the copula function is a CDF, its output is a probability of observing a particular combination of uniformly distributed values $\mathbf{U} = [u_1, \ldots, u_{N_f}]$. Through the experiment, for each measurement sequence q, an FNAC structure is built using uniform matrix $\mathbf{U}_q$. The process is shown in Fig. 5.

The calculated values from the initial fault-free measurements $q = 1$ are used as a baseline for CI. Since a deterioration in the condition will alter the impedance statistical characteristics, for the initially calculated copula, such a state will be regarded as a random event with a low likelihood. The low likelihood events (i.e., faults) lie in the tails of the PDF. As the output of CDFs is the probability $P[U \leq u]$, the output of the copula will be close to one for events that lie in the tail that is in the $(+,+,\ldots,+)$ hyperoctant.[1] On the other hand, the output of the copula will be close to zero for events that lie in the tail that is in the $(-,-,\ldots,-)$ hyperoctant. For a two-dimensional PDF, the $(+,+)$ quadrant is marked with 1 and the $(-,-)$ quadrant is marked with 2 in Fig. 6. The CI baseline will be located somewhere in between.

5. Evaluation results

For the purpose of evaluation of the proposed approach, a set of $q \in [1,105]$ impedance characteristics were estimated, each based on 40-s measurements. Fig. 7 shows an example of the measured current $i(t)$ and voltage $u(t)$ signals, which were further used for feature extraction.

5.1. Experimental procedure

The experiment was performed on a commercially available PEM fuel cell system HyPM HD 8 produced by the Hydrogenics Corporation. The stack consists of 80 PEM fuel cells, each with surface area of 200 cm^2, providing 8.5 kW of electric power in total. The fuel cell system operates on pure hydrogen and ambient air. The impedance was measured on individual cells of the stack, where the PRBS perturbation signal was applied in galvanostatic mode.

During the experiment, the fuel cell system was kept at constant operating and environmental conditions at a temperature of 50 °C, stoichiometry 2.5. The temperature of the airflow was kept constant at 50 °C, and the relative humidity was controlled in order to introduce drying or flooding conditions. At the anode side, the fuel cell was fed with pure and dry hydrogen at a constant temperature of 20 °C. The DC current operating point I_{dc} was set to 70 A, resulting in the stack voltage of 55 V, whereas the amplitude of the superposed PRBS waveform was set to 2 A.

[1] The notation $(+,+,\ldots,+)$ specifies the area determined by positive semiaxes in all dimensions. A two-dimensional special case is shown in Fig. 6.

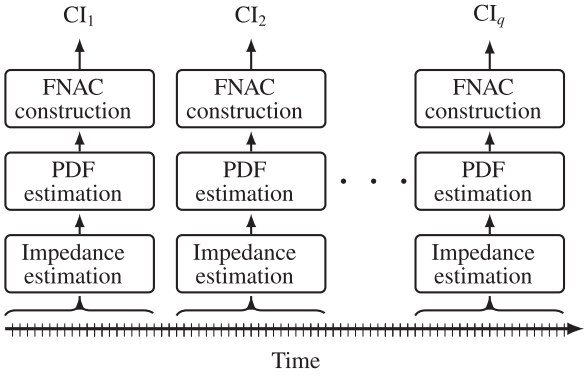


Fig. 5. Measurement sequences in time.

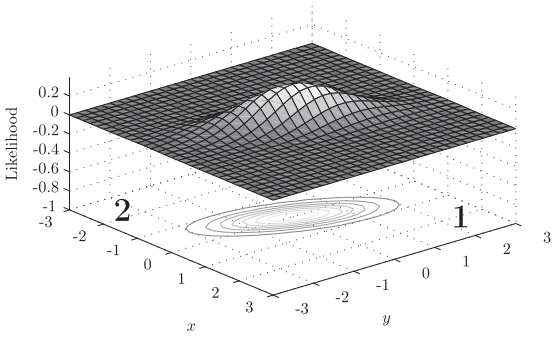


Fig. 6. Description of the regions for high and low copula outputs.

The experiment went through five stages. In the first stage of approximately 11 min, 18 measurement sets were acquired in the fault-free state at which the relative humidity of the inlet air was kept at 9%. Then air fed to the fuel cell was slightly dried down to a relative humidity of 5% for about 10 min, between the 12th and the 22nd min, in order to induce membrane drying, and again humidified to 9%. Afterwards, between the 34th and the 58th minute, saturated air with a relative humidity of 100% was fed into the fuel cell system, inducing the flooding of fuel cells. Finally, the air humidity was decreased down to the initial 9%. Using such a cycle, the response of the fuel cell under different fault scenarios with various fault severities was evaluated.

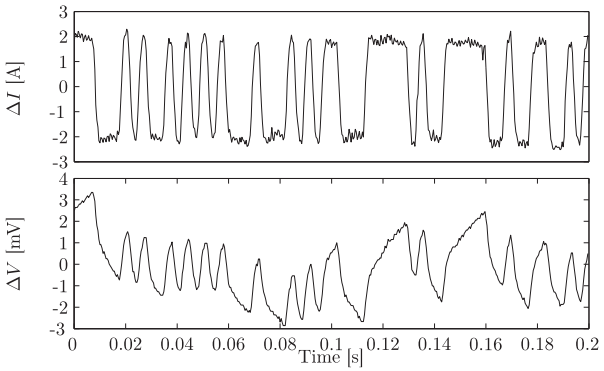


Fig. 7. Example of current and voltage signals during the experiment.

5.2. Time evolution of condition indicator

Following the procedure described in Section 4, the CI was computed for each of the $q \in [1,105]$ measurements. The time evolution of the CI is presented in Fig. 8, where the experiment time is represented on x-axis.

At the beginning of the experiment, the copula value defines the CI baseline of a fault-free condition. Dry inlet air of 5% relative humidity causes fuel cells to dry out, hence the increase of the CI. This indicates that some of the impedance components changed, and consequently, the observed measurements belong to a low likelihood tail. On the other hand, the saturated inlet air with a relative humidity of 100% causes the flooding of fuel cells. As a result, the CI reaches almost zero. At the end of the experiment, the humidity of the inlet air was set back to nominal values, resulting in fuel cell recovery, causing the CI to return to the baseline values similar to the ones from the beginning of the experiment.

It has to be noted that the experiment was performed on an industrial-grade fuel cell system. As such, the built-in controls managed various parameters such as air and fuel flow (stoichiometry) as well as temperature. Therefore, these parameters were not strictly held within sharp boundaries with laboratory precision. As a result, some fluctuations can be observed in the CI values throughout the experiment (Fig. 8). Regardless of these fluctuations, the fault regions are distinctly visible, which confirms the link between CI and the actual fuel cell condition.

The results show that the proposed CI (i.e., copula output) can also be directly related to the fault severity. The departure of the copula values for the drying fault from the baseline level is smaller compared with the copula values during the flooding fault, which corresponds to the induced fault severity.

6. Conclusion

This paper presents an approach for fuel cell condition monitoring by employing PRBS excitation signals, CWT for impedance estimation and copula functions for information fusion. The calculated large cardinality feature set comprises dependent complex random variables, which represent fuel cell impedance at individual frequencies. The fuel cell condition is hidden in the dependence structure of these complex random variables. The application of copula functions allows the proper characterisation of the dependence by estimating the multidimensional joint CDF. Therefore, the CI, defined as the output of the copula structure, is a probability of observing particular impedance values and is directly related to the fuel cell condition as well as the severity of the present fault.

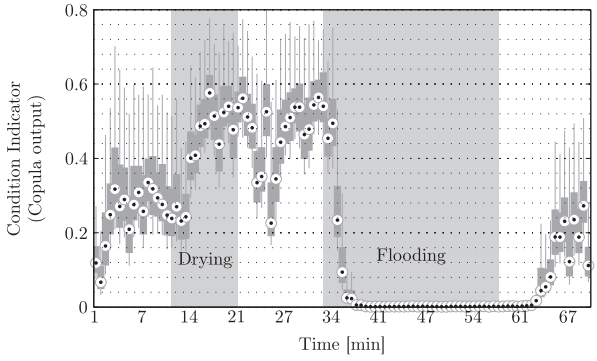


Fig. 8. Evolution of the health index (copula output).

The proposed approach has several practical merits. First, for the purpose of fault detection, the proposed CI can be implemented without any prior characterisation of the fuel cell under various faults. The CI baseline can be estimated from data acquired solely from measurements under a fault-free operation. Second, the approach is computationally efficient. Finally, the estimation of PDF parameters and the transformation of the acquired data into uniform random variables exist in closed form. This makes the proposed approach a suitable solution for an embedded condition monitoring system.

The applicability of the proposed approach is not limited either to PEM fuel cells or to water management faults. It can be applied in an unmodified form wherever the EIS approach is applicable.

Acknowledgements

The work is supported by the Creative Core FISNM-3330-13-500033 "Simulations" project funded by the European Union, the European Regional Development Fund. The authors also acknowledge the financial support of the Slovenian Research Agency through the Research Programme P2-0001.

References

[1] F. Barbir, PEM Fuel Cells: Theory and Practice, Elsevier, 2005.
[2] V. Jovan, M. Perne, J. Petrovčič, Energ. Convers. Manage. 51 (2010) 2467–2472.
[3] J. Wu, X.Z. Yuan, J.J. Martin, H. Wang, J. Zhang, J. Shen, S. Wu, W. Merida, J. Power Sources 184 (2008) 104–119.
[4] X.-Z. Yuan, H. Li, S. Zhang, J. Martin, H. Wang, J. Power Sources 196 (2011) 9107–9116.
[5] M. Fowler, R.F. Mann, J.C. Amphlett, B.A. Peppley, P.R. Roberge, Reliability Issues and Voltage Degradation, John Wiley & Sons, Ltd, 2005.
[6] F.A. de Bruijn, V.A.T. Dam, G.J.M. Janssen, Fuel Cells 8 (2008) 3–22.
[7] W. Schmittinger, A. Vahidi, J. Power Sources 180 (2008) 1–14.
[8] H.R. Colón-Mercado, B.N. Popov, J. Power Sources 155 (2006) 253–263.
[9] R. Borup, J. Meyers, B. Pivovar, Y.S. Kim, R. Mukundan, N. Garland, D. Myers, M. Wilson, F. Garzon, D. Wood, P. Zelenay, K. More, K. Stroh, T. Zawodzinski, J. Boncella, J.E. McGrath, M. Inaba, K. Miyatake, M. Hori, K. Ota, Z. Ogumi, S. Miyata, A. Nishikata, Z. Siroma, Y. Uchimoto, K. Yasuda, K.-i. Kimijima, N. Iwashita, Chem. Rev. 107 (2007) 3904–3951.
[10] P.T. Yu, Z. Liu, R. Makharia, J. Electrochem. Soc. 160 (2013) F645–F650.
[11] J.D. Fairweather, D. Spernjak, A.Z. Weber, D. Harvey, S. Wessel, D.S. Hussey, D.L. Jacobson, K. Artyushkova, R. Mukundan, R.L. Borup, J. Electrochem. Soc. 160 (2013) F980–F993.
[12] C. Farrell, C. Gardner, M. Ternan, J. Power Sources 171 (2007) 282–293.
[13] X. Cheng, Z. Shi, N. Glass, L. Zhang, J. Zhang, D. Song, Z.-S. Liu, H. Wang, J. Shen, J. Power Sources 165 (2007) 739–756.
[14] W.-M. Yan, H.-S. Chu, M.-X. Lu, F.-B. Weng, G.-B. Jung, C.-Y. Lee, J. Power Sources 188 (2009) 141–147.
[15] G. Postole, A. Auroux, Int. J. Hydrogen Energy 36 (2011) 6817–6825.
[16] H. Li, Y. Tang, Z. Wang, Z. Shi, S. Wu, D. Song, J. Zhang, K. Fatih, J. Zhang, H. Wang, Z. Liu, R. Abouatallah, A. Mazza, J. Power Sources 178 (2008) 103–117.
[17] N. Yousfi-Steiner, P. Moçotéguy, D. Candusso, D. Hissel, A. Hernandez, A. Aslanides, J. Power Sources 183 (2008) 260–274.
[18] T. Ous, C. Arcoumanis, J. Power Sources 240 (2013) 558–582.
[19] M. Jouin, R. Gouriveau, D. Hissel, M.-C. Péra, N. Zerhouni, Int. J. Hydrogen Energy 38 (2013) 15307–15317.
[20] M. Jouin, R. Gouriveau, D. Hissel, M.-C. Péra, N. Zerhouni, Int. J. Hydrogen Energy 39 (2014) 481–494.
[21] B. Pregelj, D. Vrečko, V. Jovan, J. Power Sources 196 (2011) 9419–9428.
[22] A.J. Verhage, J.F. Coolegem, M.J. Mulder, M.H. Yildirim, F.A. de Bruijn, Int. J. Hydrogen Energy 38 (2013) 4714–4724.
[23] B. Pregelj, D. Vrečko, J. Petrovčič, V. Jovan, G. Dolanc, Appl. Energy 137 (2015) 64–76.
[24] X.-Z. Yuan, H. Wang, J.C. Sun, J. Zhang, Int. J. Hydrogen Energy 32 (2007) 4365–4380.
[25] J. Wu, X.Z. Yuan, H. Wang, M. Blanco, J.J. Martin, J. Zhang, Int. J. Hydrogen Energy 33 (2008) 1735–1746.
[26] R. Petrone, Z. Zheng, D. Hissel, M. Péra, C. Pianese, M. Sorrentino, M. Becherif, N. Yousfi-Steiner, Int. J. Hydrogen Energy 38 (2013) 7077–7091.
[27] Z. Zheng, R. Petrone, M. Péra, D. Hissel, M. Becherif, C. Pianese, N.Y. Steiner, M. Sorrentino, Int. J. Hydrogen Energy 38 (2013) 8914–8926.
[28] S.M. Rezaei Niya, M. Hoorfar, J. Power Sources 240 (2013) 281–293.
[29] X.-Z. Yuan, C. Sons, H. Wang, J. Zhang, Electrochemical Impedance Spectroscopy in PEM Fuel Cells, in: Fundamentals and Applications, Springer, London, 2010.

[30] N. Fouquet, C. Doulet, C. Nouillant, G. Dauphin-Tanguy, B. Ould-Bouamama, J. Power Sources 159 (2005) 905–913.
[31] W. Merida, D. Harrington, J.L. Canut, G. McLean, J. Power Sources 161 (2006) 264–274.
[32] J.-M. Le Canut, R.M. Abouatallah, D.A. Harrington, J. Electrochem. Soc. 153 (2006) A857–A864.
[33] A. Debenjak, M. Gašperin, B. Pregelj, M. Atanasijević-Kunc, J. Petrovčič, V. Jovan, J. Mech. Eng. 59 (2013) 56–64.
[34] S. Cruz-Manzo, R. Chen, J. Electrochem. Soc. 160 (2013) F1109–F1115.
[35] M. Gašperin, P. Boškoski, A. Debenjak, J. Petrovčič, Fuel Cells 14 (2014) 457–465.
[36] A. Debenjak, P. Boškoski, B. Musizza, J. Petrovčič, Đ. Juričić, J. Power Sources 254 (2014) 112–118.
[37] P. Boškoski, A. Debenjak, J. Power Sources 268 (2014) 692–699.
[38] B.W. Silverman, Density Estimation for Statistics and Data Analysis, Chapman and Hall, 1986.
[39] M. Al-Harthy, S. Begg, R.B. Bratvold, J. Petrol. Sci. Eng 57 (2007) 195–208.
[40] M. Fischer, C. Kock, S. Schluter, F. Weigert, Quant. Financ. 9 (2009) 839–854.
[41] E. Bouyé, V. Durrleman, A. Nikeghbaliand, G. Riboulet, T. Roncalli, Copulas for Finance – A Reading Guide and Some Applications, 2000.
[42] C. Genest, A.C. Favre, J. Hydrol. Eng. 12 (4) (2007) 347–368.
[43] J.M. Kim, Y.S. Jung, E.A. Sungur, K.H. Han, C. Park, I. Sohn, BMC Bioinforma. 9 (1) (2008) 225.
[44] G. Mercier, G. Moser, S.B. Serpico, IEEE T. Geosci. Remote 46 (2008).
[45] B. Mileva Boshkoska, M. Bohanec, P. Boškoski, Đ. Juričić, J. Intell. Manuf. (2013) 1–13.
[46] S. Jaimungal, E.K.H. Ng (Eds.), ECML PKDD, 2009, pp. 628–643.
[47] C. Brunetto, A. Moschetto, G. Tina, Electr. Power Syst. Res. 79 (2008) 17–26.
[48] E.O. Doebelin, System Modeling and Response, John Wiley & Sons Inc, 1980.
[49] I. Daubechies, Ten Lectures on Wavelets, CBMS-NSF Regional Conference Series in Applied Mathematics, Society for Industrial and Applied Mathematics, 1992.
[50] P.O. Amblard, M. Gaeta, J.L. Lacoume, Signal Proc. 53 (1996) 1–13.
[51] M.K. Simon, Probability Distributions Involving Gaussian Random Variables, Springer Science, New York, 2006.
[52] E. Ollila, IEEE Signal Process. Lett. 15 (2008) 841–844.
[53] A. Khurshid, Z. Al-Hemyari, S. Kamal, Pak. J. Stat. Oper. Res. 8 (2012) 645–654.
[54] R.B. Nelsen, An Introduction to Copulas, second ed., Springer, New York, 2006.
[55] A. Sklar, Distributions with Fixed Marginals and Related Topics – Random Variables, Distribution Functions, and Copulas, in: A Personal Look Backward and Forward, vol. 28, Institute of Mathematical Statistics, Hayward, CA, 1996.
[56] L.M. Leemis, S.K. Park, Discrete-event Simulation: A First Course, Prentice-Hall, Inc., Upper Saddle River, NJ, USA, 2005.
[57] H. Joe, Multivariate Models and Dependence Concepts, Chapman and Hall, 1997.
[58] Savu C, Trade M, in: International Conference on High Frequency Finance, Konstanz, Germany.
[59] D. Berg, K. Aas, Eur. J. Financ. 15 (2009) 639–659.
[60] P. Trivedi, Z. David, Copula Modeling: An Introduction for Practitioners, World Scientific Publishing, 2006.
[61] M. Hofert (Ed.), Copula Theory and its Applications, Proceedings of the Workshop Held in Warsaw 25–26 September, 2009, Springer, 2010, pp. 147–160. Lecture Notes in Statistics.
[62] S.T. Rachev (Ed.), Handbook of Heavy Tailed Distributions in Finance, Elsevier/North Holland, 2003.
[63] B. Mileva Boshkoska, M. Bohanec, Int J. Decis. Support Syst. Technol. 4 (2012) 42–58.
[64] R. Onanena, L. Oukhellou, D. Candusso, F. Harel, D. Hissel, P. Aknin, Int. J. Hydrogen Energy 36 (2011) 1730–1739.
[65] D. Benouioua, D. Candusso, F. Harel, L. Oukhellou, Int. J. Hydrogen Energy 39 (2014) 21631–21637.

Chapter 5

Embedded Condition Monitoring System

The optimal exploitation of PEM fuel cells requires a number of supporting subsystems. Among them, an effective online CM system facilitates the fulfillment of reliability and durability requirements. Contemporary commercial PEM fuel cell power systems are equipped with DC-DC converters and voltage monitors, which provide only basic information (i.e., voltage and voltage measurements at low sampling rates and resolution). The designed embedded CM system extends the basic functionalities of a DC-DC converter and a FCVM with the CM capabilities.

The originally devised concept of the designed CM system is the interconnection between a DC-DC converter and a FCVM. The designed system incorporates:

- a DC-DC converter module capable of injecting excitation signals, which are required for the CM purposes,
- a high resolution FCVM monitor capable of acquiring voltage and current measurements on all of the cells within the fuel cell stack, and
- a CM algorithm capable of detecting the presence of PEM fuel cell faulty operation.

The designed embedded CM system aims at bridging the gap between the laboratory-grade measurement equipment (highly accurate and prohibitively expensive for the industrial applications) and contemporary commercial diagnostic systems (inexpensive, but capable of only basic monitoring). The designed electronics uses innovative design solutions by employing industry-standard components. In this way, the system is jointly commercially viable and precise enough to perform sophisticated diagnostic measurements.

The designed DC-DC converter (Figure 5.2) is a conversion module that converts the output voltage of a fuel cell stack into the voltage of an energy storage device (i.e., secondary battery). The converter targets medium power, stationary, and uninterruptible power supply applications, where the power bus voltage is lower than the output voltage of the fuel cell stack. To achieve high conversion efficiency, a topology with minimal number of power components is preferred. Therefore, the conversion topology employed is the current mode step-down converter, where only a small amount of energy is cycled in the power inductor during each conversion cycle.

The designed FCVM is a low-cost data acquisition device capable of performing precise voltage measurement of individual cells inside a fuel cell stack that consists of up to 90 cells. It provides the means for acquiring measurements that are required for the fast impedance estimation of individual cells of the stack. Figure 5.6 shows a typical implementation of

the FCVM connected to a PEM fuel cell stack of a commercially available power unit via spring contact pins.

To perform online EIS-based CM of PEM fuel cells, the FCVM and the DC-DC converter module were interconnected into a CM system. The interconnection enables joint injection of excitation signals and acquisition of measurements that are required for a fast online estimation of the impedance of PEM fuel cells. The scheme of the interconnected CM system is shown in Figure 5.10. To perform the current excitation of the cells, the DC-DC converter is equipped with a firmware-based excitation signal generator. The DC-DC converter's microcontroller modulates the output current of the DC-DC converter and thus injects the excitation signal to the fuel cell stack. By measuring the current excitation and minute voltage variations by the FCVM, the impedance of the cells is obtained.

This chapter includes the following publication:
Debenjak, A., Petrovčič, J., Boškoski, P., Musizza, B., & Juričić, Đ. (2015). Fuel cell condition monitoring system based on interconnected DC-DC converter and voltage monitor. *IEEE Transactions on Industrial Electronics*, *62*(8), 1–13. doi:10.1109/TIE.2015.2434792

Fuel Cell Condition Monitoring System Based on Interconnected DC-DC Converter and Voltage Monitor

Andrej Debenjak, *Student Member, IEEE*, Janko Petrovčič, Pavle Boškoski, Bojan Musizza, and Đani Juričić

***Abstract*—This paper presents a comprehensive solution for condition monitoring of PEM fuel cell systems. It comprises a modular DC-DC converter, a 90-channel fuel cell voltage monitor, and embedded diagnostics algorithms. Besides providing its basic functionality, the DC-DC converter is designed to perform diagnostic probing of fuel cells by injecting current excitation waveforms. The designed voltage monitor enables the precise voltage measurement of all individual cells in the stack. The interconnection between the DC-DC converter and the voltage monitor provides a platform for an embedded condition monitoring system. It employs a novel algorithm for fast electrochemical impedance estimation and automatic tuning of the thresholds used in the fault detection algorithm. The final output is a unit-free condition indicator that describes the overall condition of the fuel cell stack. As such, the designed condition monitoring system allows the seamless integration and optimal exploitation of fuel cell power systems. The complete solution has been evaluated on an 8.5 kW PEM fuel cell power system.**

***Index Terms*—PEM Fuel Cell, Condition Monitoring, Condition Indicator, DC-DC Converter, Voltage Monitor**

I. Introduction

BY its very nature, the proton exchange membrane (PEM) fuel cell technology offers efficient energy conversion along with low ecological footprint [1]. The energy conversion is done through electrochemical reaction of combining hydrogen and oxygen at a peak efficiency of 55% [2], [3]. High conversion efficiency combined with no greenhouse emissions is promoting PEM fuel cells as an energy source of the future.

A set of supporting subsystems is a prerequisite for the optimal exploitation of PEM fuel cells. This set comprises, but is not limited to, balance of plant (BoP) components, direct-current-to-direct-current (DC-DC) converter, precise voltage monitor, and supervisory control unit [4]–[6]. On top of these hardware subsystems, an effective online condition monitoring (CM) system enables real-time assessment of fuel cell health. A typical structure of such a PEM fuel cell-based system is presented in Fig. 1.

Manuscript received June 9, 2014; revised November 4, 2014 and April 14, 2015; accepted April 27, 2015.

Copyright © 2015 IEEE. Personal use of this material is permitted. However, permission to use this material for any other purposes must be obtained from the IEEE by sending a request to pubs-permissions@ieee.org.

This work was jointly supported by the Slovenian Research Agency (Programme P2-0001) and by the Centre of Excellence for Low-Carbon Technologies – CO NOT.

The authors are with the Department of Systems and Control, Jožef Stefan Institute, Jamova cesta 39, SI-1000 Ljubljana, Slovenia. Andrej Debenjak is also with the Jožef Stefan International Postgraduate School, Jamova cesta 39, SI-1000 Ljubljana, Slovenia. Corresponding author: Andrej Debenjak (e-mail: andrej.debenjak@ijs.si).

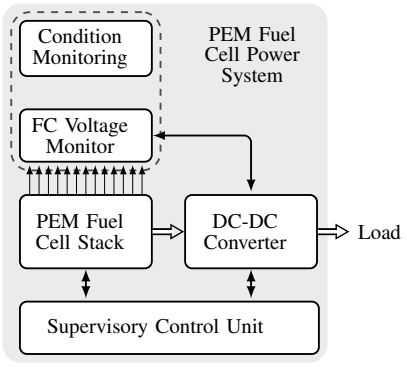


Fig. 1. Block diagram of a PEM fuel cell power system.

Contemporary commercial fuel cell systems are equipped with DC-DC converters and voltage monitors that fulfill only basic requirements for output power conditioning (e.g., [7]–[15]) and monitoring (e.g., [16], [17]), respectively. Such systems fail in providing accurate information about system condition. The diagnostic aspect is of a significant practical merit since the durability and reliability of PEM fuel cells are vitally influenced by several kinds of faults [18], [19]. Therefore, timely and precise information about the health condition of the fuel cell system allows optimal exploitation with respect to its momentary capabilities in various applications (e.g., [20]–[23]).

All things considered, the aim of the present study is to bridge the gap between the laboratory-grade measurement equipment and contemporary commercial diagnostic systems. The designed electronics use innovative design solutions by employing industry-standard components. Consequently, the constructed system is both (i) commercially viable and (ii) precise enough to perform sophisticated diagnostic measurements. The combination of the designed DC-DC converter with the 90-channel fuel cell voltage monitor (FCVM) represents a capable platform for accurate online CM. Hence, this paper addresses the following subsystems:

- A DC-DC converter with the capability of generating probing signals for diagnostic purposes
- A 90-channel FCVM capable of precise voltage measurement of each cell of a fuel cell stack and extraction of small voltage variations
- An algorithm for fast impedance estimation by employing

pseudorandom binary sequence (PRBS) signal
- A systematic approach for tuning of the threshold of the CM system and calculation of an overall unit-free condition indicator (CI)

Deterioration in operation conditions (i.e., presence of faults) of PEM fuel cells affects their electrochemical impedance characteristic. Consequently, faults can be detected with a multitude of approaches based on electrochemical impedance spectroscopy (EIS) [24]–[29]. Despite the sufficiently high diagnostic resolution of this technique, two obstacles hinder the usage of EIS for online CM system:

1) Typical EIS estimation using single-sine excitation signals is time-consuming (typically a few minutes) and is therefore unsuitable for fast online CM purposes.
2) Proper selection of diagnostic threshold requires a rich set of historical records at various conditions of fuel cell system.

To address the first issue, an algorithm for fast estimation of the fuel cell impedance was developed that employs small-amplitude PRBS excitation signal with a duration of less than 60 seconds. The DC-DC converter superimposes the PRBS excitation signal onto the stack electrical current. Using the FCVM for data acquisition and signal processing, the impedance is estimated using continuous wavelet transform (CWT) with the complex Morlet mother wavelet [30].

With regard to the second issue, the thresholds of the CM system can be easily determined by employing the probability of false alarm (PFA) through the analysis of the statistical properties of the electrical impedance at different frequencies [31]. As a result, a unit-free CI is obtained whose value is directly related to the overall condition of the fuel cell system.

For the purpose of the complete system presentation, first, the hardware components are presented: DC-DC converter in Section II and FCVM in Section III. Afterward, a brief overview of the method for fast impedance estimation using CWT as well as implementation of the CM algorithms is given in Section IV. Finally, the evaluation results are presented in Section V.

II. DC-DC CONVERTER

The presented DC-DC converter is a conversion module that converts the output voltage of a fuel cell power module into the voltage of an energy storage device (e.g., rechargeable lithium battery or storage capacitor). The input device (i.e., fuel cell stack) and the output device (i.e., secondary battery) are current source and current drain, respectively. Therefore, the DC-DC converter should be treated and designed as a current-transforming device. Yet this is uncommon for nearly all commercially available converters, which mostly operate as voltage-transforming devices.

The DC-DC converter targets medium power, stationary auxiliary, and uninterruptible power supply applications, where the power bus voltage is lower than the output voltage of the fuel cell stack. This dictates the use of the step-down DC-DC converter topology. However, the use of the step-up topology would have some benefits in comparison with the step-down one. For the solutions presented in this paper, the most notable would be a direct input current modulation and low input (i.e., fuel cell stack) current ripple. As a consequence of a lower current ripple, a smaller input capacitor bank would be required. The step-up topology is of great interest in automotive, aviation, and other fields of applications. However, in the presented case, the overall system design dictates the use of a less favorable topology.

The DC-DC converter module presented in this paper is designed as a current-transforming device. Consequently, the stack current is under the primary control, while the stack voltage is monitored in order to ensure safety and operation in an appropriate range. The same applies to the output side, where the current is under primary control, and the output voltage is supervised in order to stay in the predefined range.

To achieve high conversion efficiency, a topology with the lowest number of power components is preferred. The conversion topology employed is the step-down converter. For such a converter, the main energy flow goes only through a single-pole double-throw electronic switch and the power inductor. As a result, only a small amount of energy is cycled in the power inductor during each conversion cycle.

This topology suffers from three drawbacks: (i) the input voltage must always be higher than the output voltage, (ii) the input and output ports are not galvanically separated, and (iii) the input current ripple is high. The first issue is not critical for medium-sized power systems. The second one can be overcome, as fuel cell stacks can be made electrically floating or grounded at one side. The third one is of real concern, and it has to be properly handled since ripple current at the input side negatively affects the fuel cell stack. The ripple influence is effectively mitigated by the use of an electrolytic capacitor bank at the input side of the DC-DC converter.

It should be noted that the electrolytic capacitors may be easily replaced with the power-film ones [32], [33]. This would enhance the reliability of the system and reduce the weight, which is particularly beneficial for transportation applications. The usage of power-film capacitors would be even more justified in the case of the step-up DC-DC conversion topology because of higher voltages [32].

Given the current mode of operation, several DC-DC converter modules can be paralleled to obtain higher output currents. The external master controller can be programmed to dynamically share the load between several parallel converters in order to fulfill the current load requirements and to optimize the efficiency of conversion. At low current loads, the master controller can switch off some of the modules and drive the others to a higher conversion power. In this way, the switching losses of the less loaded modules are eliminated and the overall conversion efficiency is increased.

In the present configuration, the solution is limited to a maximum of eight parallel DC-DC converter modules, each handling up to 80 A of output current. When eight units are paralleled, the overall current reaches up to 640 A, attaining the capacity of power conversion of nearly 16 kW in 24 V systems. An example of an implemented 5 kW conversion block is shown in Fig. 2. The assembly consists of three parallel DC-DC converter modules, two capable of delivering 80 A and one 40 A of current.

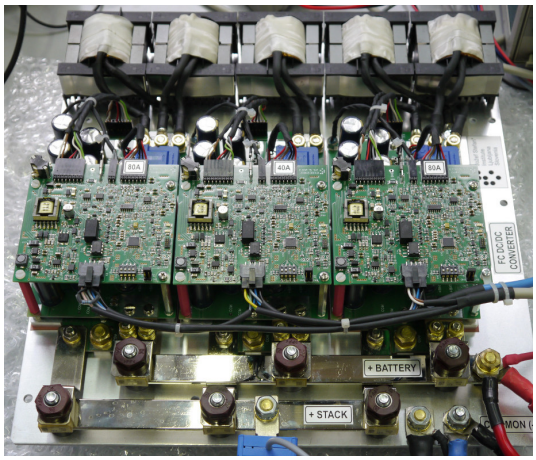


Fig. 2. Assembly of three DC-DC converter modules paralleled together providing 5 kW of power conversion capability.

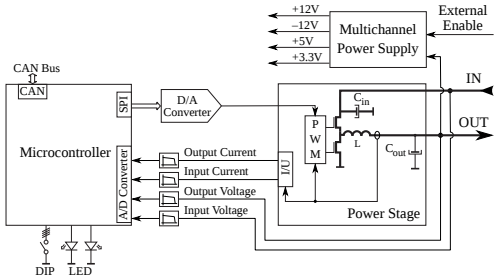


Fig. 3. Block diagram of the DC-DC module.

By paralleling several DC-DC converter modules, a lower input current ripple is achieved by the asynchronously operated modules. The current mode step-down converter with constant OFF-time inherently operates with variable frequency. As confirmed by the performed test, three paralleled modules have never fallen into synchronism, even if they were driven by the same current set-point. This allows further optimization (i.e., reduction) of the size of the input capacitor bank.

The block diagram in Fig. 3 depicts the conceptual arrangement of the DC-DC module. Roughly, the module can be divided into three functional blocks, namely,

- multichannel power supply,
- microcontroller circuitry, and
- step-down power output stage.

A. Microcontroller circuitry

The microcontroller circuitry is powered by a multichannel power supply. The supply voltages are generated by a flyback converter topology. The multichannel power supply must be enabled by an external digital signal. With this signal, the external master controller can switch ON or OFF the complete DC-DC converter module. This enables isolation of the defective module as well as increases the efficiency of operation at low loads.

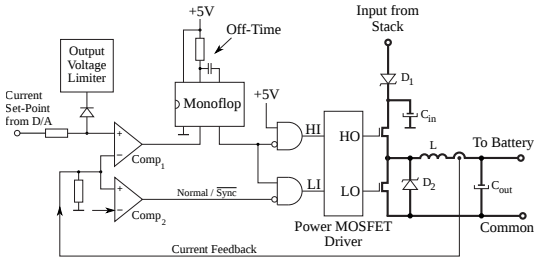


Fig. 4. Power output stage of the current-mode DC-DC converter.

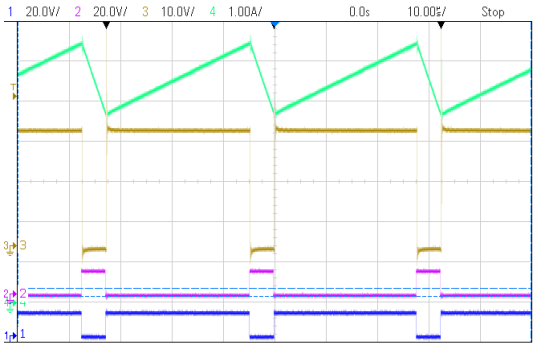
The DC-DC module is managed over a controller area network (CAN) bus communication line. The primary task of the microcontroller is to receive CAN messages with set-point values for the DC-DC converter and to adjust the peak current of the output stage accordingly. The set-points that can be sent to the microcontroller of a DC-DC converter module via the CAN bus are: (i) the peak value of the output current, (ii) the maximum output voltage, (iii) the amplitude of the excitation signal for the impedance measurements, and (iv) the frequency of the excitation signal. The only way the embedded microcontroller can affect the power stage is by means of a control signal through an external 12-bit D/A converter. The microcontroller supervises the operation of the DC-DC conversion across four analogue inputs (see Fig. 3).

B. Power output stage

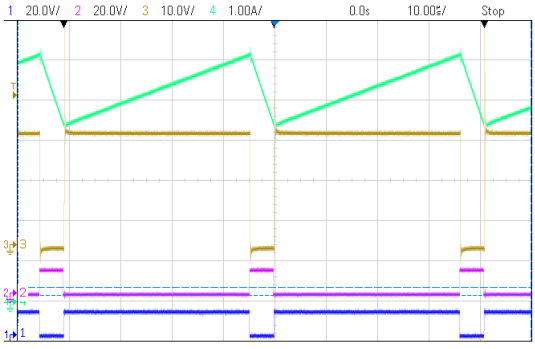
The step-down power output stage is designed as a self-sufficient block. It needs no microcontroller intervention to oscillate and to control the output current. Hence, the safety of the power control is not affected by possible software errors or strong external transients, which would cause the microcontroller to operate temporarily in an undefined state.

The energy flow of the power output stage of the DC-DC converter is controlled by pulse-width modulation (PWM). The design of the output stage is presented in Fig. 4. PWM cycles power metal-oxide-semiconductor field-effect transistors (MOSFETs) in a synchronous mode. This mode reduces power dissipation during the OFF cycle of the converter. Power inductor L filters the modulating current variations and, together with the output capacitor C_{out}, provides necessary low-pass filtering. Input current variations are filtered out with input capacitor bank C_{in}, which eliminates fuel cell stack current ripple. Stack current is delivered through the Schottky diode D_1 intended to prevent back current flow that would otherwise cause an irreparable damage to the fuel cell stack.

The standard current mode converter with constant frequency is most often employed, although it suffers from the inherent low-frequency instability [34]–[37]. As the stack voltage is frequently close to the required output voltage, the DC-DC conversion is subjected to operation at high PWM duty cycles. The constant-OFF mode of the current control is a particularly convenient method for this purpose. Therefore, at the design of the DC-DC converter, a *current mode step-down converter with a constant OFF-time and synchronous switching mode* was used. The constant-OFF type encounters



(a) U_{in} = 32 V, I_{out} = 5.5 A



(b) U_{in} = 28 V, I_{out} = 5.5 A

Fig. 5. Key waveforms of the DC-DC converter operating at two different input voltages U_{in} and the same output current I_{out} (CH1[blue]: LI signal, CH2[magenta]: HI signal, CH3[brown]: voltage of the power inductor's entry point, CH4[cyan]: power inductor current).

no inherent instability problems and enables cycle-by-cycle peak current control of the output stage.

Fig. 4 shows that the output pair of N-type MOSFETs is driven by a high-side/low-side MOSFET driver. When the upper MOSFET bank is switched ON, electrical current starts to flow from the fuel cell stack and the input capacitor bank into the output capacitor bank and the load. The current in the inductor increases until the current sensor detects a set-point value, as shown in Fig. 5. When output current exceeds the set-point value, the Comp_1 triggers the monostable flip-flop. This causes the top MOSFET bank to switch OFF and the bottom MOSFET bank to switch ON (the driving signals for the MOSFET banks are shown in Fig. 5). The inductor current recirculates through the lower transistor bank and decreases linearly for a defined amount of time (constant-OFF). When the predefined time elapses, the top MOSFETs switch ON again and allow the passage of stack current to the output.

The OFF-time is determined by the RC constant of the monoflop constant. The ON-time is variable and depends on the input voltage. If the input voltage from the stack is high, the ON-time becomes short, and vice versa. When the input voltage approaches the output voltage, the oscillation ceases away, and the current goes straight through. With the present design, the OFF-time is set to 4 μs. When the fuel cell stack output voltage is near twice the required DC-DC converter output voltage, the output stage oscillates at 125 kHz. The switching frequency increases with the input-output voltage ratio. When the input voltage is only a few volts above the output voltage, the switching frequency drops to a few kilohertz. At the ultimate situation, the switching stops completely. In this way, a very wide range of input voltages are covered. Given the backflow protection diode D_1, the input voltage must be at least one diode drop higher than the output voltage. To illustrate the constant-OFF mode, the waveforms shown in Fig. 5 were acquired under the same output current I_{out} but at two different input voltages U_{in}. The OFF-time is identical in both cases, whereas the ON-time is longer in the case of lower input voltage U_{in} (i.e., Fig. 5b) in order to fulfill the requirements of the output current.

When a battery is connected to the output of the converter, the implementation of the synchronous mode is not a straightforward task. The backflow current might flow from the battery back through the power inductor and the lower bank of MOSFETs (e.g., at zero current set-point). In such a case, the inductor current would rise to values at which the circuitry would be damaged instantly. To avoid this, the circuitry actually switches between the normal mode (when the diode D_2 is used to recirculate the inductor current) and the synchronous mode (when low-side MOSFETs are used instead). The switchover is performed by the comparator Comp_2. At low output currents, the output stage operates in normal mode, and lower MOSFETs are never switched ON. At higher output currents, the synchronous mode takes over and keeps the switching losses low.

The DC-DC converter strictly operates in current-transforming mode. However, when the output voltage reaches the gassing level of the battery, the output current is reduced. In this situation, the output voltage limiter (see Fig. 4) reduces the current set-point. It operates as a secondary voltage control loop and fixes the battery voltage at the set-value by forcing lower output current as demanded.

III. Fuel Cell Voltage Monitor

A significant voltage drop is an indication that either the operating conditions or the health of the fuel cell is seriously impaired. Therefore, even low-cost fuel cell-based power systems require some kind of cell voltage monitoring. A significant discrepancy exists between the laboratory-grade and the commercially available diagnostic and measurement equipment. The trade-off is between the capability of handling fast and precise measurements on one hand and the price on the other [38], [39]. Most of the commercially installed FCVM systems are capable of measuring only the joint voltage of two or more adjacent fuel cells with a rather low sample rate and resolution. Notwithstanding the cost-effectiveness, such equipment suffices only for detecting severe deteriorations in the fuel cell condition. As a result, it is incapable of performing total stack monitoring or providing more sophisticated diagnostic information.

The proposed solution bridges the gap between the laboratory-grade measurement equipment and the contemporary commercial diagnostic systems. The proposed FCVM is a

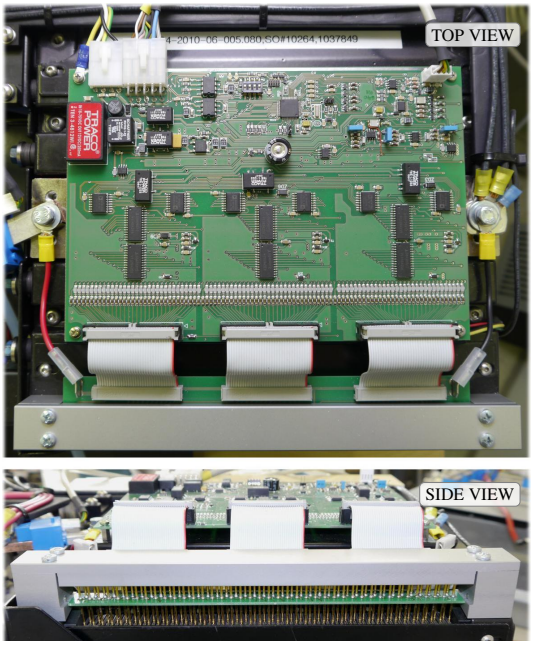


Fig. 6. FCVM connected to an 8.5 kW PEM fuel cell system Hydrogenics HyPM-HD 8-200 (top view: FCVM's PCB; side view: realization of contacts to all of the fuel cells).

low-cost data acquisition device capable of performing precise voltage measurement of individual cells inside a fuel cell stack that consists of up to 90 cells. Additionally, it provides a platform for conducting EIS measurements on every cell of the stack. Fig. 6 shows a typical implementation of the FCVM connected to a PEM fuel cell stack of a commercially available power unit via spring contact pins.

A. Resolving high common-mode voltage potential issue

One of the biggest issues when measuring the voltage of an individual cell within a larger stack is a high common-mode potential, which builds up from the potentially low cell to the highest cell in the stack. The signal acquisition system must be capable of measuring only a few hundred millivolts superimposed on several tens of volts. Such high common-mode potential poses two limiting factors: the ability of a multiplexer to select the individual cell within this very wide common-mode voltage range and the ability of instrumentation amplifiers or floating A/D converters to extract the relatively small cell voltage in the presence of high voltage offset [40].

The issue of high common-mode voltage range of multiplexers remains unsolved by readily available low-cost measurement devices. The proposed solution employs standard CMOS analogue multiplexers. By proper biasing and using an isolated DC-DC power supply, making an analogue multiplexer floating is possible. Fig. 7 shows that an isolated DC-DC converter provides voltage supply to the multiplexer. Two Zener diodes regulates the bias for the multiplexer for maximum input range, while an NPN transistor supplies current to a digital signal isolator, which selects the particular

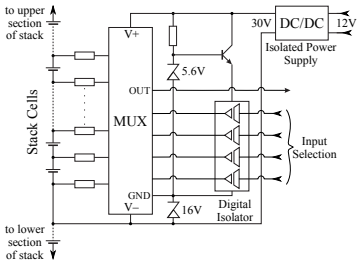


Fig. 7. Floating power supply scheme, which allows an industry-standard multiplexer to operate in floating mode.

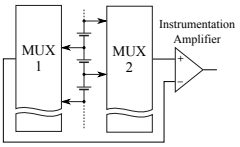


Fig. 8. Connection of two industry-standard multiplexers to measure up to 30 fuel cell leads in order to reduce component count.

input. The selected voltage is then transferred to the difference amplifier for further signal preparation and A/D conversion. One such circuitry is capable of handling signals from up to 30 fuel cells.

To decrease the number of multiplexers, two multiplexers are interlaced as shown in Fig. 8. In this way, only one input is effectively used per cell. Thus, selecting 30 cells is possible by using a pair of standard 16-to-1 multiplexers. One spare channel is used for automatic autozero measurement, which eliminates the offset voltage of the difference amplifier.

An ARM Cortex-based microcontroller performs synchronization among different AD channels required for proper data acquisition. Additionally, the microcontroller controls the communication interfaces and provides the necessary computational resources for the execution of the diagnostic algorithms.

B. FCVM measurement modes

The FCVM can perform two types of measurements:

- Voltage monitoring of all the cells of the stack
- Impedance measurement of individual cells

In the first mode, the FCVM measures the voltage of each individual cell inside a stack with a resolution of 62.5 μV. The stack voltage and current are also measured with a resolution of 24 mV and 10 mA, respectively. The stack voltage and current are measured through a simple voltage divider and Hall-effect current transducer, respectively. In the monitoring mode, the refresh rate is 400 ms.

The second measurement mode provides a powerful tool for performing measurements intended for EIS-based diagnostics. The relevant AC diagnostic signals are superimposed on the operational DC signals of the fuel cell and have small amplitudes with respect to the DC component. Measuring such low-amplitude AC signals at low noise is of utmost importance.

To achieve the required high resolution at low noise, the voltage of an individual cell undergoes two preprocessing

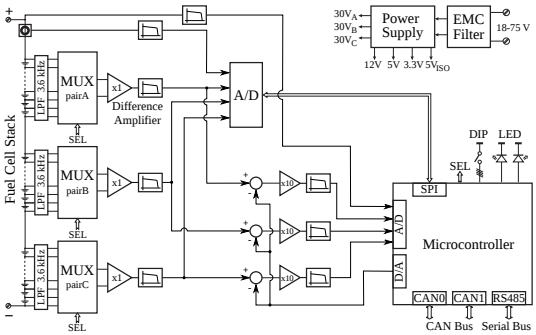


Fig. 9. Block diagram of the FCVM.

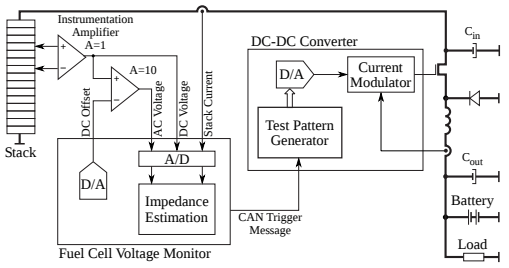


Fig. 10. Connection scheme between the FCVM and the DC-DC converter for online CM.

steps. In the first step, the DC component is subtracted by employing the analogue subtraction circuit. In the second step, the remaining AC component of the signal is amplified by a factor of 10 in order to attain low noise and a higher resolution of A/D conversion, as shown in Fig. 9. Consequently, the FCVM measures the AC voltage of sequentially selected cells inside a stack with a high resolution of 80 μV at a sampling rate of 5 kHz. A special care was taken to keep the frequency response of voltage and current measuring paths as equal as possible as the impedance is actually proportional to their ratio in the amplitude/phase space.

Normally, extraction of AC signals in the presence of a DC signal is performed by using a high-pass analogue filter. However, switching among cells would cause a long settling time of the filter, which would significantly prolong the data acquisition time. Since the DC voltage of the cell, obtained by the first measuring mode, is already known to the microcontroller, the value is sent to the subtraction circuitry via the D/A converter, as shown in Fig. 9. The result is the AC component of the signal with a small DC residue caused by circuit imperfections and slow cell voltage variations. This composite signal is then amplified to gain higher resolution and to keep a high signal-to-noise ratio. As the DC residue is also amplified, it is removed later by digital signal processing within the microcontroller.

C. DC-DC converter and FCVM as a condition monitoring system

To perform online EIS-based CM of PEM fuel cells, the DC-DC converter module and the FCVM were interconnected into a CM system. The interconnection enables performing measurements that are required for a fast online estimation of the impedance of PEM fuel cells. The FCVM manages the estimation procedure, performs the voltage and current measurements, and conducts the signal processing tasks. The DC-DC converter performs the DC-DC conversion, and when prompted by the FCVM, it executes the current excitation of fuel cells. The scheme of the interconnected CM system is shown in Fig. 10.

To perform the current excitation of the cells, the DC-DC converter module is equipped with a firmware-based excitation pattern generator, as shown in Fig. 10. Using the selected pattern, the microcontroller modulates the output current of the DC-DC converter. As this variation of the output current is filtered out by the output capacitor bank, the modulation is not affecting the load significantly. On the input side of the DC-DC converter, the current modulation affects the current through the fuel cell stack. The stack becomes excited enough to respond with minute variations of the cells' voltages. By measuring these variations with the FCVM, the information on the impedance of the cells is obtained.

The excitation of the fuel cell stack is affected by the presence of the input capacitor bank of the DC-DC converter and its dynamics. The capacitor bank must be present to reduce stack current ripple. This capacitance is paralleled to the stack, and its influence is most prominent at high frequencies, while the information on the cells' condition is present at low frequencies.

IV. Condition monitoring

The embedded CM approach builds on top of a method for fast impedance estimation [30]. This method employs a PRBS excitation signal and CWT signal processing tool. It enables a substantially faster estimation of the PEM fuel cell impedance characteristic compared with other conventional methods, which utilize single-sine signals. Due to the specific statistical properties of the PRBS waveform, the CM thresholds are determined based on the probability distribution of impedance at particular frequencies and a desired value of PFA [31]. Finally, a unit-free CI indicator is formulated, which provides an overall assessment of the PEM fuel cell condition.

A. Fast impedance estimation using CWT and PRBS

1) CWT based on the complex Morlet wavelet: Following the procedure described by Debenjak et al. [30], the impedance characteristic can be efficiently estimated by using complex wavelet coefficients of the CWT of the fuel cell's current $i(t)$ and voltage $u(t)$ using the complex Morlet mother wavelet. The CWT of a square integrable function $f(t) \in \mathbf{L}^2(\mathbb{R})$ is defined as follows [41]:

$$Wf(u,s) = \langle f(t), \psi_{u,s}(t) \rangle = \int_{-\infty}^{\infty} f(t) \psi^*_{u,s}(t)\, dt, \qquad (1)$$

where $\psi_{u,s}(t)$ is a scaled and translated version of the mother wavelet $\psi(t)$:

$$\psi_{u,s}(t) = \frac{1}{\sqrt{s}} \psi \left(\frac{t-u}{s} \right), \qquad (2)$$

which in the present study is the complex Morlet wavelet with parameter ω_0 [42]:

$$\psi(t) = \pi^{-1/4}\left(e^{-j\omega_0 t} - e^{-\omega_0^2/2}\right)e^{-t^2/2}. \tag{3}$$

The wavelet coefficients (1) fully characterize the analyzed signal $f(t)$ on the time-scale plane. The translation between scale s and frequency f is straightforward by using the following [41]:

$$\frac{1}{f} = \frac{4\pi s}{\omega_0 + \sqrt{2+\omega_0^2}}. \tag{4}$$

Therefore, in the remainder of the paper, all subsequent relations will rely on the actual frequency f.

2) PRBS as excitation signal: PRBS can be regarded as sufficiently close to stationary random noise with a power spectral density similar to that of white noise. Furthermore, the probability distribution of the amplitude of its frequency components can be regarded as Gaussian [43]. Analyzing such a signal with CWT preserves its statistical properties within the wavelet coefficients. As the DC-DC converter superimposes the PRBS signal on the current $i(t)$ drawn by the load, the voltage $u(t)$ will response accordingly. Analyzing both signals with CWT results into wavelet coefficients:

$$\begin{aligned} Wi(t,f) &= \Re\{Wi(t,f)\} + j\Im\{Wi(t,f)\}, \\ Wu(t,f) &= \Re\{Wu(t,f)\} + j\Im\{Wu(t,f)\}. \end{aligned} \tag{5}$$

The wavelet coefficients at a particular frequency can be regarded as a zero-mean Gaussian circular complex random [44]. Therefore, the complex wavelet coefficients have the following properties:

$$\begin{aligned} \Re\{Wi(t,f)\}, \Im\{Wi(t,f)\} &\sim \mathcal{N}\left(0, \frac{\sigma_i^2}{2}\right), \\ \Re\{Wu(t,f)\}, \Im\{Wu(t,f)\} &\sim \mathcal{N}\left(0, \frac{\sigma_u^2}{2}\right), \end{aligned} \tag{6}$$

where the corresponding variances σ_u^2 and σ_i^2 are parameters that should be estimated. Using the complex wavelet coefficients (6), the impedance at a particular frequency $f = f_0$ can be calculated as a ratio of the complex wavelet coefficients:

$$z(t) = \left.\frac{Wu(t,f)}{Wi(t,f)}\right|_{f=f_0} = z_r(t) + jz_i(t). \tag{7}$$

B. Probability density function of the complex impedance $z(t)$

Current $i(t)$ and voltage $u(t)$ in (7) are correlated, which can be expressed with the covariance matrix [45]–[47]:

$$\Sigma = \frac{1}{2}\begin{bmatrix} \sigma_u^2 & \rho\sigma_u\sigma_i \\ \rho^*\sigma_u\sigma_i & \sigma_i^2 \end{bmatrix}, \tag{8}$$

where $\rho = \rho_r + j\rho_i$ is a complex correlation coefficient, such that $|\rho| \leq 1$. As a result, the probability density function (PDF) of the ratio (7) reads as follows [48]:

$$p_z(z) = \frac{1-|\rho|^2}{\pi\sigma_u^2\sigma_i^2}\left(\frac{|z|^2}{\sigma_u^2} + \frac{1}{\sigma_i^2} - 2\frac{\rho_r z_r - \rho_i z_i}{\sigma_u\sigma_i}\right)^{-2}. \tag{9}$$

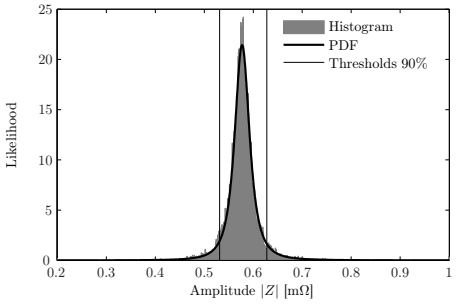


Fig. 11. Probability distribution function of $|Z|$ at 157 Hz.

The distribution of the real z_r and imaginary z_i components of the impedance (7) can be derived from the distribution (9). The PDF of the imaginary component z_i reads as follows [48]:

$$p_{z_i}(z_i|\rho_r,\rho_i) = \frac{\left(1-|\rho|^2\right)\sigma_x^2\sigma_y}{2\left(\left(1-\rho_r^2\right)\sigma_x^2 + 2z_i\rho_i\sigma_x\sigma_y + z_i^2\sigma_y^2\right)^{3/2}}. \tag{10}$$

For the real component z_r, the PDF has the same shape and reads as follows:

$$p_{z_r}(z_r|\rho_r,\rho_i) = p_{z_i}(z_r| - \rho_i, -\rho_r). \tag{11}$$

Besides the probability distribution of the real z_r and imaginary z_i components of the impedance, in many cases, the module of the complex impedance can be used as a feature in CM. For the circular Gaussian complex random variables (6), the corresponding modules $|Wu(t,f_0)|$ and $|Wi(t,f_0)|$ are distributed according to the Rayleigh distribution:

$$\begin{aligned} |Wu(t,f_0)| &\sim \text{Rayleigh}(\sigma_u), \\ |Wi(t,f_0)| &\sim \text{Rayleigh}(\sigma_i). \end{aligned} \tag{12}$$

As the current $i(t)$ and voltage $u(t)$ are correlated, the PDF of the module of the ratio (7) reads as follows [49]:

$$p_{|Z|}(|z|) = \frac{2\sigma_i^2\sigma_u^2(1-\rho^2)|z|(\sigma_i^2|z|+\sigma_u^2)}{\left[(\sigma_i^2|z|^2+\sigma_u^2)^2 - 4\rho^2\sigma_u^2\sigma_i^2|z|^2\right]^{3/2}}, |z| \geq 0, \tag{13}$$

where $|\rho| \leq 1$ is the correlation coefficient, as defined in (8). The probability distribution function (13) is positively skewed and defined on the nonnegative semiaxis. A typical realization of the probability distribution function (13) is shown in Fig. 11.

C. Fuel cell condition indicator based on PFA

Determining the optimal threshold values at which the deterioration can be regarded as significant is of great importance for a CM system. Too-high thresholds decrease the sensitivity of the diagnostic system to faults and hence increase the probability of missed alarms. At the same time, the probability of false alarms is decreased. Too-low thresholds increase the chances of false alarms, which can easily ruin the credibility of the monitoring system. The most commonly used criterion for determining the thresholds is not by explicitly defining their values, but rather by defining the permitted PFA [50].

A CM system based on low PFA will raise alarms only when the condition of the fuel cell is suboptimal. Having derived

the PDF (13), upper and lower thresholds can be handily found as critical values of a two-sided test using its cumulative distribution function (CDF) $P_{|Z|}(z)$:

$$\begin{aligned} T_{\downarrow} &= P_{|Z|}^{-1}\left(\frac{p_{FA}}{2}\right) = \inf\left\{P_{|Z|}(z) \geq \frac{p_{FA}}{2}\right\}, \\ T_{\uparrow} &= P_{|Z|}^{-1}\left(1-\frac{p_{FA}}{2}\right) = \inf\left\{P_{|Z|}(z) \geq 1-\frac{p_{FA}}{2}\right\}. \end{aligned} \tag{14}$$

Note that expression $\frac{p_{FA}}{2}$ is used to split the PFA between both ends of the PDF since the presence of different faults can increase or decrease the value of $|z|$. The CDF $P_{|z|}(z)$ that corresponds to (13) reads as follows [49]:

$$P_{|z|}(z) = \frac{1}{2} - \frac{\sigma_u^2 - z^2\sigma_i^2}{2\sqrt{4z^2\left(1-\rho^2\right)\sigma_i^2\sigma_u^2 + \left(\sigma_u^2 - z^2\sigma_i^2\right)^2}}. \tag{15}$$

The steps of the proposed method for threshold selection are listed in Algorithm 1. The threshold values have to be separately calculated for each individual fuel cell. The algorithm has to be performed for each fuel cell only once (e.g., when commissioning a new system), under fault-free conditions. The only design parameter is the desired PFA value.

Algorithm 1 Determining threshold values

1: **Apply** PRBS excitation signal.
2: **Measure** voltage $u(t)$ and current $i(t)$ signals under fault-free condition.
3: **Estimate** impedance $z(t)$ using (7).
4: **Estimate** covariance Σ using (8).
5: **Compute** CM thresholds (14) using CDF (15) and the desired PFA value.

Condition indicator: Selected threshold values (14) can be additionally employed for mapping the complex impedance values into a so-called CI, which is an abstract feature that can be directly related to the condition of the system [50]. For a healthy system, the CI should acquire low values (i.e., $CI = 0$). As the condition deteriorates, the value of the CI should increase in accordance with the severity of the fault(s) present in the system. Using the desired PFA value, the values of the CI are typically scaled in such a way that values close to 1 should indicate imminent failure. Thus, the CI offers two advantages:

1) It gives a unified and unit-free view of the overall system condition.
2) Its trend over time can be used for prognostics (i.e., estimation of the remaining useful life[1]).

In the context of fuel cells, the presence of a fault can either increase or decrease certain impedance components. Therefore, for a fault-free operation, the value of the CI will be in the middle of the region bounded by thresholds at a certain PFA, as shown in Fig. 11.

The mapping into the corresponding CI can be achieved by using the CDF (15). As a result, the impedance components of the fault-free region will acquire values in the vicinity of $1/2$.

[1]The problems of prognostics are not treated by this paper.

Setting the maximal value for the CI to be the chosen PFA, the final scaling relation reads as follows:

$$CI = 2 \times (1-p_{FA})^{-1}\left|P_{|Z|}(z) - \frac{1}{2}\right|, \tag{16}$$

where $P_{|Z|}(z)$ is the CDF of the corresponding impedance component.

D. Computationally efficient CWT with the Morlet wavelet

By substituting the mother wavelet $\psi(t)$ with

$$\tilde{\psi}_s(t) = \frac{1}{\sqrt{s}}\psi^*\left(-\frac{t}{s}\right), \tag{17}$$

the relation (1) transforms into the following convolution:

$$Wf(u,s) = \frac{1}{\sqrt{s}}\int_{-\infty}^{\infty} f(t)\tilde{\psi}_s(u-t)\,dt. \tag{18}$$

In the Fourier domain, the convolution (18) becomes

$$Wf(u,s) = \frac{1}{2\pi}\int_{-\infty}^{\infty} \hat{f}(\omega)\sqrt{s}\hat{\psi}(s\omega)e^{j\omega u}d\omega, \tag{19}$$

where $\hat{f}(\omega)$ is the Fourier transform of the original signal $f(t)$ and $\hat{\psi}(\omega)$ is the Fourier transform of the Morlet wavelet (3) [42]:

$$\hat{\psi}(\omega) = \pi^{-\frac{1}{4}}\left(e^{-\frac{(\omega-\omega_0)^2}{2}} - e^{-\frac{\omega^2}{2}}e^{-\frac{\omega_0^2}{2}}\right). \tag{20}$$

V. Experimental validation

Among other faults, the water management ones vitally affect PEM fuel cell operation reliability and efficiency [19]. The diagnosis of these faults is of great practical value, providing information for efficient fuel cell system management. For validation of the proposed CM solution, a commercial PEM fuel cell system was employed, which was subjected to water management faults.

A number of studies show that water management faults affect the electrochemical impedance of a PEM fuel cell and can therefore be detected by utilizing EIS-based approaches [51]–[61]. Water content affects the transport of the involved chemical species (i.e., reactant gases and protons) in different ways [24], [29]. In the case of flooding, the formed water droplets block the pathways to the reaction sites, thus preventing the oxygen from being involved and consumed as a reactant. Conversely, when the water level is low, the membrane of a PEM fuel cell is subjected to drying. The PEM is made of an ionomer that has to be sufficiently hydrated in order to conduct protons. If the cell is subjected to drying, the water content of the PEM is reduced, and consequently, the proton conductivity of the membrane is decreased. Additionally, due to a lower water content, the volume of the ionomer is reduced, and it results in a decrease of the contact surface area.

A. Experimental procedure

During the experiments, the fuel cell system was kept at constant operating and environmental conditions. The DC current operating point I_{dc} was set to 70 A, whereas the peak-to-peak amplitude of the superimposed PRBS waveform was set to 4 A. Such an amplitude was high enough to sufficiently perturb the PEM fuel cells in order to obtain reliable impedance estimations, but small enough not to cause difficulties due to nonlinearity of the PEM fuel cells.

The frequency f_s of the PRBS excitation signal was set to 600 Hz. The frequency f_s defines the rate at which the PRBS signal can switch its value. In other words, the value of the signal can change every 1.67 ms ($\Delta t = 1/f_s$). According to the theory, the PRBS signal has a nonzero power spectrum (and therefore provides the excitation energy) at all frequencies, except at those with values of integer multiples of the frequency f_s [62, pp. 164–172]. However, for practical impedance estimation purposes, the useful bandwidth f_B of the PRBS excitation signal is limited to approximately one-third of the frequency f_s ($f_B \simeq f_s/3$) [30]. For the case at hand, the useful frequency band f_B covers frequencies from 0 to approximately 200 Hz. On the other hand, the data acquisition sampling frequency f_{DAQ}, at which the voltage and current signals were acquired, was set to 5 kHz. During the experiment, the impedance was estimated every 40 seconds. Within that time interval, the PRBS excitation was applied for 10 seconds. At the same time, the required voltage and current signals were acquired.

Fig. 12 shows an example of the current and voltage signals of a PEM fuel cell during the experiment, which were acquired by the FCVM and used for the impedance estimation. As can be seen from Fig. 12, the actual fuel cell current is not of an ideal PRBS waveform. The shape is affected by the presence of the input capacitor bank of the DC-DC converter and its dynamics, as discussed in Subsection III-C. It should be stressed that the proposed impedance estimation method (i.e., CWT-based signal processing) neither assumes nor requires that the current is of pure PRBS waveform. Based on the actual frequency components in the voltage and current signals, the method estimates the impedance and provides the corresponding confidence intervals of the estimation. However, the CI methodology assumes the complex circularity of the signals' frequency components (presented in Section IV-A2). The PRBS complies with the requirement, and the circularity is retained as long as the signal is subjected to any kind of linear transformation. Consequently, the CI methodology is capable of handling affected PRBS signals as long as the DC-DC converter does not modify them in a nonlinear fashion.

The experiment went through five stages: fault free, dried, fault free, flooded, and back to fault free. The first fault-free stage lasted 10 minutes during which the relative humidity of the inlet air was kept at 10%. During the second stage, between the 10th and the 17th minute, the air fed to the fuel cell was dried down to a relative humidity of 2%. Afterward, the inlet air was humidified back to 10% relative humidity to simulate the fault-free stage again. In the fourth stage, between the 30th and the 47th minute, saturated air with a relative humidity of

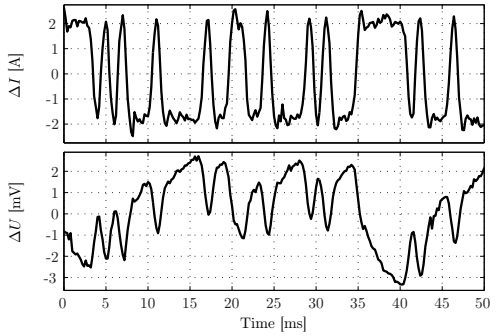


Fig. 12. Example of acquired current and voltage signals.

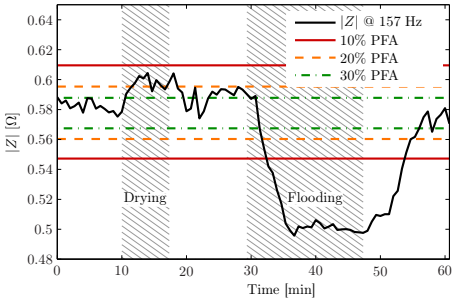


Fig. 13. Trend of $|Z|$ at 157 Hz throughout the experiment.

100% was fed into the fuel cell system, inducing flooding of fuel cells. Finally, the air humidity was decreased down to the initial 10%. Such an experiment profile enables analysis of the fuel cell response under different fault scenarios with various fault severities. These stages of the experiment are clearly indicated in Fig. 13.

B. Time evolution of particular impedance components

The parameters ρ, σ_u^2, and σ_i^2 of the PDF (13) were estimated at a frequency of 157 Hz. Note that the exact value of the selected frequency is the consequence of the parameters chosen for the CWT. The proposed CM algorithm performs efficiently also if any other frequency in the range between 10 and 200 Hz is selected. Based on the estimated parameters, the threshold values were calculated at three different $PFAs = \{10\%,\ 20\%,\ 30\%\}$. The resulting CM thresholds and the trend of $|z|$ at the selected frequency are shown in Fig. 13.

The time evolution of $|z|$ corresponds with the five experiment stages, as shown in Fig. 13. The shaded regions mark the occurrence of drying and flooding of the fuel cell. In the drying region, the module of the impedance increased and surpassed the threshold of 70%. Despite the minute changes in the relative humidity of the inflow air, there are clear changes in the value of the impedance, with 30% PFA. Unlike the minor changes caused by the mild decrease in humidity, the flooding with 100% saturated air inflow shows significant changes in all three impedance components. The values of $|z|$ indicate that the condition of the fuel cell departed from the

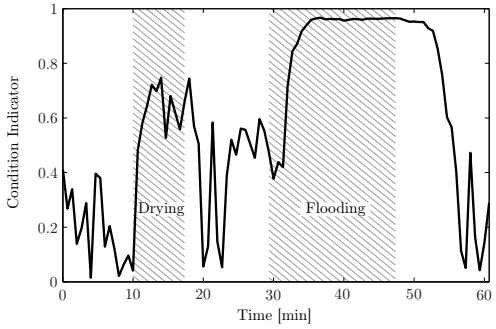


Fig. 14. Trend of the CI throughout the experiment.

fault-free area, with less than 10% PFA. Finally, when the relative humidity of the air inflow was returned to normal, the impedance components returned to the initial values within the fault-free region.

C. Time evolution of the CI

The time evolution of the CI (16) is shown in Fig. 14. The values of the CI were calculated for $PFA = 10\%$. As expected, during the fault-free operation, the CI acquired low values. As the first fault was induced, the values of the CI increased up to 0.5, which indicates deterioration of the fuel cell condition. The acquired value of 0.5 clearly shows a departure from fault-free operation and at the same time is in line with the low severity of the induced drying and relative humidity change of 8%. Unlike the low severity of the drying fault, during the flooding phase of the experiment, the value of the CI surpasses the limit value of 1. The overwhelming flooding of the system is directly reflected in the high value of the CI. Finally, at the end of the experiment, when the air condition was back to nominal, the values of the CI decreased, indicating an almost fault-free operation.

The results confirm that the CI is sufficiently sensitive to the water management faults. At the same time, the values of the CI are directly related to the severity of the fault. As such, the CI in its present form is applicable for performing fault detection and fault evaluation. In order to perform fault identification and localization, an extension of the proposed CI is required. A possible solution to this problem could be reached through the utilization and aggregation of impedance information at multiple frequencies.

VI. Conclusion

This study presents a versatile online CM system for PEM fuel cells, which builds on an integrated DC-DC converter and FCVM. As a result, a fuel cell system is enriched with information about its current health condition, which in essence enables optimal exploitation.

The system encompasses a DC-DC converter with diagnostics capabilities, a 90-channel voltage monitor, and embedded algorithms for signal processing and CM. The developed DC-DC converter module can be grouped in parallel with what the overall output power is increased. Besides power conditioning, the DC-DC converter enables system probing with arbitrary signals that can be used for diagnostic purposes. Together with the FCVM, it provides the basic hardware platform for online CM of commercial PEM fuel cell-based power systems. Both devices are built to meet tight requirements regarding size and costs imposed by commercially oriented applications and at the same time to fulfill accuracy requirements set by the diagnostic methodology.

On top of the designed hardware, the online CM system also includes the method for fast estimation of the fuel cell impedance. The benefits of the proposed methodologies are twofold. First, it considerably shortens the time required to conduct measurements, which makes it viable for commercial applications. Second, the threshold selection methodology is based on PFA, which allows unambiguous threshold specifications. Based on these thresholds, a unit-free CI is calculated, which describes the overall health of the fuel cell stack. These pieces of information are of significant practical merit for both integrators and end users.

The proposed hardware and methodology were validated on a commercially available 8.5 kW PEM fuel cell-based system. The results show that the overall system performs as expected and that it provides the desired information about the operational condition of the system.

References

[1] O. Z. Sharaf and M. F. Orhan, "An overview of fuel cell technology: Fundamentals and applications," *Renew. Sustain. Energy Rev.*, vol. 32, pp. 810–853, 2014.
[2] F. Barbir, *PEM Fuel Cells: Theory and Practice*. Elsevier, 2005.
[3] V. Jovan, M. Perne, and J. Petrovčič, "An assessment of the energetic flows in a commercial PEM fuel-cell system," *Energy Convers. Manag.*, vol. 51, no. 12, pp. 2467–2472, 2010.
[4] X. Yu, M. R. Starke, L. M. Tolbert, and B. Ozpineci, "Fuel cell power conditioning for electric power applications: A summary," *IET Electr. Power Appl.*, vol. 1, no. 5, pp. 643–656, 2007.
[5] L. Palma, M. Harfman Todorovic, and P. N. Enjeti, "Analysis of common-mode voltage in utility-interactive fuel cell power conditioners," *IEEE Trans. Ind. Electron.*, vol. 56, no. 1, pp. 20–27, 2009.
[6] S. N. Motapon, L. A. Dessaint, and K. Al-Haddad, "A comparative study of energy management schemes for a fuel-cell hybrid emergency power system of more-electric aircraft," *IEEE Trans. Ind. Electron.*, vol. 61, no. 3, pp. 1320–1334, 2014.
[7] R. J. Wai, C. Y. Lin, R. Y. Duan, and Y. R. Chang, "High-efficiency DC-DC converter with high voltage gain and reduced switch stress," *IEEE Trans. Ind. Electron.*, vol. 54, no. 1, pp. 354–364, 2007.
[8] M. Harfman Todorovic, L. Palma, and P. N. Enjeti, "Design of a wide input range DC-DC converter with a robust power control scheme suitable for fuel cell power conversion," *IEEE Trans. Ind. Electron.*, no. 3, pp. 1247–1255, 2008.
[9] G. Wu, X. Ruan, and Z. Ye, "Non-isolated high step-up DC-DC converters adopting switched-capacitor cell," *IEEE Trans. Ind. Electron.*, vol. 62, no. 1, pp. 383–393, 2015.
[10] P. Xuewei and A. K. Rathore, "Novel bidirectional snubberless naturally commutated soft-switching current-fed full-bridge isolated DC/DC converter for fuel cell vehicles," *IEEE Trans. Ind. Electron.*, vol. 61, no. 5, pp. 2307–2315, 2014.
[11] V. Valdivia, A. Barrado, A. Lazaro, M. Sanz, D. Lopez del Moral, and C. Raga, "Black-box behavioral modeling and identification of DC-DC converters with input current control for fuel cell power conditioning," *IEEE Trans. Ind. Electron.*, vol. 61, no. 4, pp. 1891–1903, 2014.
[12] K. C. Tseng and C. C. Huang, "High step-up high-efficiency interleaved converter with voltage multiplier module for renewable energy system," *IEEE Trans. Ind. Electron.*, vol. 61, no. 3, pp. 1311–1319, 2014.
[13] X. Hu and C. Gong, "A high gain input-parallel output-series DC/DC converter with dual coupled inductors," *IEEE Trans. Power Electron.*, vol. 30, no. 3, pp. 1306–1317, 2015.

[14] Y. P. Siwakoti, P. C. Loh, F. Blaabjerg, S. J. Andreasen, and G. E. Town, "Y-source boost DC/DC converter for distributed generation," *IEEE Trans. Ind. Electron.*, vol. 62, no. 2, pp. 1059–1069, 2015.

[15] Y. Tang, D. Fu, T. Wang, and Z. Xu, "Hybrid switched-inductor converters for high step-up conversion," *IEEE Trans. Ind. Electron.*, vol. 62, no. 3, pp. 1480–1490, 2015.

[16] S. Burany, R. B. Gopal, N. A. Freeman, and S. Masse, "Method and apparatus for monitoring fuel cell voltages," American Patent US 7,148,654, 2006.

[17] M. Ordonez, M. O. Sonnaillon, J. E. Quaicoe, and M. T. Iqbal, "An embedded frequency response analyzer for fuel cell monitoring and characterization," *IEEE Trans. Ind. Electron.*, vol. 57, no. 6, pp. 1925–1934, 2010.

[18] F. A. de Bruijn, V. A. T. Dam, and G. J. M. Janssen, "Review: Durability and degradation issues of PEM fuel cell components," *Fuel Cells*, vol. 8, no. 1, pp. 3–22, 2008.

[19] W. Schmittinger and A. Vahidi, "A review of the main parameters influencing long-term performance and durability of PEM fuel cells," *J. Power Sources*, vol. 180, no. 1, pp. 1–14, 2008.

[20] B. Pregelj, D. Vrečko, and V. Jovan, "Improving the operation of a fuel-cell power unit with supervision control - a simulation study," *J. Power Sources*, vol. 196, no. 22, pp. 9419–9428, 2011.

[21] S. B. Silva, M. M. Severino, and M. A. G. de Oliveira, "A stand-alone hybrid photovoltaic, fuel cell and battery system: A case study of Tocantins, Brazil," *Renew. Energy*, vol. 57, pp. 384–389, 2013.

[22] A. J. L. Verhage, J. F. Coolegem, M. J. J. Mulder, M. H. Yildirim, and F. A. de Bruijn, "30,000 h operation of a 70 kW stationary PEM fuel cell system using hydrogen from a chlorine factory," *Int. J. Hydrogen Energy*, vol. 38, no. 11, pp. 4714–4724, 2013.

[23] B. Pregelj, D. Vrečko, J. Petrovčič, V. Jovan, and G. Dolanc, "A model-based approach to battery selection for truck onboard fuel cell-based APU in an anti-idling application," *Appl. Energy*, vol. 137, pp. 64–76, 2015.

[24] X.-Z. Yuan, H. Wang, J. C. Sun, and J. Zhang, "AC impedance technique in PEM fuel cell diagnosis – A review," *Int. J. Hydrogen Energy*, vol. 32, pp. 4365–4380, 2007.

[25] J. Wu, X. Z. Yuan, H. Wang, M. Blanco, J. J. Martin, and J. Zhang, "Diagnostic tools in PEM fuel cell research: Part I Electrochemical techniques," *Int. J. Hydrogen Energy*, vol. 33, no. 6, pp. 1735–1746, 2008.

[26] R. Petrone, Z. Zheng, D. Hissel, M. Péra, C. Pianese, M. Sorrentino, M. Becherif, and N. Yousfi-Steiner, "A review on model-based diagnosis methodologies for PEMFCs," *Int. J. Hydrogen Energy*, vol. 38, no. 17, pp. 7077–7091, 2013.

[27] Z. Zheng, R. Petrone, M. Péra, D. Hissel, M. Becherif, C. Pianese, N. Yousfi-Steiner, and M. Sorrentino, "A review on non-model based diagnosis methodologies for PEM fuel cell stacks and systems," *Int. J. Hydrogen Energy*, vol. 38, no. 21, pp. 8914–8926, 2013.

[28] S. M. Rezaei Niya and M. Hoorfar, "Study of proton exchange membrane fuel cells using electrochemical impedance spectroscopy technique – A review," *J. Power Sources*, vol. 240, pp. 281–293, 2013.

[29] X.-Z. Yuan, C. Sons, H. Wang, and J. Zhang, *Electrochemical Impedance Spectroscopy in PEM Fuel Cells, Fundamentals and Applications*. London: Springer, 2010.

[30] A. Debenjak, P. Boškoski, B. Musizza, J. Petrovčič, and Đ. Juričić, "Fast measurement of proton exchange membrane fuel cell impedance based on pseudo-random binary sequence perturbation signals and continuous wavelet transform," *J. Power Sources*, vol. 254, pp. 112–118, 2014.

[31] P. Boškoski and A. Debenjak, "Optimal selection of proton exchange membrane fuel cell condition monitoring thresholds," *J. Power Sources*, vol. 268, pp. 692–699, 2014.

[32] G. Terzulli and B. W. Peace, *Film technology to replace electrolytic technology*, AVX, 2004.

[33] H. Wang and F. Blaabjerg, "Reliability of capacitors for DC-link applications in power electronic converters - an overview," *IEEE Trans. Ind. Appl.*, vol. 50, no. 5, pp. 3569–3578, 2014.

[34] T. L. Skvarenina, Ed., *The Power Electronics Handbook*, ser. Industrial Electronics. CRC Press, 2001.

[35] W. A. Kester, *Analog Devices Practical Design Techniques For Power And Thermal Management, Analog Devices technical reference books*. Analog Devices, 1998.

[36] *Modulated Constant off-Time Control Mechanism, Application Note*, Linfinity Microelectronics, 1998.

[37] S. H. Chee, *A New, High Efficiency Monolithic Buck Converter*. Linear Technology, 1995.

[38] D. Webb and S. Møller-Holst, "Measuring individual cell voltages in fuel cell stacks," *J. Power Sources*, vol. 103, pp. 54–60, 2001.

[39] D. Brunner, A. K. Prasad, S. G. Advani, and B. W. Peticolas, "A robust cell voltage monitoring system for analysis and diagnosis of fuel cell or battery systems," *J. Power Sources*, vol. 195, no. 24, pp. 8006–8012, 2010.

[40] B. Dobkin and J. Williams, Eds., *Analog Circuit Design - A Tutorial Guide to Applications and Solutions*. Elsevier, 2011.

[41] S. Mallat, *A Wavelet Tour of Signal Processing: The Sparse Way*, 3rd ed. Elsevier Academic Press, 2008.

[42] I. Daubechies, *Ten Lectures on Wavelets*, ser. CBMS-NSF Regional Conference Series in Applied Mathematics. Society for Industrial and Applied Mathematics, 1992.

[43] E. O. Doebelin, *System Modeling and Response*. John Wiley & Sons Inc, 1980.

[44] P. O. Amblard, M. Gaeta, and J. L. Lacoume, "Statistics for complex variables and signals – Part I: Variables," *Signal Process.*, vol. 53, pp. 1–13, 1996.

[45] N. Goodman, "Statistical analysis based on a certain multivariate complex Gaussian distribution," *Ann. Math. Stat.*, vol. 34, no. 1, pp. 152–177, 1963.

[46] E. Ollila, "On the circularity of a complex random variable," *IEEE Signal Process. Lett.*, vol. 15, pp. 841–844, 2008.

[47] A. Khurshid, Z. Al-Hemyari, and S. Kamal, "On complex random variables," *Pak. J. Stat. Oper. Res.*, vol. 8, no. 3, pp. 645–654, 2012.

[48] R. J. Baxley, B. T. Walkenhorst, and G. Acosta-Marum, "Complex Gaussian ratio distribution with applications for error rate calculation in fading channels with imperfect CSI," in *IEEE GLOBECOM 2010*, 2010.

[49] M. K. Simon, *Probability Distributions Involving Gaussian Random Variables*. Springer Science, 2006.

[50] E. Bechhoefer and A. P. F. Bernhard, "A generalized process for optimal threshold setting in HUMS," in *IEEE Aerospace Conference*, 2007.

[51] N. Fouquet, C. Doulet, C. Nouillant, G. Dauphin-Tanguy, and B. Ould-Bouamama, "Model based PEM fuel cell state-of-health monitoring via AC impedance measurements," *J. Power Sources*, vol. 159, pp. 905–913, 2006.

[52] J.-M. Le Canut, R. M. Abouatallah, and D. A. Harrington, "Detection of membrane drying, fuel cell flooding, and anode catalyst poisoning on PEMFC stack by electrochemical impedance spectroscopy," *J. Electrochem. Soc.*, vol. 153, pp. A857–A864, 2006.

[53] T. Kadyk, R. Hanke-Rauschenbach, and K. Sundmacher, "Nonlinear frequency response analysis of PEM fuel cells for diagnosis of dehydration, flooding and co-poisoning," *J. Electroanal. Chem.*, vol. 630, no. 1-2, pp. 19–27, 2009.

[54] M. A. Rubio, A. Urquia, and S. Dormido, "Diagnosis of performance degradation phenomena in PEM fuel cells," *Int. J. Hydrogen Energy*, vol. 35, no. 7, pp. 2586–2590, 2010.

[55] T. Kadyk, R. Hanke-Rauschenbach, and K. Sundmacher, "Nonlinear frequency response analysis of dehydration phenomena in polymer electrolyte membrane fuel cells," *Int. J. Hydrogen Energy*, vol. 37, no. 9, pp. 7689–7701, 2012.

[56] A. Debenjak, M. Gašperin, B. Pregelj, M. Atanasijević-Kunc, J. Petrovčič, and V. Jovan, "Detection of flooding and drying inside a PEM fuel cell stack," *Stroj. Vest. – J. Mech. Eng.*, vol. 59, no. 1, pp. 56–64, 2013.

[57] J. Kim, I. Lee, Y. Tak, and B. H. Cho, "Impedance-based diagnosis of polymer electrolyte membrane fuel cell failures associated with a low frequency ripple current," *Renew. Energy*, vol. 51, pp. 302–309, 2013.

[58] G. Dotelli, R. Ferrero, P. G. Stampino, S. Latorrata, and S. Toscani, "Diagnosis of PEM fuel cell drying and flooding based on power converter ripple," *IEEE Trans. Instrum. Meas.*, vol. 63, no. 10, pp. 2341–2348, 2014.

[59] M. Gašperin, P. Boškoski, A. Debenjak, and J. Petrovčič, "Signal processing and stochastic filtering for EIS based PHM of fuel cell systems," *Fuel Cells*, vol. 14, no. 3, pp. 457–465, 2014.

[60] S. Tant, S. Rosini, P. X. Thivel, F. Druart, A. Rakotondrainibe, T. Geneston, and Y. Bultel, "An algorithm for diagnosis of proton exchange membrane fuel cells by electrochemical impedance spectroscopy," *Electrochim. Acta*, vol. 135, pp. 368–379, 2014.

[61] G. Dotelli, R. Ferrero, P. G. Stampino, S. Latorrata, and S. Toscani, "PEM fuel cell drying and flooding diagnosis with signals injected by a power converter," *IEEE Trans. Instrum. Meas.*, vol. PP, no. 99, pp. 1–8, 2015.

[62] R. Isermann and M. Münchhof, *Identification of Dynamic Systems: An Introduction with Applications*, ser. Advanced textbooks in control and signal processing. Springer-Verlag Berlin Heidelberg, 2011.



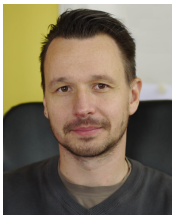
Andrej Debenjak (S'11) received his B.Sc. degree in electrical engineering from the University of Ljubljana, Slovenia, in 2011. Currently, he is employed as a young researcher at the Jožef Stefan Institute, and he is pursuing his Ph.D. degree at the Jožef Stefan International Postgraduate School in Ljubljana, Slovenia. His research is mainly focused on fault detection and diagnostics of PEM fuel cell systems and prognostics and health management of lithium-based batteries. Areas of his expertise include embedded programming, digital signal processing, statistical analysis, and diagnostics algorithm design. In the last few years, he was involved in the design of an approach for fast online diagnostics of PEM fuel cells, he was responsible for algorithms and firmware design for a modular Li-Ion BMS, and he was working on the development of a measurement equipment for fast online impedance estimation of Li-S cells.



Janko Petrovčič received his Ph.D. degree from the Faculty of Electrical and Computer Engineering, University of Ljubljana, Slovenia, in 1992. He joined the Jožef Stefan Institute, Ljubljana, Slovenia, in 1983 and since then works at the Department of Systems and Control. He is currently an R&D advisor. His main activities are in the fields of process control engineering, process control algorithms, industrial diagnostic, signal acquisition, and electronic design. He works mainly on research and development projects for industry and is responsible for the hardware support of basic research activities of the Department of Systems and Control. He was leading an electronic design of a control coprocessor module for Mitsubishi Electric Europe. Recently, he led the design of several diagnostic systems for vacuum cleaner and EC motors for Domel d.d., Slovenia. He also participated in the design of new BLDC-driven valve actuators for Danfoss Trata. Currently, he works on EU's FP7 projects, concerning the application of fuel cell-based power systems.



Pavle Boškoski received his B.Sc. in 2002 and Ms.C. in 2007 at the University "Ss. Cyril and Methodius," R. Macedonia. In 2011 he received his Ph.D. with the topic "Condition monitoring of mechanical drives," at the Jožef Stefan International Postgraduate School in Ljubljana, Slovenia. Since 2011, he has been employed at the Jožef Stefan Institute in Ljubljana, Department of Systems and Control. His research work was focused on the development of signal processing methods for prognostics and health management of mechanical drives. Since 2012, his work has been focused on the development of methods for diagnostics of fuel cell-based systems. He authored or coauthored more than 40 journal and conference papers.



Bojan Musizza received his B.Sc. in 2003 and Ph.D. in 2008 with the topic "Methods for analysis of phase interactions and causality analysis between brain and cardio-respiratory oscillations," at the University of Ljubljana. Since 2003, he has been employed at the Jožef Stefan Institute in Ljubljana, Department of Systems and Control. His research work was focused on the development of methods for causality detection between biological oscillators with the application to the problem of depth of anesthesia monitoring. Since 2009, his work has been focused on the development and application of purpose-build electronic modules and software tools for diagnostics and control of fuel cell-based systems, and the development and implementation of signal processing methods for tackling problems in industrial diagnostics. In these fields, he authored or coauthored more than 60 journal and conference papers.



Đani Juričić has earned his Ph.D. in automatic control in 1990 from the University of Ljubljana, Slovenia. Since 1981, he has been affiliated with the Jožef Stefan Institute as head deputy of the Department of Systems and Control. Since 2013, he has been full professor at the University of Nova Gorica, Slovenia. His interests span condition monitoring, with particular focus on fault detection, diagnosis, and prognosis; nonlinear dynamic system identification; statistical signal processing; and optimal control. He has (co)authored more than 200 journal and conference papers with peer review and delivered 10 invited talks. He has been coordinator or person responsible in nearly 40 research projects and projects for the industry. He received several awards, including DAAD Fellowship (2001) and ISA Transactions Best Paper Award for 2009. He is a member of IFAC Technical Committee SAFEPROCESS and a member of the General Assembly and Council of the European Control Association.

Chapter 6

Conclusions

This dissertation addresses the problem of reliable condition monitoring of PEM fuel cells. The work can be summarised in the following original scientific contributions:

- *The approach for fast impedance estimation* that provides a fast and high time-frequency resolution estimate of the impedance characteristic of a PEM fuel cell.
- *The method for optimal selection of condition monitoring thresholds* that offers an analytical solution to the problem of tuning the threshold values of an EIS-based diagnostic system for PEM fuel cells.
- *The unit-free condition indicator* that encompasses the overall condition of a PEM fuel cell and presents it in a clear manner.
- *The condition monitoring system for PEM fuel cells* that consists of a modular DC-DC converter and a 90-channel FCVM. The DC-DC converter, interconnected with the FCVM, forms a self-sufficient diagnostic system capable of performing various diagnostic tasks.

The approach for fast impedance estimation uses excitation signals of the PRBS waveform. The computational procedure of the impedance estimation is based on the CWT with Morlet mother wavelet. Due to the PRBS excitation and the CWT, the approach provides a high time-frequency resolution estimate of the impedance characteristic of a PEM fuel cell. The main advantage of the approach, compared to the conventional one (i.e., single-sine), is the shorter probing time. To estimate the frequency characteristic of a fuel cell in a frequency band from 0.1 Hz to 500 Hz, the required probing time is 60 s. This is approximately five times faster compared to the single-sine approach. Short probing time decreases the invasivity level subjected to a fuel cell or stack under the test. Consequently, the utilisation of the EIS-based CM becomes feasible also for the out-of-laboratory PEM fuel cell systems. Moreover, since the PRBS is a broadband signal, the value of the impedance can be estimated at any frequency of interest.

The method for optimal selection of CM thresholds builds on the fast impedance estimation approach. It exploits one of the statistical properties of the PRBS signal, namely the complex Gaussian circularity of the PRBS's frequency components. The main novelty of the method is the concept of treating the impedance at individual frequency as a complex random variable. The method outlines an analytical solution to the problem of tuning the threshold values of an EIS-based diagnostic system for PEM fuel cells. The decision thresholds are determined based on the CDF of the impedance amplitude and the value of the predetermined PFA. The main advantage of the method is that it requires no prior information about the operation of the fuel cell under the faulty conditions. The threshold

values are determined solely based on the characteristic data under fault-free operation of the cell and the desired level of the PFA.

The unit-free CI for fault detection in PEM fuel cells is constructed from a set of fuel cell impedance values at a number of frequencies. These impedance values at individual frequencies are treated as dependent complex random variables. The information aggregation of the set of the impedance values into the CI is performed by the copula functions. The CI is defined as the output of the constructed copula. The sensitivity of copula to the changes of the underlaying distributions of the impedance at individual frequencies enables the detection of the departure of the system condition away from the reference condition. The proposed CI describes a probability of observing a particular combination of the impedance values. Thus, it is directly related to the condition of a PEM fuel cell as well as the severity of the present fault.

The CM system for PEM fuel cells consists of the modular DC-DC converter and the 90-channel FCVM. The systems bridges the gap between the laboratory-grade measurement equipment and the commercial diagnostic systems. It is both commercially viable and accurate enough to perform the measurements required for the diagnostic purposes. The interconnection enables joint injection of excitation signals and acquisition of measurements that are required for fast online estimation of the impedance of PEM fuel cells. The embedded CM system provides the user or the high-level supervisory control system with the basic monitoring information as well as with the sophisticated CM information in the form of the CI. Furthermore, it is also a capable platform for future development of the CM approaches.

The work presented in this dissertation is focused on PEM fuel cells. However, the majority of the contributions is applicable to any type of electrochemical cell with rather slight modifications. The approach for fast impedance estimation has been applied to laboratory-grade lithium-sulphur battery cells and to a commercially available lithium-ion battery pack.

Further Work

Five research and development topics have been identified that are worth taking into consideration and pursuing:

Extension to other faults in PEM fuel cell and fault isolation
: The dissertation provides the methodology for CM of PEM fuel cells. However, the answer to which fault is present remains open. Therefore, the fault isolation is the next logical step. In a part, this issue is relatively straightforward to tackle, since the individual faults tend to move into specific regions of the multidimensional space of the copula structure. However, with a high number of the possible faults that have to be isolated, the isolation becomes harder to tackle.

Prognostics
: First, the proposed CI should be extended to the health indicator (HI), describing the overall state of health of a PEM fuel cell system. Then, the prognostics approaches should be explored in order to come up with a suitable prognostics model for the prediction of the remaining useful life of the system.

Non-stationary operating conditions
: The operating conditions of the PEM fuel cell are not necessarily stationary. During operation, a fuel cell system can be subjected to different load currents, temperatures, etc. The state-of-the-art CM methodologies are too sensitive to these changes in the operating conditions, which makes them unsuitable for some of the applications.

Further development of the embedded CM platform

The platform should be further developed and improved. The primary focus should be widening of the frequency band to higher frequencies. The stack loading capacitance should be optimised toward lower values in order to reduce the influence to the impedance measurements.

Transfer of the methodology to other scientific areas

The fast impedance estimation approach is easily applicable to any type of electrochemical cell. It has been already successfully applied to lithium-based battery cells (Figure A.1 shows the impedance characteristic of a lithium-sulphur battery cell obtained by the fast impedance estimation approach). The approach has a potential of being successfully applied for the CM and prognostics of lithium-based batteries.

Appendix A

Matlab Code for Fast Impedance Estimation

The Matlab code for fast impedance estimation, together with the sample dataset, is publicly available on the website of the Department of Systems and Control, Jožef Stefan Institute. The package can be directly accessed at http://dsc.ijs.si/files/datasets_files/fast_eis.zip. The package includes two Matlab script files and three data files with the current and voltage measurements conducted on a laboratory-grade lithium-sulphur battery cell according to the fast impedance estimation approach. Listing A.1 lists `compute_impedance.m` Matlab script. The script loads the data files and calls the `fc_impedance_cwtft.m` function (listed by Listing A.2). The `fc_impedance_cwtft.m` function performs the CWT signal processing and estimates the impedance. As a final result, the Nyquist plot of the estimated impedance is produced, as presented in Figure A.1.

Listing A.1: `compute_impedance.m` Matlab script.

```
%% Estimation of electrochemical cell impedance
%  using CWT with complex Morlet mother wavelet
%
%  This .m file is intended to show how the impedance can be estimated
%  based on the procedure described by Debenjak et. el (2014). The paper
%  talks about PEM fuel cell impedance, however, the exact procedure can be
%  used on any kind of electrochemical cell.
%
%  In the .mat files are voltage and current measurements taken on a
%  laboratory-grade Li-S cell. Voltage and Current are measured in mV and
%  mA, respectively. Each .mat file contains measurements at specific PRBS
%  sampling frequency covering specific frequency region. The final
%  impedance characteristic is therefore constructed from three parts.
%
%  Please cite as:
%  A. Debenjak, P. Boskoski, B. Musizza, J. Petrovcic, D. Juricic. Fast
%  measurement of proton exchange membrane fuel cell impedance based on
%  pseudo-random binary sequence perturbation signals and continuous
%  wavelet transform. Journal of Power Sources (254), pp. 112-118, 2014.
%
%% Low frequency part from 0.05 to 5 Hz
disp('Low frequency part');
```

```
load meas_prbs__low.mat %load data file

nb = 20; %number of frequencies at which the CWT will be computed
cwt_data = zeros(6, nb); %prepare output data matrix

f_min = 0.05;          %lower frequency bound in Hz
f_max = 5;             %higher frequency bound in Hz
fs = 100000;           %sampling rate in Hz
decimate_factor = 10;  %decimate factor for resampling (down-sampling)
f0 = 5;                %Morlet central frequency

[Z f varA varPhi stat Wz c_u c_i ts] = ...
    fc_impedance_cwtft(u_ac, i_ac, f_min, f_max, fs, decimate_factor, ...
    f0, nb);

for kk=1:length(stat.real)
    % voltage CWT coefficients
    cwt_data(1, kk) = stat.real(kk).median;
    cwt_data(2, kk) = stat.real(kk).prctile10;
    cwt_data(3, kk) = stat.real(kk).prctile90;

    % current CWT coefficients
    cwt_data(4, kk) = stat.imag(kk).median;
    cwt_data(5, kk) = stat.imag(kk).prctile10;
    cwt_data(6, kk) = stat.imag(kk).prctile90;
end

% compute the impedance
Z_low = (cwt_data(1,:) + j*cwt_data(4,:));
f_low = f;

%% Medium frequency part from 1 to 500 Hz
disp('Medium frequency part');
load meas_prbs__med.mat %load data file

nb = 40; %number of frequencies at which the CWT will be computed
cwt_data = zeros(6, nb); %prepare output data matrix

f_min = 1;             %lower frequency bound in Hz
f_max = 500;           %higher frequency bound in Hz
fs = 100000;           %sampling rate in Hz
decimate_factor = 1;   %decimate factor for resampling
f0 = 15;               %Morlet central frequency

[Z f varA varPhi stat Wz c_u c_i ts] = ...
    fc_impedance_cwtft(u_ac, i_ac, f_min, f_max, fs, decimate_factor, ...
    f0, nb);

for kk=1:length(stat.real)
    % voltage CWT coefficients
```

```
    cwt_data(1, kk) = stat.real(kk).median;
    cwt_data(2, kk) = stat.real(kk).prctile10;
    cwt_data(3, kk) = stat.real(kk).prctile90;

    % current CWT coefficients
    cwt_data(4, kk) = stat.imag(kk).median;
    cwt_data(5, kk) = stat.imag(kk).prctile10;
    cwt_data(6, kk) = stat.imag(kk).prctile90;
end

% compute the impedance
Z_med = (cwt_data(1,:) + j*cwt_data(4,:));
f_med = f;

%% High frequency part from 400 to 20000 Hz
disp('High frequency part');
load meas_prbs_high.mat %load data file

nb = 20; %number of frequencies at which the CWT will be computed
cwt_data = zeros(6, nb); %prepare output data matrix

f_min = 400;          %lower frequency bound in Hz
f_max = 20000;        %higher frequency bound in Hz
fs = 200000;          %sampling rate in Hz
decimate_factor = 1;  %decimate factor for resampling
f0 = 50;              %Morlet central frequency

[Z f varA varPhi stat Wz c_u c_i ts] = ...
    fc_impedance_cwtft(u_ac, i_ac, f_min, f_max, fs, decimate_factor, ...
    f0, nb);

for kk=1:length(stat.real)
    % voltage CWT coefficients
    cwt_data(1, kk) = stat.real(kk).median;
    cwt_data(2, kk) = stat.real(kk).prctile10;
    cwt_data(3, kk) = stat.real(kk).prctile90;

    % current CWT coefficients
    cwt_data(4, kk) = stat.imag(kk).median;
    cwt_data(5, kk) = stat.imag(kk).prctile10;
    cwt_data(6, kk) = stat.imag(kk).prctile90;
end

% compute the impedance
Z_high = (cwt_data(1,:) + j*cwt_data(4,:));
f_high = f;
%% Plot the impedance characteristic
figure();
hold on

```

```
plot(Z_low, 'b', 'linewidth', 2);
plot(Z_med, 'b', 'linewidth', 2);
plot(Z_high, 'b', 'linewidth', 2);
axis equal
grid on
title('Impedance characteristic [50 mHz --- 20 kHz]')
xlabel('Re [\Omega]')
ylabel('Im [\Omega]')
```

Listing A.2: `fc_impedance_cwtft.m` Matlab script.

```
function [Z,fr,varA, varPhi,stats,Wz,c_u,c_i,ts]=fc_impedance_cwtft(voltage,
    current,f_min,f_max,fs,decimate_factor,f0,nb)
% Function returns the CWT coefficients of the input current and voltage
% signals and the coefficients' statistics

    % decimate signals if requested
    if (decimate_factor > 1)
        u_fc = decimate(voltage,decimate_factor);
        i_fc = decimate(current,decimate_factor);
        fs = fs/decimate_factor;
    else
        u_fc = voltage;
        i_fc = current;
    end

    % compute the scale-frequency factor
    MorletFourierFactor = 4*pi/(f0+sqrt(2+f0^2));

    % create wavelet structure
    WAV={'morl',f0};

    % create scales structure
    s0 = fs/(f_max * MorletFourierFactor);
    mx = fs/(f_min * MorletFourierFactor);
    ds = log(mx/s0)/log(2)/(nb-1);
    scales = struct('s0',s0,'ds',ds,'nb',nb,'type','pow','pow',2);

    % compute the CWT
    disp('Starting CWT..');
    c_u = cwtft(u_fc,'wavelet',WAV,'scales',scales);
    c_i = cwtft(i_fc,'wavelet',WAV,'scales',scales);
    disp('CWT Done..');
    % compute instantaneous impedance
    Wz=c_u.cfs./c_i.cfs;

    % cone of influence for the Morlet wavelet
    s=c_u.scales;
    ts=ceil(sqrt(2)*s);
```

```
38
39      % determin the statistics
40      varA = zeros(size(ts));
41      varPhi = zeros(size(ts));
42      Z = zeros(size(ts));
43      disp(['Calculating stat for ' num2str(length(ts)) ' scales...']);
44      for ii=1:length(ts)
45          if (size(Wz,2) <= ts(ii))
46              varA(ii) = NaN;
47              varPhi(ii) = NaN;
48              Z(ii) = NaN;
49              fr(ii) = NaN;
50
51              stats.angle(ii).median = NaN;
52              stats.angle(ii).prctile10 = NaN;
53              stats.angle(ii).prctile90 = NaN;
54
55              stats.abs(ii).median = NaN;
56              stats.abs(ii).prctile10 = NaN;
57              stats.abs(ii).prctile90 = NaN;
58
59              stats.real(ii).median = NaN;
60              stats.real(ii).prctile10 = NaN;
61              stats.real(ii).prctile90 = NaN;
62
63              stats.imag(ii).median = NaN;
64              stats.imag(ii).prctile10 = NaN;
65              stats.imag(ii).prctile90 = NaN;
66          else
67              varA(ii) = var(abs(Wz(ii,ts(ii):end-ts(ii))));
68              varPhi(ii) = var(angle(Wz(ii,ts(ii):end-ts(ii))));
69              Z(ii) = mean(real( Wz(ii,ts(ii):end-ts(ii)) ) ) ...
70                  + 1i*mean(imag( Wz(ii,ts(ii):end-ts(ii)) ) );
71
72              stats.real(ii).median = median(real(Wz(ii,ts(ii):end-ts(ii))));
73              stats.real(ii).prctile10 = prctile(real(Wz(ii,ts(ii):end-ts(ii))
                    ),10);
74              stats.real(ii).prctile90 = prctile(real(Wz(ii,ts(ii):end-ts(ii))
                    ),90);
75
76              stats.imag(ii).median = median(imag(Wz(ii,ts(ii):end-ts(ii))));
77              stats.imag(ii).prctile10 = prctile(imag(Wz(ii,ts(ii):end-ts(ii))
                    ),10);
78              stats.imag(ii).prctile90 = prctile(imag(Wz(ii,ts(ii):end-ts(ii))
                    ),90);
79
80              fr(ii) = 1./(c_u.scales(ii)*MorletFourierFactor)*fs;
81
82              if isnan(fr(ii))
83                  disp(c_u.scales(ii));
```

```
84                  disp(MorletFourierFactor);
85                  disp(fs);
86              end
87          end
88      end
89  end
```

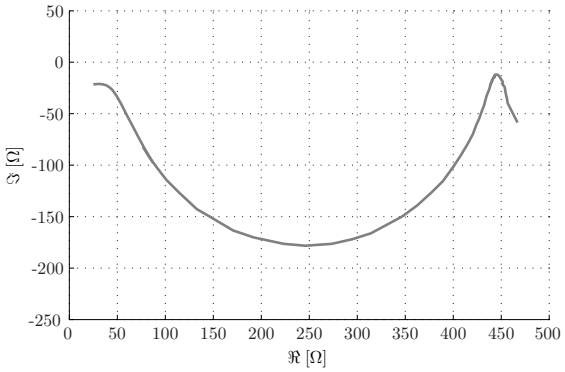


Figure A.1: An impedance characteristic from 50 mHz to 20 kHz – the output of the publicly available package.

References

Amblard, P. O., Gaeta, M., & Lacoume, J. L. (1996). Statistics for complex variables and signals – Part I: Variables. *Signal Processing*, *53*, 1–13.

Barbir, F. (2005). *PEM fuel cells: theory and practice*. Burlington, MA: Elsevier Academic Press.

Baxley, R. J., Walkenhorst, B. T., & Acosta-Marum, G. (2010). Complex Gaussian ratio distribution with applications for error rate calculation in fading channels with imperfect CSI. In *2010 IEEE Global Telecommunications Conference (GLOBECOM 2010)* (pp. 1–5).

Bechhoefer, E. & Bernhard, A. (2007). A generalized process for optimal threshold setting in HUMS. In *2007 IEEE Aerospace Conference* (pp. 1–9).

Benouioua, D., Candusso, D., Harel, F., & Oukhellou, L. (2014). PEMFC stack voltage singularity measurement and fault classification. *International Journal of Hydrogen Energy*, *39*(36), 21631–21637. doi:10.1016/j.ijhydene.2014.09.117

Berg, D. & Aas, K. (2009). Models for construction of multivariate dependance: A comparison study. *The European Journal of Finance*, *15*(7-8), 639–659. doi:10.1080/13518470802588767

Boghani, H. C., Kim, J. R., Dinsdale, R. M., Guwy, A. J., & Premier, G. C. (2013). Analysis of the dynamic performance of a microbial fuel cell using a system identification approach. *Journal of Power Sources*, *238*, 218–226. doi:10.1016/j.jpowsour.2013.03.061

Borup, R. L., Davey, J. R., Garzon, F. H., Wood, D. L., & Inbody, M. A. (2006). PEM fuel cell electrocatalyst durability measurements. *Journal of Power Sources*, *163*(1), 76–81. doi:10.1016/j.jpowsour.2006.03.009

Borup, R., Meyers, J., Pivovar, B., Kim, Y. S., Mukundan, R., Garland, N., ... Iwashita, N. (2007). Scientific aspects of polymer electrolyte fuel cell durability and degradation. *Chemical Reviews*, *107*(10), 3904–3951. doi:10.1021/cr050182l

Boškoski, P. & Debenjak, A. (2014). Optimal selection of proton exchange membrane fuel cell condition monitoring thresholds. *Journal of Power Sources*, *268*, 692–699. doi:10.1016/j.jpowsour.2014.06.110

Boškoski, P. & Juričić, Đ. (2012). Fault detection of mechanical drives under variable operating conditions based on wavelet packet Rényi entropy signatures. *Mechanical Systems and Signal Processing*, *31*, 369–381. doi:10.1016/j.ymssp.2012.04.016

Bouyé, E., Durrleman, V., Nikeghbaliand, A., Riboulet, G., & Roncalli, T. (2000). *Copulas for finance - A reading guide and some applications*. Social Science Research Network. doi:10.2139/ssrn.1032533

Brunetto, C., Moschetto, A., & Tina, G. (2008). PEM fuel cell testing by electrochemical impedance spectroscopy. *Electric Power System Research*, *79*, 17–26. doi:10.1016/j.epsr.2008.05.012

Brunner, D., Prasad, A. K., Advani, S. G., & Peticolas, B. W. (2010). A robust cell voltage monitoring system for analysis and diagnosis of fuel cell or battery systems. *Journa of Power Sources*, *195*(24), 8006–8012. doi:10.1016/j.jpowsour.2010.06.054

Büchi, F. N., Marek, A., & Scherer, G. G. (1995). In situ membrane resistance measurements in polymer electrolyte fuel cells by fast auxiliary current pulses. *Journal of The Electrochemical Society*, *142*(6), 1895–1901. doi:10.1149/1.2044211

Burany, S., Gopal, R. B., Freeman, N. A., & Masse, S. (2006). *Method and apparatus for monitoring fuel cell voltages*. US patent 7,148,654.

Chee, S. H. (1995). *A new, high efficiency monolithic buck converter*. Linear Technology.

Cheng, X., Shi, Z., Glass, N., Zhang, L., Zhang, J., Song, D., ... Shen, J. (2007). A review of PEM hydrogen fuel cell contamination: impacts, mechanisms, and mitigation. *Journal of Power Sources*, *165*(2), 739–756. doi:10.1016/j.jpowsour.2006.12.012

Ciureanu, M. (2004). Effects of Nafion dehydration in PEM fuel cells. *Journal of Applied Electrochemistry*, *34*(7), 705–714. doi:10.1023/B:JACH.0000031102.32521.c6

Colón-Mercado, H. R. & Popov, B. N. (2006). Stability of platinum based alloy cathode catalysts in PEM fuel cells. *Journal of Power Sources*, *155*(2), 253–263. doi:10.1016/j.jpowsour.2005.05.011

Cruz-Manzo, S. & Chen, R. (2013). An electrical circuit for performance analysis of polymer electrolyte fuel cell stacks using electrochemical impedance spectroscopy. *Journal of The Electrochemical Society*, *160*(10), F1109–F1115. doi:10.1149/2.025310jes

Daubechies, I. (1992). *Ten lectures on wavelets*. Philadelphia, PA: Society for Industrial and Applied Mathematics.

Davies, W. (1970). *System identification for self-adaptive control*. New York, NY: John Wiley & Sons.

de Bruijn, F. A., Dam, V. A. T., & Janssen, G. J. M. (2008). Review: durability and degradation issues of PEM fuel cell components. *Fuel Cells*, *8*(1), 3–22. doi:10.1002/fuce.200700053

Debenjak, A., Boškoski, P., Musizza, B., Petrovčič, J., & Juričić, Đ. (2014). Fast measurement of proton exchange membrane fuel cell impedance based on pseudo-random binary sequence perturbation signals and continuous wavelet transform. *Journal of Power Sources*, *254*, 112–118. doi:10.1016/j.jpowsour.2013.12.094

Debenjak, A., Gašperin, M., & Petrovčič, J. (2013). On-line tracking of fuel cell system impedance using extended kalman filter. In *Chemical Engineering Transactions: 2013 Prognostics and System Health Management Conference* (Vol. 33, pp. 1003–1008). doi:10.3303/CET1333168

Debenjak, A., Gašperin, M., Pregelj, B., Atanasijević-Kunc, M., Petrovčič, J., & Jovan, V. (2013). Detection of flooding and drying inside a PEM fuel cell stack. *Strojniški vestnik – Journal of Mechanical Engineering*, *59*(1), 56–64. doi:10.5545/sv-jme.2012.640

Debenjak, A., Petrovčič, J., Boškoski, P., Musizza, B., & Juričić, Đ. (2015). Fuel cell condition monitoring system based on interconnected DC-DC converter and voltage monitor. *IEEE Transactions on Industrial Electronics*, *62*(8), 1–13. doi:10.1109/TIE.2015.2434792

Dobkin, B. & Williams, J. (Eds.). (2011). *Analog circuit design - A tutorial guide to applications and solutions*. Amsterdam: Elsevier.

Doebelin, E. O. (1980). *System modeling and response*. New York, NY: John Wiley & Sons Inc.

Dotelli, G., Ferrero, R., Stampino, P. G., Latorrata, S., & Toscani, S. (2014). Diagnosis of PEM fuel cell drying and flooding based on power converter ripple. *IEEE Transac-*

tions on Instrumentation and Measurement, *63*(10), 2341–2348. doi:10.1109/TIM.2014.2318371

Dotelli, G., Ferrero, R., Stampino, P. G., Latorrata, S., & Toscani, S. (2015). PEM fuel cell drying and flooding diagnosis with signals injected by a power converter. *IEEE Transactions on Instrumentation and Measurement*, *PP*(99), 1–8. doi:10.1109/TIM.2015.2406051

Fairweather, A., Foster, M., & Stone, D. (2012). Modelling of VRLA batteries over operational temperature range using pseudo random binary sequences. *Journal of Power Sources*, *207*, 56–59. doi:10.1016/j.jpowsour.2012.02.024

Fairweather, J. D., Spernjak, D., Weber, A. Z., Harvey, D., Wessel, S., Hussey, D. S., ... Borup, R. L. (2013). Effects of cathode corrosion on through-plane water transport in proton exchange membrane fuel cells. *Journal of The Electrochemical Society*, *160*(9), F980–F993. doi:10.1149/2.024309jes

Farrell, C., Gardner, C., & Ternan, M. (2007). Experimental and modelling studies of CO poisoning in PEM fuel cells. *Journal of Power Sources*, *171*(2), 282–293. doi:10.1016/j.jpowsour.2007.07.006

Fischer, M., Kock, C., Schluter, S., & Weigert, F. (2009). An empirical analysis of multivariate copula models. *Quantitative Finance*, *9*(7), 839–854.

Fouquet, N., Doulet, C., Nouillant, C., Dauphin-Tanguy, G., & Ould-Bouamama, B. (2006). Model based PEM fuel cell state-of-health monitoring via AC impedance measurements. *Journal of Power Sources*, *159*, 905–913. doi:10.1016/j.jpowsour.2005.11.035

Fowler, M., Mann, R. F., Amphlett, J. C., Peppley, B. A., & Roberge, P. R. (2005). Reliability issues and voltage degradation. In W. Vielstich, A. Lamm, & H. A. Gasteiger (Eds.), *Handbook of fuel cells*. Chichester, England: John Wiley & Sons, Ltd. doi:10.1002/9780470974001.f303056

Gašperin, M., Boškoski, P., Debenjak, A., & Petrovčič, J. (2014). Signal processing and stochastic filtering for EIS based PHM of fuel cell systems. *Fuel Cells*, *14*(3), 457–465. doi:10.1002/fuce.201300217

Genest, C. & Favre, A. C. (2007). Everything you always wanted to know about copula modeling but were afraid to ask. *Journal of Hydrologic Engineering*, *12*(4), 347–368. doi:10.1061/(ASCE)1084-0699(2007)12:4(347)

Goodman, N. (1963). Statistical analysis based on a certain multivariate complex Gaussian distribution. *The Annals of Mathematical Statistics*, *34*(1), 152–177.

Harfman Todorovic, M., Palma, L., & Enjeti, P. N. (2008). Design of a wide input range DC-DC converter with a robust power control scheme suitable for fuel cell power conversion. *IEEE Transactions on Industrial Electronics*, (3), 1247–1255. doi:10.1109/TIE.2007.911200

Al-Harthy, M., Begg, S., & Bratvold, R. B. (2007, May). Copulas: a new technique to model dependence in petroleum decision making. *Journal of Petroleum Science and Engineering*, *57*(1-2), 195–208. doi:10.1016/j.petrol.2005.10.015

Hofert, M. (2010). Construction and sampling of nested archimedean copulas. In P. Jaworski, F. Durante, W. K. Härdle, & T. Rychlik (Eds.), *Copula theory and its applications* (Vol. 198, pp. 147–160). Springer Berlin Heidelberg. doi:10.1007/978-3-642-12465-5_7

Hu, X. & Gong, C. (2015). A high gain input-parallel output-series DC/DC converter with dual coupled inductors. *IEEE Transactions on Power Electronics*, *30*(3), 1306–1317. doi:10.1109/TPEL.2014.2315613

Isermann, R. & Ballé, P. (1997). Trends in the application of model-based fault detection and diagnosis of technical processes. *Control Engineering Practice*, *5*(5), 709–719. doi:10.1016/S0967-0661(97)00053-1

Isermann, R. & Münchhof, M. (2011). *Identification of dynamic systems: An introduction with applications*. Springer-Verlag Berlin Heidelberg. doi:10.1007/978-3-540-78879-9

Jaimungal, S. & Ng, E. K. H. (2009). Kernel-based copula processes. In W. Buntine, M. Grobelnik, D. Mladenić, & J. Shawe-Taylor (Eds.), *Machine learning and knowledge discovery in databases* (Vol. 5781, pp. 628–643). doi:10.1007/978-3-642-04180-8_58

Jardine, A., Lin, D., & Banjevic, D. (2006). A review on machinery diagnostics and prognostics implementing condition-based maintenance. *Mechanical Systems and Signal Processing*, *20*(6), 1483–1510. doi:10.1016/j.ymssp.2005.09.012

Joe, H. (1997). *Multivariate models and dependence concepts*. London: Chapman and Hall.

Jouin, M., Gouriveau, R., Hissel, D., Péra, M.-C., & Zerhouni, N. (2013). Prognostics and health management of PEMFC – state of the art and remaining challenges. *International Journal of Hydrogen Energy*, *38*(35), 15307–15317. doi:10.1016/j.ijhydene.2013.09.051

Jouin, M., Gouriveau, R., Hissel, D., Péra, M.-C., & Zerhouni, N. (2014). Prognostics of PEM fuel cell in a particle filtering framework. *International Journal of Hydrogen Energy*, *39*(1), 481–494. doi:10.1016/j.ijhydene.2013.10.054

Jovan, V., Perne, M., & Petrovčič, J. (2010). An assessment of the energetic flows in a commercial PEM fuel-cell system. *Energy Conversion and Management*, *51*(12), 2467–2472. doi:10.1016/j.enconman.2010.04.014

Kadyk, T., Hanke-Rauschenbach, R., & Sundmacher, K. (2009). Nonlinear frequency response analysis of PEM fuel cells for diagnosis of dehydration, flooding and co-poisoning. *Journal of Electroanalytical Chemistry*, *630*(1-2), 19–27. doi:10.1016/j.jelechem.2009.02.001

Kadyk, T., Hanke-Rauschenbach, R., & Sundmacher, K. (2011). Nonlinear frequency response analysis for the diagnosis of carbon monoxide poisoning in PEM fuel cell anodes. *Journal of Applied Electrochemistry*, *41*(9), 1021–1032. doi:10.1007/s10800-011-0298-8

Kadyk, T., Hanke-Rauschenbach, R., & Sundmacher, K. (2012). Nonlinear frequency response analysis of dehydration phenomena in polymer electrolyte membrane fuel cells. *International Journal of Hydrogen Energy*, *37*(9), 7689–7701. 7th Petite Workshop on the Defect Chemical Nature of Energy Materials, 14-17 March 2011, Storaas, Kongsberg, Norway. doi:10.1016/j.ijhydene.2012.01.148

Kester, W. A. (1998). *Analog devices practical design techniques for power and thermal management, analog devices technical reference books*. Analog Devices.

Khurshid, A., Al-Hemyari, Z., & Kamal, S. (2012). On complex random variables. *Pakistan Journal of Statistics and Operation Research*, *8*(3), 645–654.

Kim, J. M., Jung, Y. S., Sungur, E. A., Han, K. H., Park, C., & Sohn, I. (2008). A copula method for modeling directional dependence of genes. *BMC Bioinformatics*, *9*(1), 225–236. doi:10.1186/1471-2105-9-225

Kim, J., Lee, I., Tak, Y., & Cho, B. H. (2013). Impedance-based diagnosis of polymer electrolyte membrane fuel cell failures associated with a low frequency ripple current. *Renewable Energy*, *51*, 302–309. doi:10.1016/j.renene.2012.09.053

Kvandal, P., Sheppard, L., Landsverk, S. A., Stefanovska, A., & Kirkeboen, K. A. (2013). Impaired cerebrovascular reactivity after acute traumatic brain injury can be detected by wavelet phase coherence analysis of the intracranial and arterial blood pressure signals. *Journal of Clinical Monitoring and Computing*, *27*(4), 375–383. doi:10.1007/s10877-013-9484-z

Le Canut, J.-M., Abouatallah, R. M., & Harrington, D. A. (2006). Detection of membrane drying, fuel cell flooding, and anode catalyst poisoning on PEMFC stack by elec-

trochemical impedance spectroscopy. *Journal of The Electrochemical Society*, *153*, A857–A864. doi:10.1149/1.2179200

Lee, J. S., Quan, N. D., Hwang, J. M., Lee, S. D., Kim, H., Lee, H., & Kim, H. S. (2006). *Journal of Industrial and Engineering Chemistry*, *12*(2), 175–183.

Leemis, L. M. & Park, S. K. (2005). *Discrete-event simulation: A first course*. Upper Saddle River, NJ: Prentice-Hall, Inc.

Li, H., Tang, Y., Wang, Z., Shi, Z., Wu, S., Song, D., ... Mazza, A. (2008). A review of water flooding issues in the proton exchange membrane fuel cell. *Journal of Power Sources*, *178*(1), 103–117. doi:10.1016/j.jpowsour.2007.12.068

Liu, W. & Tang, B. (2011). A hybrid time-frequency method based on improved morlet wavelet and auto terms window. *Expert Systems with Applications*, *38*(6), 7575–7581. doi:10.1016/j.eswa.2010.12.107

Ljung, L. (1999). *System identification: Theory for the user* (2nd ed.). Englewood Cliffs, NJ: Prentice-Hall.

Mallat, S. (2008). *A wavelet tour of signal processing: the sparse way* (3rd ed.). Amsterdam: Elsevier Academic Press.

Mercier, G., Moser, G., & Serpico, S. B. (2008). Conditional copulas for change detection in heterogeneous remote sensing images. *IEEE Transactions on Geoscience and Remote Sensing*, *46*(5), 1428–1441. doi:10.1109/TGRS.2008.916476

Merida, W., Harrington, D., Canut, J. L., & McLean, G. (2006). Characterisation of proton exchange membrane fuel cell (PEMFC) failures via electrochemical impedance spectroscopy. *Journal of Power Sources*, *161*(1), 264–274. doi:10.1016/j.jpowsour.2006.03.067

Mileva Boshkoska, B. & Bohanec, M. (2012). A method for ranking non-linear qualitative decision preferences using copulas. *International Journal of Decision Support System Technology*, *4*(2), 42–58. doi:10.4018/jdsst.2012040103

Mileva Boshkoska, B., Bohanec, M., Boškoski, P., & Juričić, Đ. (2015). Copula-based decision support system for quality ranking in the manufacturing of electronically commutated motors. *Journal of Intelligent Manufacturing*, *26*(2), 281–293. doi:10.1007/s10845-013-0781-7

Mileva Boshkoska, B., Boškoski, P., Debenjak, A., & Juričić, Đ. (2015). Dependence among complex random variables as a fuel cell condition indicator. *Journal of Power Sources*, *284*, 566–573. doi:10.1016/j.jpowsour.2015.03.044

Motapon, S. N., Dessaint, L. A., & Al-Haddad, K. (2014). A comparative study of energy management schemes for a fuel-cell hybrid emergency power system of more-electric aircraft. *IEEE Transactions on Industrial Electronics*, *61*(3), 1320–1334. doi:10.1109/TIE.2013.2257152

Mulyazmi, Daud, W. R. W., Majlan, E. H., & Rosli, M. I. (2013). Water balance for the design of a PEM fuel cell system. *International Journal of Hydrogen Energy*, *38*(22), 9409–9420. doi:10.1016/j.ijhydene.2012.12.014

Musizza, B., Stefanovska, A., McClintock, P. V., Paluš, M., Petrovčič, J., Ribarič, S., & Bajrović, F. F. (2007). Interactions between cardiac, respiratory and EEG-δ oscillations in rats during anaesthesia. *The Journal of Physiology*, *580*(1), 315–326. doi:10.1113/jphysiol.2006.126748

Nelsen, R. B. (2006). *An introduction to copulas* (2nd ed.). New York, NY: Springer.

Ollila, E. (2008). On the circularity of a complex random variable. *IEEE Signal Processing Letters*, *15*, 841–844. doi:10.1109/LSP.2008.2005050

Onanena, R., Oukhellou, L., Candusso, D., Harel, F., Hissel, D., & Aknin, P. (2011). Fuel cells static and dynamic characterizations as tools for the estimation of their ageing

time. *International Journal of Hydrogen Energy*, *36*(2), 1730–1739. doi:10.1016/j.ijhydene.2010.10.064

Ordonez, M., Sonnaillon, M. O., Quaicoe, J. E., & Iqbal, M. T. (2010). An embedded frequency response analyzer for fuel cell monitoring and characterization. *IEEE Transactions on Industrial Electronics*, *57*(6), 1925–1934. doi:10.1109/TIE.2009.2028295

Modulated constant off-time control mechanism, application note. (1998). Linfinity Microelectronics.

The department of energy hydrogen and fuel cells program plan. (2011). U.S. Department of Energy. Retrieved from http://www.hydrogen.energy.gov/pdfs/program_plan2011.pdf

Ous, T. & Arcoumanis, C. (2013). Degradation aspects of water formation and transport in proton exchange membrane fuel cell: A review. *Journal of Power Sources*, *240*, 558–582. doi:10.1016/j.jpowsour.2013.04.044

Palma, L., Harfman Todorovic, M., & Enjeti, P. N. (2009). Analysis of common-mode voltage in utility-interactive fuel cell power conditioners. *IEEE Transactions on Industrial Electronics*, *56*(1), 20–27. doi:10.1109/TIE.2008.2004382

Petrone, R., Zheng, Z., Hissel, D., Péra, M., Pianese, C., Sorrentino, M., ... Yousfi-Steiner, N. (2013). A review on model-based diagnosis methodologies for PEMFCs. *International Journal of Hydrogen Energy*, *38*(17), 7077–7091. doi:10.1016/j.ijhydene.2013.03.106

Postole, G. & Auroux, A. (2011). The poisoning level of pt/c catalysts used in PEM fuel cells by the hydrogen feed gas impurities: the bonding strength. *International Journal of Hydrogen Energy*, *36*(11), 6817–6825. doi:10.1016/j.ijhydene.2011.03.018

Pregelj, B., Vrečko, D., & Jovan, V. (2011). Improving the operation of a fuel-cell power unit with supervision control - A simulation study. *Journal of Power Sources*, *196*(22), 9419–9428. doi:10.1016/j.jpowsour.2011.06.077

Pregelj, B., Vrečko, D., Petrovčič, J., Jovan, V., & Dolanc, G. (2015). A model-based approach to battery selection for truck onboard fuel cell-based APU in an anti-idling application. *Applied Energy*, *137*, 64–76. doi:10.1016/j.apenergy.2014.10.007

Priestley, M. (1981). *Spectral analyses and time series.* London: Academic Press.

Rachev, S. T. (Ed.). (2003). *Handbook of heavy tailed distributions in finance.* Amsterdam: Elsevier.

Rezaei Niya, S. M. & Hoorfar, M. (2013). Study of proton exchange membrane fuel cells using electrochemical impedance spectroscopy technique – A review. *Journal of Power Sources*, *240*, 281–293. doi:10.1016/j.jpowsour.2013.04.011

Roy, S. K. & Orazem, M. E. (2007). Error analysis of the impedance response of PEM fuel cells. *Journal of the Electrochemical Society*, *154*(8), B883–B891. doi:10.1149/1.2747533

Roy, S. K., Orazem, M. E., & Tribollet, B. (2007). Interpretation of low-frequency inductive loops in PEM fuel cells. *Journal of The Electrochemical Society*, *154*(12), B1378–B1388. doi:10.1149/1.2789377

Rubio, M. A., Urquia, A., & Dormido, S. (2010). Diagnosis of performance degradation phenomena in PEM fuel cells. *International Journal of Hydrogen Energy*, *35*(7), 2586–2590. doi:10.1016/j.ijhydene.2009.03.054

Sadiq Al-Baghdadi, M. A. R. (2013). *PEM fuel cells: Fundamentals, modeling, and applications.* International Energy and Environment Foundation.

Savu, C. & Trade, M. (2006). Hierarchical Archimedean copulas. In *Proceedings of the international conference on high frequency finance.*

Schmittinger, W. & Vahidi, A. (2008). A review of the main parameters influencing long-term performance and durability of PEM fuel cells. *Journal of Power Sources*, *180*(1), 1–14. doi:10.1016/j.jpowsour.2008.01.070

Sethuraman, V. A. & Weidner, J. W. (2010). Analysis of sulfur poisoning on a PEM fuel cell electrode. *Electrochimica Acta*, *55*(20), 5683–5694. doi:10.1016/j.electacta.2010.05.004

Sharaf, O. Z. & Orhan, M. F. (2014). An overview of fuel cell technology: Fundamentals and applications. *Renewable and Sustainable Energy Reviews*, *32*, 810–853. doi:10.1016/j.rser.2014.01.012

Silva, S. B., Severino, M. M., & de Oliveira, M. A. G. (2013). A stand-alone hybrid photovoltaic, fuel cell and battery system: a case study of Tocantins, Brazil. *Renewable Energy*, *57*, 384–389. doi:10.1016/j.renene.2013.02.004

Silverman, B. W. (1986). *Density estimation for statistics and data analysis*. London: Chapman and Hall.

Simon, M. K. (2006). *Probability distributions involving Gaussian random variables*. New York, NY: Springer Science.

Siwakoti, Y. P., Loh, P. C., Blaabjerg, F., Andreasen, S. J., & Town, G. E. (2015). Y-Source boost DC/DC converter for distributed generation. *IEEE Transactions on Industrial Electronics*, *62*(2), 1059–1069. doi:10.1109/TIE.2014.2345336

Sklar, A. (1996). Distributions with fixed marginals and related topics - Random variables, distribution functions, and copulas - A personal look backward and forward. In L. Rüschendorf, B. Schweizer, & M. Taylor (Eds.), (Vol. 28, pp. 1–14). Hayward, CA: Institute of Mathematical Statistics.

Skvarenina, T. L. (Ed.). (2001). *The power electronics handbook*. New York, NY: CRC Press.

Stefanovska, A. & Bračič, M. (1999). Physics of the human cardiovascular system. *Contemporary Physics*, *40*(1), 31–55. doi:10.1080/001075199181693

Stumper, J., Löhr, M., & Hamada, S. (2005). Diagnostic tools for liquid water in PEM fuel cells. *Journal of Power Sources*, *143*(1-2), 150–157. doi:10.1016/j.jpowsour.2004.11.036

Tang, Y., Fu, D., Wang, T., & Xu, Z. (2015). Hybrid switched-inductor converters for high step-up conversion. *IEEE Transactions on Industrial Electronics*, *62*(3), 1480–1490. doi:10.1109/TIE.2014.2364797

Tant, S., Rosini, S., Thivel, P. X., Druart, F., Rakotondrainibe, A., Geneston, T., & Bultel, Y. (2014). An algorithm for diagnosis of proton exchange membrane fuel cells by electrochemical impedance spectroscopy. *Electrochimica Acta*, *135*, 368–379. doi:10.1016/j.electacta.2014.04.108

Terzulli, G. & Peace, B. W. (2004). *Film technology to replace electrolytic technology*. AVX.

Torrence, C. & Compo, G. P. (1998). A practical guide to wavelet analysis. *Bulletin of the American Meteorological Society*, *79*, 61–78. doi:10.1175/1520-0477(1998)079<0061:APGTWA>2.0.CO;2

Trivedi, P. & David, Z. (2007). Copula modeling: An introduction for practitioners. *Foundations and Trends in Econometrics*, *1*(1), 1–111. doi:10.1561/0800000005

Tseng, K. C. & Huang, C. C. (2014). High step-up high-efficiency interleaved converter with voltage multiplier module for renewable energy system. *IEEE Transactions on Industrial Electronics*, *61*(3), 1311–1319. doi:10.1109/TIE.2013.2261036

Vachtsevanos, G., Lewis, F. L., Roemer, M., Hess, A., & Wu, B. (2006). *Intelligent fault diagnosis and prognosis for engineering systems*. Hoboken, NJ: John Wiley & Sons, Inc.

Valdivia, V., Barrado, A., Lazaro, A., Sanz, M., Lopez del Moral, D., & Raga, C. (2014). Black-box behavioral modeling and identification of DC-DC converters with input current control for fuel cell power conditioning. *IEEE Transactions on Industrial Electronics*, *61*(4), 1891–1903. doi:10.1109/TIE.2013.2267692

Verhage, A. J. L., Coolegem, J. F., Mulder, M. J. J., Yildirim, M. H., & de Bruijn, F. A. (2013). 30,000 h operation of a 70 kW stationary PEM fuel cell system using hydrogen from a chlorine factory. *International Journal of Hydrogen Energy*, *38*(11), 4714–4724. doi:10.1016/j.ijhydene.2013.01.152

Wai, R. J., Lin, C. Y., Duan, R. Y., & Chang, Y. R. (2007). High-efficiency DC-DC converter with high voltage gain and reduced switch stress. *IEEE Transactions on Industrial Electronics*, *54*(1), 354–364. doi:10.1109/TIE.2006.888794

Wang, H. [Huai] & Blaabjerg, F. (2014). Reliability of capacitors for DC-link applications in power electronic converters - an overview. *IEEE Transactions on Industry Applications*, *50*(5), 3569–3578. doi:10.1109/TIA.2014.2308357

Wasterlain, S., Candusso, D., Harel, F., Hissel, D., & François, X. (2011). Development of new test instruments and protocols for the diagnostic of fuel cell stacks. *Journal of Power Sources*, *196*(12), 5325–5333. doi:10.1016/j.jpowsour.2010.08.029

Webb, D. & Møller-Holst, S. (2001). Measuring individual cell voltages in fuel cell stacks. *Journal of Power Sources*, *103*, 54–60. doi:10.1016/S0378-7753(01)00831-X

Wilkinson, D. P. & St-Pierre, J. (2010). Durability. In W. Vielstich, A. Lamm, & H. A. Gasteiger (Eds.), *Handbook of fuel cells*. Chichester, England: John Wiley & Sons, Ltd. doi:10.1002/9780470974001.f303053

Wu, B., Zhao, M., Shi, W., Liu, W., Liu, J., Xing, D., ... Zou, Z. (2014). The degradation study of Nafion/PTFE composite membrane in PEM fuel cell under accelerated stress tests. *International Journal of Hydrogen Energy*, *39*(26), 14381–14390. doi:10.1016/j.ijhydene.2014.02.142

Wu, G., Ruan, X., & Ye, Z. (2015). Non-isolated high step-up DC-DC converters adopting switched-capacitor cell. *IEEE Transactions on Industrial Electronics*, *62*(1), 383–393. doi:10.1109/TIE.2014.2327000

Wu, J., Yuan, X.-Z., Martin, J. J., Wang, H., Zhang, J., Shen, J., ... Merida, W. (2008). A review of PEM fuel cell durability: degradation mechanisms and mitigation strategies. *Journal of Power Sources*, *184*(1), 104–119. doi:10.1016/j.jpowsour.2008.06.006

Wu, J., Yuan, X.-Z., Wang, H. [Haijiang], Blanco, M., Martin, J. J., & Zhang, J. (2008). Diagnostic tools in PEM fuel cell research: Part I Electrochemical techniques. *International Journal of Hydrogen Energy*, *33*(6), 1735–1746. doi:10.1016/j.ijhydene.2008.01.013

Xuewei, P. & Rathore, A. K. (2014). Novel bidirectional snubberless naturally commutated soft-switching current-fed full-bridge isolated DC/DC converter for fuel cell vehicles. *IEEE Transactions on Industrial Electronics*, *61*(5), 2307–2315. doi:10.1109/TIE.2013.2271599

Yan, Q., Toghiani, H., Lee, Y.-W., Liang, K., & Causey, H. (2006). Effect of sub-freezing temperatures on a {pem} fuel cell performance, startup and fuel cell components. *Journal of Power Sources*, *160*(2), 1242–1250. doi:10.1016/j.jpowsour.2006.02.075

Yan, W.-M., Chu, H.-S., Lu, M.-X., Weng, F.-B., Jung, G.-B., & Lee, C.-Y. (2009). Degradation of proton exchange membrane fuel cells due to CO and CO_2 poisoning. *Journal of Power Sources*, *188*(1), 141–147. doi:10.1016/j.jpowsour.2008.11.107

Yi, J. S., Yang, J. D., & King, C. (2004). Water management along the flow channels of PEM fuel cells. *AIChE Journal*, *50*(10), 2594–2603. doi:10.1002/aic.10307

Yousfi-Steiner, N., Hissel, D., Moçotéguy, P., & Candusso, D. (2011). Non intrusive diagnosis of polymer electrolyte fuel cells by wavelet packet transform. *International Journal of Hydrogen Energy*, *6*(1), 740–746. doi:10.1016/j.ijhydene.2010.10.033

Yousfi-Steiner, N., Moçotéguy, P., Candusso, D., Hissel, D., Hernandez, A., & Aslanides, A. (2008). A review on PEM voltage degradation associated with water management: impacts, influent factors and characterization. *Journal of Power Sources*, *183*(1), 260–274. doi:10.1016/j.jpowsour.2008.04.037

Yu, P. T., Liu, Z., & Makharia, R. (2013). Investigation of carbon corrosion behavior and kinetics in proton exchange membrane fuel cell cathode electrodes. *Journal of The Electrochemical Society*, *160*(6), F645–F650. doi:10.1149/2.120306jes

Yu, X., Starke, M. R., Tolbert, L. M., & Ozpineci, B. (2007). Fuel cell power conditioning for electric power applications: a summary. *IET Electric Power Applications*, *1*(5), 643–656.

Yuan, X.-Z., Li, H., Zhang, S., Martin, J., & Wang, H. (2011). A review of polymer electrolyte membrane fuel cell durability test protocols. *Journal of Power Sources*, *196*(22), 9107–9116. doi:10.1016/j.jpowsour.2011.07.082

Yuan, X.-Z., Sons, C., Wang, H., & Zhang, J. (2010). *Electrochemical impedance spectroscopy in PEM fuel cells, fundamentals and applications*. London: Springer.

Yuan, X.-Z., Wang, H., Sun, J. C., & Zhang, J. (2007). AC impedance technique in PEM fuel cell diagnosis – A review. *International Journal of Hydrogen Energy*, *32*, 4365–4380. doi:10.1016/j.ijhydene.2007.05.036

Zheng, Z., Petrone, R., Péra, M., Hissel, D., Becherif, M., Pianese, C., ... Sorrentino, M. (2013). A review on non-model based diagnosis methodologies for PEM fuel cell stacks and systems. *International Journal of Hydrogen Energy*, *38*(21), 8914–8926. doi:10.1016/j.ijhydene.2013.04.007

Bibliography

Publications Related to the Dissertation

Journal Articles

Debenjak, A., Boškoski, P., Musizza, B., Petrovčič, J., & Juričić, Đ. (2014). Fast measurement of proton exchange membrane fuel cell impedance based on pseudo-random binary sequence perturbation signals and continuous wavelet transform. *Journal of Power Sources*, *254*, 112–118. doi:10.1016/j.jpowsour.2013.12.094

Author Contributions. Andrej Debenjak devised the underlying idea of using the PRBS waveform as a perturbation signal for the impedance estimation and coordinated the research work flow. He set up the experiment testbed, designed and performed the experiments, collected the data, developed the methodology and performed the analysis. Pavle Boškoski assisted in the methodology development, software implementation for data acquisition and analysis. The manuscript was jointly written by Andrej Debenjak and Pavle Boškoski. Bojan Musizza advised on the tuning of the CWT parameters. Janko Petrovčič designed the hardware part of the embedded measurement equipment and assisted at the experiment testbed formation. Đani Juričić coordinated the scientific aspect of the research.

Boškoski, P. & Debenjak, A. (2014). Optimal selection of proton exchange membrane fuel cell condition monitoring thresholds. *Journal of Power Sources*, *268*, 692–699. doi:10.1016/j.jpowsour.2014.06.110

Author Contributions. Pavle Boškoski conceived the main idea of treating the impedance values as random complex variables and developed the methodology. Andrej Debenjak designed and performed the experiments and assisted in the methodology development. Both authors contributed equally to the other aspects of the research work.

Mileva Boshkoska, B., Boškoski, P., Debenjak, A., & Juričić, Đ. (2015). Dependence among complex random variables as a fuel cell condition indicator. *Journal of Power Sources*, *284*, 566–573. doi:10.1016/j.jpowsour.2015.03.044

Author Contributions. Biljana Mileva Boshkoska advised on the copula functions methodology and conducted the copulas-based information aggregation analysis. Pavle Boškoski devised the copula functions statistical framework as a pathway to the construction of a unit-free CI and helped on the data analysis. Andrej Debenjak designed and conducted the experiments, performed the feature extraction analysis and contributed to the interpretation of the data. Andrej Debenjak, Pavle Boškoski and Biljana Mileva Boshkoska wrote the manuscript. Đani Juričić coordinated and supervised the scientific aspect of the research and revised the manuscript.

Debenjak, A., Petrovčič, J., Boškoski, P., Musizza, B., & Juričić, Đ. (2015). Fuel cell condition monitoring system based on interconnected DC-DC converter and voltage monitor. *IEEE Transactions on Industrial Electronics*, *62*(8), 1–13. doi:10.1109/TIE.2015.2434792

Author Contributions. Janko Petrovčič proposed the interconnected fuel cell voltage monitor and DC-DC converter for the CM purpose, designed the electronic hardware of the platform and coordinated the project. Bojan Musizza and Andrej Debenjak designed software and implemented the CM algorithms. Janko Petrovčič, Bojan Musizza and Andrej Debenjak tested and validated the platform. Andrej Debenjak and Pavle Boškoski conducted the experiments. Andrej Debenjak, Pavle Boškoski and Janko Petrovčič wrote the manuscript. Đani Juričić supervised the scientific aspect of the project and revised the manuscript.

Other Publications

Journal Articles

Debenjak, A., Gašperin, M., Pregelj, B., Atanasijević-Kunc, M., Petrovčič, J., & Jovan, V. (2013). Detection of flooding and drying inside a PEM fuel cell stack. *Strojniški vestnik – Journal of Mechanical Engineering*, *59*(1), 56–64. doi:10.5545/sv-jme.2012.640

Debenjak, A., Musizza, B., Gašperin, M., & Petrovčič, J. (2013a). Diagnostični modul za gorivne celice s protonsko prevodno membrano. *Ventil*, *19*(3), 200–206.

Gašperin, M., Boškoski, P., Debenjak, A., & Petrovčič, J. (2014). Signal processing and stochastic filtering for EIS based PHM of fuel cell systems. *Fuel Cells*, *14*(3), 457–465. doi:10.1002/fuce.201300217

Conference Papers

Boškoski, P., Debenjak, A., & Juričić, Đ. (2015). Spremljanje stanja gorivnih celic PEM. In *Zbornik devete konference Avtomatizacija v industriji in gospodarstvu AIG'15*.

Debenjak, A. (2011). Uporaba elektrokemične impedančne spektroskopije v sistemih s PEM gorivnimi celicami. In *Zbornik dvajsete mednarodne Elektrotehniške in računalniške konference ERK 2011* (pp. 467–468).

Debenjak, A. (2012). Diagnostika sistemov z gorivnimi celicami in izboljšanje njihovega delovanja. In *Zbornik 4. študentske konference Mednarodne podiplomske šole Jožefa Stefana*.

Debenjak, A., Gašperin, M., & Petrovčič, J. (2013). On-line tracking of fuel cell system impedance using extended kalman filter. In *Chemical Engineering Transactions: 2013 Prognostics and System Health Management Conference* (Vol. 33, pp. 1003–1008). doi:10.3303/CET1333168

Debenjak, A., Jovan, V., Petrovčič, J., Gašperin, M., & Pregelj, B. (2012). An assessment of water conditions in a PEM fuel cell stack using electrochemical impedance spectroscopy. In *2012 IEEE Conference on Prognostics and System Health Management* (pp. 1–6). doi:10.1109/PHM.2012.6228846

Debenjak, A., Musizza, B., Gašperin, M., & Petrovčič, J. (2013b). Modul za sprotno diagnostiko PEM gorivnih celic. In *Zbornik osme konference Avtomatizacija v industriji in gospodarstvu AIG'13*.

Debenjak, A., Papa, G., & Petrovčič, J. (2015). Modularni sistem za upravljanje Li-Ion baterije. In *Zbornik devete konference Avtomatizacija v industriji in gospodarstvu AIG'15*.

Debenjak, A., Pregelj, B., Gašperin, M., & Petrovčič, J. (2012). Koncept diagnostike sistemov s PEM gorivnimi celicami. In *Vir znanja in izkušenj za stroko: Zbornik foruma IRT 2012*.

Pregelj, B., Fritz, J., Vrečko, D., Petrovčič, J., Jovan, V., & Debenjak, A. (2013). Model of an 8-kW fuel cell based power unit for operation monitoring, optimization and control testing. In *2013 8th EUROSIM congress on modelling and simulation* (pp. 433–438). doi:10.1109/EUROSIM.2013.80

Biography

Andrej Debenjak was born on 24th January 1987 in Šempeter pri Gorici, Slovenia. He completed the secondary education at the Nova Gorica comprehensive school in 2005. In the same year, he enrolled in the undergraduate programme at the Faculty of Electrical Engineering, University of Ljubljana. During his study, he had been a Zois Scholarship holder and later he received the scholarship of the Jožef Stefan Institute. His undergraduate study was in the field of systems engineering and process control. He received his diploma degree in electrical engineering from the University of Ljubljana in 2011. For his diploma thesis, he was awarded the Dr. Vratislav Bedjanič Award.

In 2011 he was accepted to the Young Researchers Programme of the Slovenian Research Agency under the supervision of Dr. Janko Petrovčič. In the same time he started with his Ph.D. study at the Jožef Stefan International Postgraduate School, Information and Communication Technologies programme.

His research is mainly focused on fault detection and diagnostics of PEM fuel cell systems and prognostics and health management of lithium-based batteries. Areas of his expertise include embedded programming, digital signal processing, statistical analysis, and diagnostic algorithm design. In the last few years, he has been involved in the design of an approach for time-efficient estimation of electrochemical impedance with applicability to condition monitoring. He was responsible for algorithms and firmware design of a modular battery management system for lithium-ion batteries. He has also been working on the design of an embedded measurement equipment for fast online impedance estimation of lithium-sulphur battery cells. Lately, he has be involved in the design of firmware for the embedded controller for auxiliary power unit based on diesel reforming and PEM fuel cells.